January 2015

The Effect of Body Weight Support on Squat Biomechanics

Najam R. Syed
Purdue University

Graduate School Form 30
Updated 1/15/2015

PURDUE UNIVERSITY
GRADUATE SCHOOL
Thesis/Dissertation Acceptance

This is to certify that the thesis/dissertation prepared

By Najam R. Syed

Entitled

The Effect of Body Weight Support on Squat Biomechanics

For the degree of Master of Science in Mechanical Engineering

Is approved by the final examining committee:

Dr. Justin Seipel
Chair

Dr. Eric Nauman

Dr. Bradley Duerstock

To the best of my knowledge and as understood by the student in the Thesis/Dissertation Agreement, Publication Delay, and Certification Disclaimer (Graduate School Form 32), this thesis/dissertation adheres to the provisions of Purdue University's "Policy of Integrity in Research" and the use of copyright material.

Approved by Major Professor(s): Dr. Justin Seipel

Approved by: Jay P. Gore 12/11/2015

Head of the Departmental Graduate Program Date

THE EFFECT OF BODY WEIGHT SUPPORT ON SQUAT BIOMECHANICS

A Thesis

Submitted to the Faculty

of

Purdue University

by

Najam R. Syed

In Partial Fulfillment of the

Requirements for the Degree

of

Master of Science in Mechanical Engineering

December 2015

Purdue University

West Lafayette, Indiana

ACKNOWLEDGMENTS

First, I would like to give my utmost thanks to my advisor, Dr. Justin Seipel, for giving me the opportunity to work with him and on this project. His academic guidance, support, and encouragement have been invaluable and have helped me navigate the maze that is graduate school. Perhaps equally important, his enthusiasm for biomechanics and robotics has inspired a sense of excitement about the field in me, too.

Next, I would like to thank all the other individuals whose help enabled this project and thesis to come to fruition. I am immensely grateful to Ginina Vitucci, with whom I worked side by side to design and build the experimental setup, for sharing her knowledge and expertise with me. Without her efforts, this project would not have been possible. I thank Jeffrey Ackerman for his sage advice and recommendations at every step of the way, and for acting as a sort of compass whenever I was unsure in which direction to travel. I want to thank Manish Anand for his advice and for helping me with motion capture and data acquisition. I would like to thank Michelle Yuen for her assistance with developing and testing parts of the experimental setup, and for her willingness to discuss ideas and issues. I am also thankful to all the other members of the Spira Lab, particularly Harshal Upadhyay and Sashank Allu, for giving me someone to bounce ideas off of or simply to commiserate with.

Finally, I am wholeheartedly grateful to my friends and family, who have kept me sane over the past few years, and with whom I have shared numerous memorable conversations, experiences, and adventures. I am especially indebted to my parents, whose continual love and support have kept me afloat.

TABLE OF CONTENTS

Page

LIST OF TABLES

LIST OF FIGURES

Figure Page

Figure Page

ABBREVIATIONS

ACL	Anterior cruciate ligament
BW	Body weight
BWS	Body weight support
COM	Center of mass
CoP	Center of pressure
FBD	Free body diagram
GRF	Ground reaction force
IR	Infrared
PD	Proportional–Derivative

ABSTRACT

Syed, Najam. MSME, Purdue University, December 2015. The Effect of Body Weight Support on Squat Biomechanics. Major Professor: Justin Seipel, School of Mechanical Engineering.

To yield insights into how assistive technology can impact basic human motion, here we investigate the effects of varied body weight support on the biomechanics of human subjects rising from a squatted position. This rising motion occurs when individuals rise from a seated squat, rise from a chair, or lift up an object, and may occur as a component of other motions as well. To study the effect of weight support on this motion we designed an apparatus that utilizes controlled pneumatic actuators allowing for variable load profiles on either side of the body. In this experiment, a vertical load was applied at the hips during the rising phase of the squatting motion. Two levels of load supported motions, 20% BW and 35% BW, were compared to unsupported squats. There were statistically significant differences in the joint moments and forces when squatting with BW support versus squatting without, based on the results of two-way, repeated measures ANOVA ($p < 0.01$). Presented as mean ± SD, peak knee moments decreased from 4.725 ± 0.747 (%BW*height) without support, at the beginning of the squat, to 3.660 ± 1.010 (%BW*height) with 35% BW support. Peak hip moments declined from 3.433 ± 0.755 (%BW*height) without support, at the beginning of the squat, to 2.627 ± 0.815 (%BW*height) at 35% BW support. We developed a simplified dynamic model of

the squatting motion that predicts and explains these changes. However, despite the overall agreement with our model, the assistive load support also induced kinematic adaptations in the subjects that were not predicted by the model. Subjects tended to maintain a relatively high trunk tilt under the influence of load support until nearing the end of the squat, causing the actual forces, moments, and CoP to deviate from the predicted values during this final phase of the squat.

CHAPTER 1. INTRODUCTION

In recent decades, there has been a surge of research and development of orthoses, exoskeletons, and devices that attempt to assist the human body. The applications of such devices are diverse. They can multiply the strength and capabilities of manual materials handlers, like freight and warehouse employees, or soldiers who must carry and sometimes lift heavy loads, or they can restore lost function in individuals with musculoskeletal or neurological impairments—amputees, stroke patients, paraplegics—or they can act as rehabilitative aids in clinical and therapeutic settings. By their very nature, these devices exert loads and moments on the human body, so it is imperative to understand the effects of these loads on how the body works.

One way which devices may assist motion is by providing vertical load support at the lower limbs, as many lower limb exoskeletons and orthotics do. The legs provide for several important functions, obviously, one of which is squatting. The squat and related motions like the sit-to-stand or stand-to-sit transition are common movements in the contexts of both athletic exercise and activities of daily living. A review of the literature reveals that, while many studies have examined the metabolic costs of using exoskeletons, the effect of body weight support on walking and running, and the joint kinetics of the squatting motion, few or none have considered the effects of squatting with weight support.

It is no secret that the lower limbs comprise a complex biomechanical system or that, consequently, repetitive use and stress injuries in the lower limbs present with complex etiologies. It is crucial to properly understand the effect of the application of moments or loads on the lower limbs, whether applied by a specialized rehabilitative device like the AlterG treadmill or by a heavily actuated, battery-powered exoskeleton like the HULC, whether for an athlete recovering from ACL surgery, or for a stroke patient retraining basic skills and coordination, or for an able-bodied soldier lifting munitions weighing hundreds of pounds.

A recent study by Gams, et al., attempted to bridge a segment of this gap by assessing the metabolic cost of an augmentative robotic knee exoskeleton during repetitive squatting motion [1]. The researchers designed a prototype for a knee exoskeleton that could be secured to the leg at the shank and thigh with Velcro straps. Their device possessed a ball joint at the ankle to allow unrestricted movement of the feet, and an active hinge joint at the knee, providing a single rotational degree of freedom at the knee. The robotic exoskeleton's knee joint was actuated by a DC motor, permitting them to compute the applied torque at any given flexion angle. The study concluded that subjects squatting with the assistance of the device expended less energy, as measured by oxygen consumption and heart rate, than they did without it. Another study by the same authors considered the joint torque reactions for the same type of robotic knee exoskeleton and found that, when the device was used without providing assistance—when it was worn but not actuated—the estimated torque at the knee increased. When the device actually assisted the user in performing squats, the torque at the knee was reduced by approximately 36%, though it should be noted that the maximum applied torque was

roughly 65% of the torque experienced by the joint during unassisted squats. In other words, the device reduced knee joint torque, but by a significantly lower margin than might have been intuitively expected [2]. This implies that the use of exoskeletons or similar assistive devices may incur, in the user, certain physiological and biomechanical costs, or impose certain kinematical constraints that are not yet well understood.

With our experiment, we aimed to address a broader class of issues by applying exclusively vertical load at the hip and considering its effect on the resultant reactions in the body. Furthermore, by utilizing an apparatus that applied upward load at the hip without burdening the wearer with additional weight, as an actual exoskeleton might, we could isolate the impact of vertical load at the hip without the confounding variables that a full device or exoskeleton might introduce. Such an approach is consistent with previous studies that have studied the effect of applied vertical load on gait and locomotion, which utilized similar harnesses and ropes or cables to reduce the apparent weight or mass of the individual [3]–[11]. Our study also attempts to address gaps in knowledge on heels down squatting during the rising phase of the squat. A number of studies have looked at heels down squatting, but few or none have sought to characterize the joint kinetics and location of the center of pressure along the foot, particularly during the rising portion of the motion [12]–[17].

It is our hope that the results of this experiment will lead to a more complete understanding of weight support and squat biomechanics.

CHAPTER 2. BACKGROUND AND LITERATURE REVIEW

2.1. Exoskeletons: History, Purpose, and Current State of the Art

Since the latter half of the twentieth century, lower-limb exoskeletons and orthoses have constituted an increasingly active area of research and design. Such devices may be broadly divided into two categories: rehabilitative and augmentative. Rehabilitative orthoses and exoskeletons, as the word implies, serve to restore normal function in individuals with lower-limb impairments or handicaps. They might serve a therapeutic function, whereby the individual uses the device periodically during physical therapy sessions or for a relatively short period of time—for example, a stroke patient who is relearning to walk, or an individual recovering from a hip or knee surgery. In other cases, an exoskeleton or lower-limb orthotic might be a permanent fixture used to replace or enable otherwise lost function—for instance, a lower-limb amputee with a prosthesis, or individuals with congenital muscular dystrophies or age-related orthopedic or muscle-related injuries. The aim of augmentative exoskeletons and devices, on the other hand, is to enhance human strength and capabilities, allowing healthy users to perform otherwise physically taxing and difficult, or altogether impossible, tasks. The potential applications of such devices are widespread and are of particular interest in areas that involve strenuous labor and manual materials handling. Information from the Bureau of Labor Statistics (BLS) indicates that, as of May 2014, there were over 2.4

million laborers in the area of (manual) freight, stock, and material moving in the United States [18]. Another report from the BLS found that, in 2013, over 40% of nonfatal occupational injuries among laborers and freight, stock, and material movers were caused by "overexertion and bodily reaction," and that musculoskeletal disorders accounted for nearly 33% of all injuries and illnesses across all occupations—a figure which jumped to 37% in the transportation and warehousing industries and resulted in a median of 19 days away from work [19]. In a study of low back injuries among Home Depot retail store employees between 1990 and 1994 found that such injuries accounted for 12.3 per million work hours of lost time, or 61% of all lost time due to work-related injuries [20].

The military and the defense industry have also shown considerable interest in powered exoskeletons, as soldiers must often cart around heavy loads and handle equipment and munitions, not unlike factory workers who may have to transport heavy objects or work in physically straining positions. These devices could also, at some point, enable aid workers or emergency rescuers, firefighters, and EMTs to provide more effective care while reducing their own risk of musculoskeletal injury.

The first known recorded design for an exoskeleton can actually be traced back to Nicholas Yagn, a Russian citizen who, in 1890, developed blueprints for an apparatus that would have relied on leaf springs to reduce compressive forces in the legs while running, though there is no evidence that Yagn's design was ever built [21], [22].

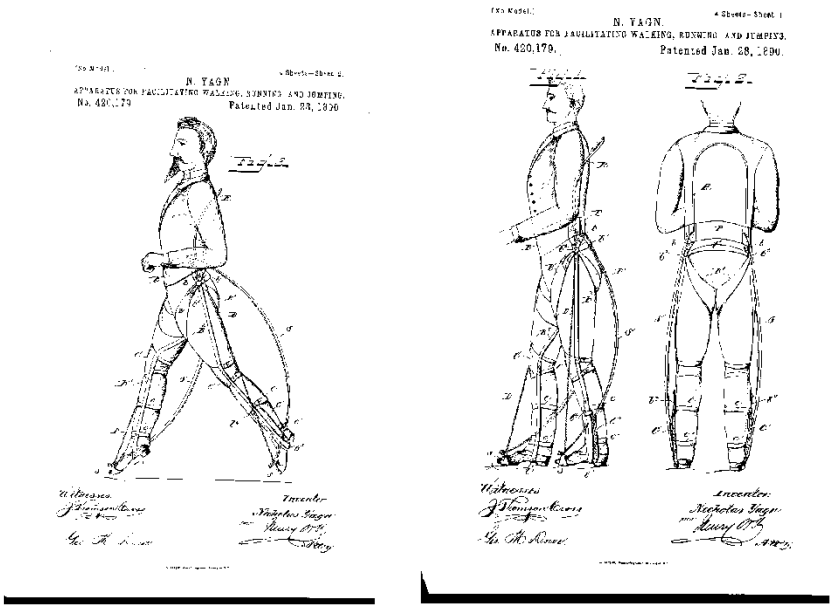

Figure 1. Nicholas Yagn's blueprints for a leaf spring–based apparatus [22].

Serge Zaroodny might be credited with inspiring the modern conception of the exoskeleton. Zaroodny, in 1963, published a report for the United States military on powered locomotion, titled "Bumpusher—a powered aid to locomotion," and though his ideas were not put into practice at the time by the military, the issues he brought up in the paper, such as weight and power consumption, are still relevant today [22], [23]. In the same decade, General Electric built the Hardiman suit, a full-body exoskeleton intended to augment typical human strength by a factor of twenty-five, though mechanical issues and safety concerns precluded testing the suit with a human inside [22]. In 1986, Jeffrey Moore published a paper in which he outlined ideas for an exoskeleton he called "Pitman," based in part on ideas from Robert Heinlein's 1959 science-fiction novel

Starship Troopers [24], [25]. Pieces of Moore's publication may have influenced the direction of the US Defense Advanced Research Project Agency's (DARPA) exoskeleton program.

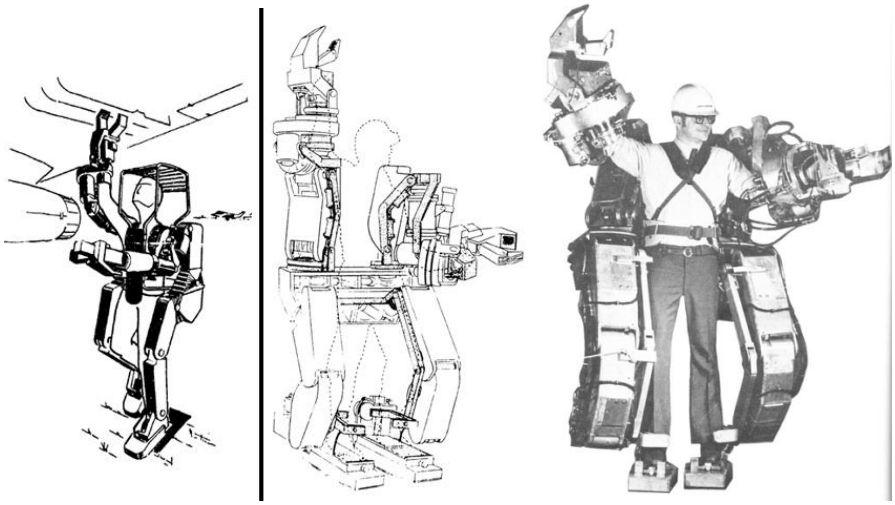

Figure 2. The General Electric Hardiman suit [22].

DARPA's Exoskeletons for Human Performance Augmentation (EHPA) began in 2001 and serves to fund research into exoskeletons and augmentative technologies that would address issues of load-carrying for soldiers [26]. Load carrying is of immense significance to the modern warfighter, as the physical demands on soldiers have increased consistently since the 19th century. Although the individual components that comprise the average infantryman's kit—body armor, radio, food, water, rifle and ammunition, gas mask, and other equipment—have gotten lighter due to advances in material science and technology, soldiers must carry increasing amounts of equipment. As a 2001 report by the Army Science Board aptly put it, "100 pounds of lightweight equipment is still 100 pounds." The report proposed that a 50-pound load ought to be the

maximum load carried by any soldier for any length of time, noting that the load on an individual soldier may be as high as 205 pounds, for instance, for an anti-tank specialist, effectively doubling their weight . Another Army report showed that average fighting loads hovered around 70 to 80 pounds, and that emergency march loads could approach 150 pounds [27]. Studies by the Navy and Marine Corps have arrived at similar conclusions; a 2007 paper by the Naval Research Advisory Committee stated that the load for a Marine rifleman should not exceed 50 pounds, yet the typical Marine rifleman carries nearly 100 pounds—a load which can increase to almost 170 pounds during certain periods—and the typical Marine squad leader hefts 134 pounds [28]. Young soldiers frequently return from deployments with musculoskeletal conditions like arthritis—conditions that, among civilians, tend not to develop until significantly later in life [29]. Between 2004 and 2007, during Operation Iraqi Freedom and Operation Enduring Freedom, medical evacuation among military personnel from military areas of operation for non–combat related musculoskeletal and spinal injuries accounted for more than 1.75 times as many evacuations as for combat-related wounds and injury [30]. Other common maladies in soldiers related to load carriage include foot blisters from friction, metatarsalgia, stress fractures, knee pain, low back injury, and rucksack palsy—a condition that may result from the compression of cervical and thoracic nerves by backpack shoulder straps [31], [32]. Bearing all this in mind, it comes as no shock that solutions which may alleviate the loads upon soldiers, such as exoskeletons, are of considerable interest to the military.

A great deal of work has been done on exoskeletons since the dawn of the new millennium, and there is no shortage of similar devices that aim to integrate wearable robotics with the human body. One product of the DARPA EHPA initiative is the Raytheon Sarcos XOS 2 exoskeleton, which utilizes hydraulic actuators to enable the user to repeatedly lift several hundred pounds for extended periods of time. The Sarcos XOS 2, which itself weighs approximately 100 kg, also allows for such feats as walking at 1.6 m/s while carrying 91 kg and supporting large payloads while standing on one leg [22], [33]–[36].

Figure 3. Raytheon Sarcos XOS 2.

Lockheed Martin's Human Universal Load Carrier (HULC), a battery-powered, untethered exoskeleton, also utilizes hydraulics to similar effect, while the Berkeley Lower Extremity Exoskeleton (BLEEX) uses electric motors to allow the user to carry a 75 kg load. The BLEEX possesses three degrees of freedom at the hip, one at the knee, and three at the ankle, four of which are actuated [22], [37]. Another exoskeleton developed fairly recently is the MIT exoskeleton, a quasi-passive lower-limb exoskeleton

that relies on numerous actuators supplemented by springs at the joints to help the user carry heavy loads. The MIT exoskeleton was found to reduce the effect of an eighty pound load on the user by 30% [38].

Figure 4. The HULC and BLEEX exoskeletons.

Other exoskeletons include Cyberdyne's HAL-5, or Hybrid Assistive Limb, which employs numerous sensing modalities—potentiometers to measure joint angles, as well as gyroscopes and accelerometers to measure acceleration and movement [22], [37]. Unlike the aforementioned exoskeletons, the HAL-5 is currently used almost exclusively rehabilitative settings, primarily in Japan and parts of Europe [39]. The utility of exoskeletons for rehabilitation and therapy is readily apparent, and numerous researchers and entrepreneurs from many parts of the globe have sought to expand the role of powered orthoses and exoskeletons in medical settings. Researchers at Sogang University in South Korea developed the EXPOS, or Exoskeleton for Patients and Old, which

combines a lower-limb exoskeleton with a more traditional locomotion aid: a walker. The walker is actively powered and wheeled, and also houses the power supply and other electromechanical components, thereby reducing the weight of the exoskeleton portion worn by the user [40].

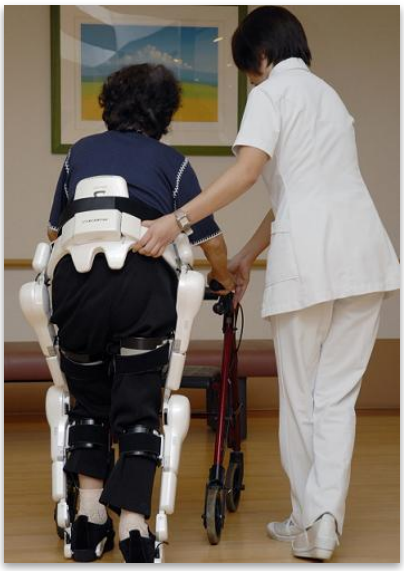

Figure 5. HAL-5 rehabilitative exoskeleton.

ReWalk Robotics, an Israeli company formerly known as Argo Medical Technologies, developed the ReWalk exoskeleton, a full lower-limb device that, with the aid of crutches, enables paraplegics and individuals with spinal cord injuries to stand, walk, and even climb stairs. Similar to the HAL-5, the ReWalk makes use of an array of sensors to detect and react to the movements and intent of the user via motorized actuators at the hip and knees. Ekso Bionics, which originally developed the HULC, also created an exoskeleton similar to the ReWalk that relies on active power, sensing, and crutches to enable paraplegics and quadriplegics to stand, walk, and perform other activities [40].

The exoskeletons discussed so far have one thing in common: they are powered and actuated and, thus, fall into the class of “active” exoskeletons and orthoses, with the partial exception of the MIT exoskeleton, whose design does involve passive elements. Although active devices like these can facilitate impressive feats and capabilities, they do so at the cost of weight and power consumption—two major challenges that virtually all actively powered devices must contend with. The BLEEX, for instance, consumes an average of 1140 W of hydraulic power and an additional 200 W of electrical power, versus the average 75 kg person, who consumes roughly 165 W while walking [41], [42]. The XOS 2 must be tethered to a power source, and the HULC, like many untethered devices, requires a bulky power supply and has a relatively limited battery life. The HAL-5, which uses feedback from its various sensors to predict the wearer’s intent, requires up to two months to calibrate the device for a single user. On the other end of the spectrum are passive devices—devices that do not rely on active power or actuation. One notable example is the Kickstart, from Cadence Biomedical, a wearable lower-limb orthotic that uses a spring placed in parallel with the thigh to provide additional thrust while walking.

Figure 6. Kickstart (Cadence Biomedical).

The spring stretches during hip extension and releases the stored potential energy during hip flexion, primarily benefiting individuals such as stroke victims who retain some lower-limb function but have reduced hip flexor capacity and coordination [43], [44].

Regardless of the mode or mechanism a particular device may utilize, all of the exoskeletons and devices discussed thus far apply or transfer some type of load to the user, either intentionally or incidentally. The effect of these loads and moments on the user may be significant and should not be discounted, though there has been little examination of the effect of such applied loads on the joints and musculoskeletal biomechanics of the user. The MIT exoskeleton, for example, though it reduced the apparent weight of a load by 30%, was found to increase the wearer's metabolic consumption by ten percent, presumably due to kinematic constraints [45]. Other devices apply considerable loads and moments at various joints, but the effect of these loads on the wearer is unclear.

2.2 Human Function, Locomotion, and Body Weight Support

Locomotion is one of the most well studied topics in human biomechanics. Human locomotion under assorted loading conditions has also been relatively well examined. Sunnerhagen, et al., looked at oxygen consumption, as a metric for metabolic rate, during walking in older adults with and without post-stroke hemiparesis, and with and without body weight support. As might be expected, mean rates of oxygen uptake were found to be higher without body weight support in both groups. The researchers conjectured that the mechanism at play might be a reduction in the mechanical work necessary to lift the center of mass when a portion of that mass is supported [46]. In an effort to better understand the phenomenon, Grabowski, et al., considered the metabolic cost of walking in healthy adults under conditions of simulated reduced gravity with and without additional load in an effort to separate the metabolic cost of supporting body weight from the metabolic cost of moving the body's mass.

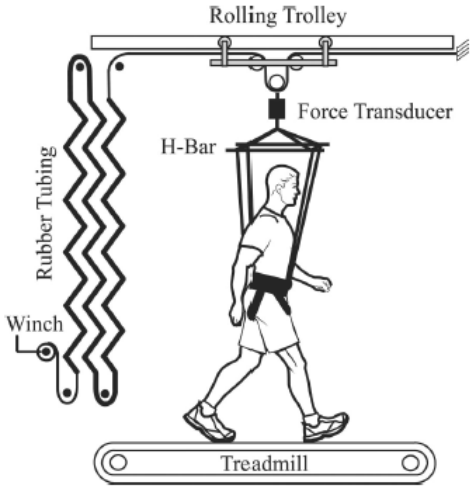

Figure 7. The apparatus Grabowski, Farley, and Kram used to provide vertical force to study body weight supported locomotion [11].

They found that work done on the center of mass due to step-to-step transitions was responsible for 45% of the metabolic cost, in line with estimates from other similar studies, while supporting body weight accounted for 28% of the total metabolic cost [11], [47]. Teunissen, Grabowski, and Kram performed a similar experiment on independently manipulating body weight and body mass and its impact on the metabolic cost of running in trained runners. Their results were relatively consistent with previous work, finding that running with reduced body weight decreased the net metabolic cost, though the reductions were not necessarily linearly proportional. Adding mass alone did not appear to appreciably increase the metabolic rate. Further, they noted that supporting body weight accounts for a significantly larger percentage of the net metabolic cost in running than it does for walking, not only due to the higher inertial forces but also because of the limb kinematics in running—joints tend to be more flexed, which may decrease the limbs' mechanical advantage [10].

Griffin, et al., also utilized a setup involving a rolling trolley above a walking subject on a treadmill. Rubber tubing, coiled around a winch, was routed through the pulleys and attached to the harnessed subject. Force was applied by turning the winch to pull the rubber tubing [5]. Barbeau, et al., developed a setup in which a subject wearing a rock climbing–style harness and walking on a treadmill was attached to a metal beam and cables that were routed through a series of pulleys overhead and then to a hydraulic actuator. A load cell sat at the base of the hydraulic cylinder, allowing them to record the supported load [8].

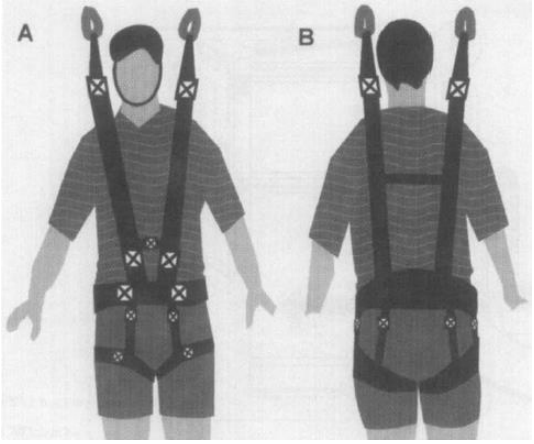

Figure 8. Representation of a modified climbing harness used to provide body weight support during treadmill walking [8].

Goldberg and Stanhope designed a similar apparatus, and used a Vicon system to obtain kinematic data [4]. In another study, by Farley and McMahon, an apparatus simulated reduced gravity for subjects walking or running on a treadmill by applying upward force via steel springs attached to a bicycle saddle. Like the approach used by Griffin, et al., they made use of a winch to adjust the tension in the springs [3].

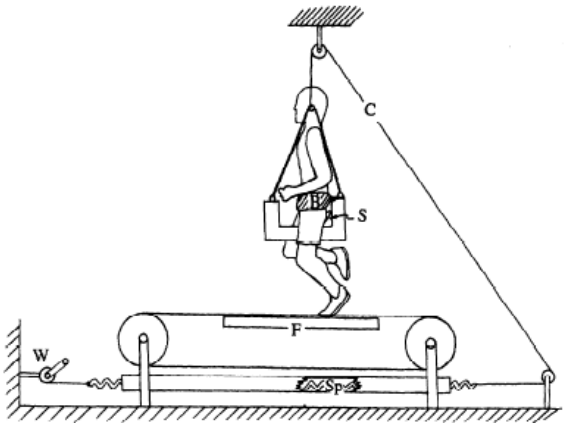

Figure 9. Farley and McMahon's body weight support system, which made use of a bicycle seat–style harness [3].

Frey, et al., introduced a novel body weight support system wherein a mechatronic system, termed the Lokolift, which incorporated both active dynamic and passive elastic components, provided vertical load support [48].

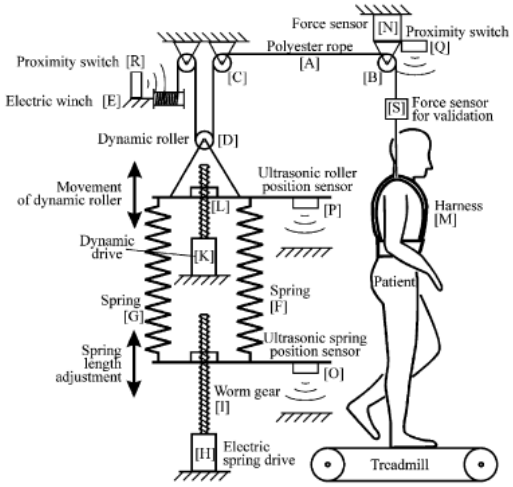

Figure 10. Frey, et al.'s mechatronic Lokolift system [48].

Aside from metabolic cost and oxygen consumption, another and perhaps more immediate measure, at least in regard to the musculoskeletal biomechanics, of the effects of BWS on the body is the change in forces and moments at the joints. Goldberg and Stanhope observed that, while walking with body weight support on a treadmill, average joint forces and peak joint moments decreased with added body weight support, but also found that the decrements were not necessarily proportional to the level of body weight support, and nonlinear in some cases [4].

Given the apparent metabolic and mechanical relief that whole or partial body weight support seems to provide for individuals, it comes as no surprise that the concept

has found its way into therapeutic and commercial settings. Among the more notable examples is the AlterG Anti-Gravity treadmill. The AlterG consists of a pressurized tent, which encircles the user's lower limbs and is fitted securely about the waist, atop a treadmill.

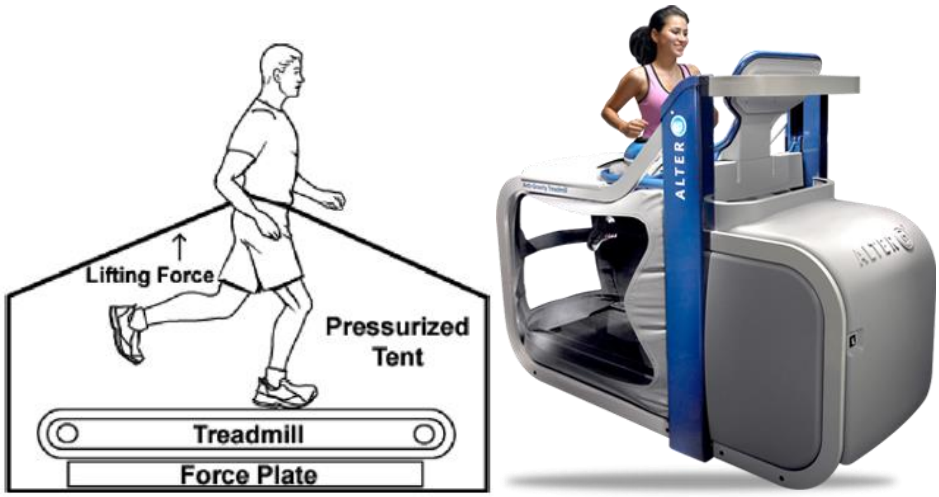

Figure 11. The AlterG positive pressure treadmill [9], [49].

Varying the pressure varies the upward force provided to the user, decreasing the overall vertical load on the user while standing, walking, or running. Kram and Grabowski studied the outcome of this lower-body positive pressure mechanism and showed that, as one might expect, weight support was a significant predictor of vertical impact and vertical loading [9]. In their paper, they also discussed some of the advantages of harness-based body weight support systems like the AlterG, in the context of sports training and therapeutic rehabilitation, over traditional methods such as water immersion. Although walking or running while immersed in water has proven to be an effective tool for building aerobic fitness and drastically reducing metabolic exertion and impulsive loading on joints, the kinematics of underwater locomotion differ considerably from

overground locomotion, reducing the efficacy of such water immersion–based techniques for certain populations of rehabilitation patients who need to relearn or retrain themselves to walk [50]–[52]. The AlterG system has also seen interest from NASA for the physical training of astronauts. Numerous other studies support the notion that body weight support treadmill training is an effective tool for rehabilitation [8].

2.3 Lower Limb Anatomy and the Squatting Motion

The ubiquity of squatting makes it essential to the study of human movement and biomechanics. The squat is one of the most common closed kinetic chain exercises in sports-related and athletic training, including but not limited to competitive weightlifting. Squatting is highly relevant to activities of daily living; a couple activities that spring to mind include picking up boxes and moving furniture. It is also related to the sit-to-stand and stand-to-sit transitions. Moreover, the squat is prescribed as a part of many rehabilitation regimens. For instance, a considerable amount of research shows that performing eccentric squats on a slightly declined surface is an effective therapy for chronic patellar tendinopathy, a tendon overuse disorder typically seen in athletes [53]. Squatting is also a key part of most postoperative rehabilitation programs for anterior cruciate ligament (ACL) injuries.

The nature of the squat also makes it prone to be detrimental if performed incorrectly, or if prescribed or monitored improperly as a therapeutic exercise. When patients engaged in physical therapy following ACL reconstructive surgery were asked to squat, they exhibited two distinct kinematic strategies between the involved limb—the limb which had undergone the ACL repair—and the noninvolved limb. In the former, the patients shifted the limb's kinematics so as to distribute greater muscular effort to the hip and less to the knee, while the kinematics of the noninvolved limb distributed muscular effort more evenly between the hip and the knee [54]. This asymmetry has the potential to limit the effectiveness of the rehabilitative process, introduce muscular deficits or

imbalances, and even cause further injury. This experiment underscores the importance of understanding the role squat kinematics play in musculoskeletal health and dynamics.

The squat makes use of the entirety of the lower body and the joints therein—ankles, knees, and hips. Naturally, this necessitates an understanding of the anatomy of the lower limbs. The translation and rotation of the body and its various segments can be described by the following planes and axes:

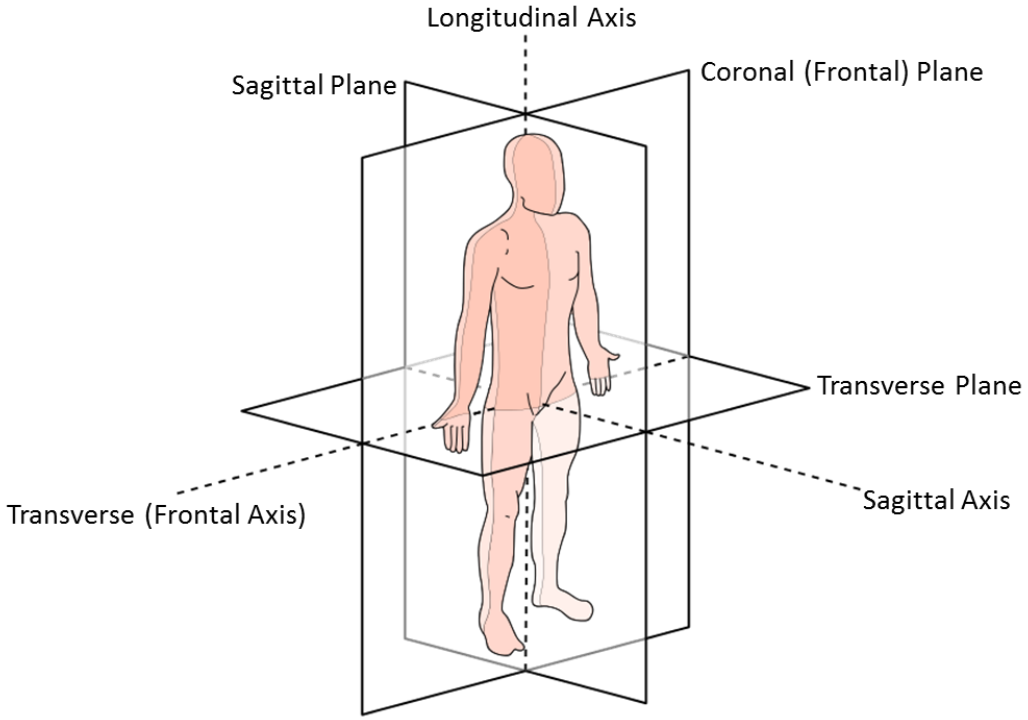

Figure 12. Anatomical planes and axes, adapted from [55].

The major sections of the body are divided into segments. Starting from the ground and moving upward, the segments with which we will primarily be concerned include 1) the foot, 2) the shank, which is the part of the leg from ankle to knee, 3) the thigh, or the part of the leg from knee to hip, and 4) the trunk, which comprises the torso and the region

from the hip up. Joint flexion angles are defined with respect to these segments. The ankle flexion angle refers to the angle between the foot and shank, the knee flexion angle to the angle between shank and thigh, and the hip flexion angle to the angle between thigh and trunk (Figure 13).

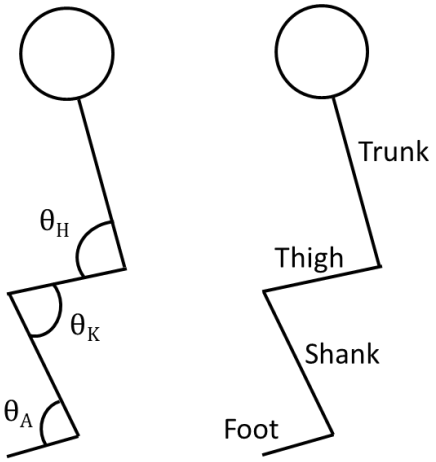

Figure 13. Definitions of the joint flexion angles and body segments, where θ_A is the ankle flexion angle, θ_K is the knee flexion angle, and θ_H is the hip flexion angle.

The locations of points on the body with respect to the body or with respect to other points can be described by the following anatomical directional terms:

Anterior, or *ventral*: Toward the front of the body or segment.

Posterior, or *dorsal*: Toward the rear of the body or segment.

Superior: Toward the top of the body (head) or segment.

Inferior: Toward the bottom of the body (feet) or segment.

Proximal: Toward the trunk, or the point of attachment nearest the trunk.

Distal: Away from the trunk, or from the point of attachment nearest the trunk.

Medial: Toward the midline of the body or segment.

Lateral: Away from the midline of the body or segment.

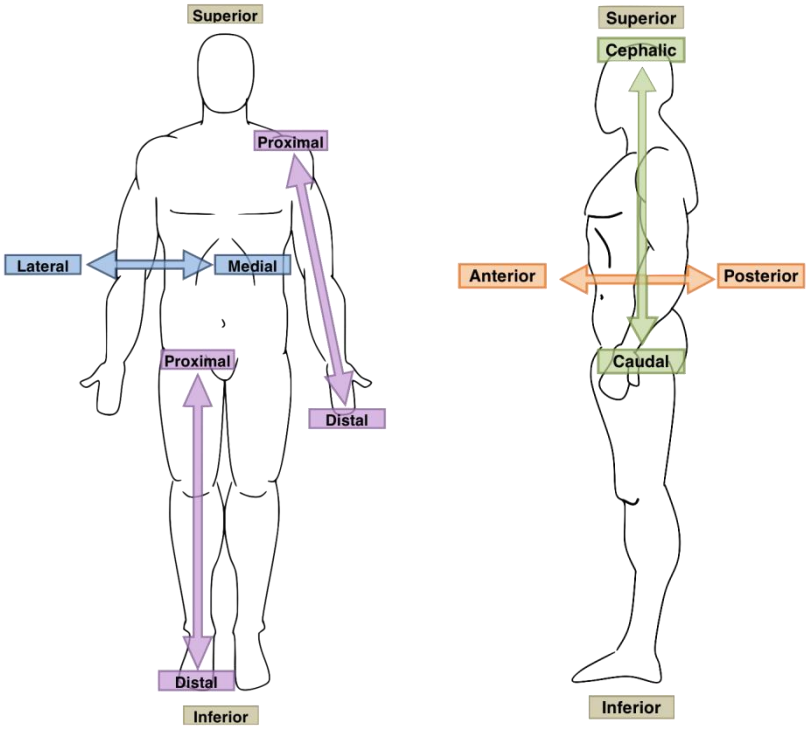

Figure 14. Anatomical directional terminology, reproduced from [56].

The ankle-foot complex consists of three joints: the talocrural joint, which is the principal joint of the ankle complex, the subtalar joint, and the inferior tibiofibular joint. The talocrural joint, located at the interface between the superior portion of the talus and the distal ends of the tibia and fibula, is responsible for plantarflexion (extension of the ankle joint, i.e., rotation of the foot in the direction of the bottom of the foot) and dorsiflexion (flexion of the ankle joint, i.e., rotation of the foot in the direction of the superior surface of the foot). The subtalar, or talocalcaneal, joint occurs between the talus and the calcaneus. The tibiofibular joint is located laterally at the distal end of the tibia and medially at the distal end of the fibula.

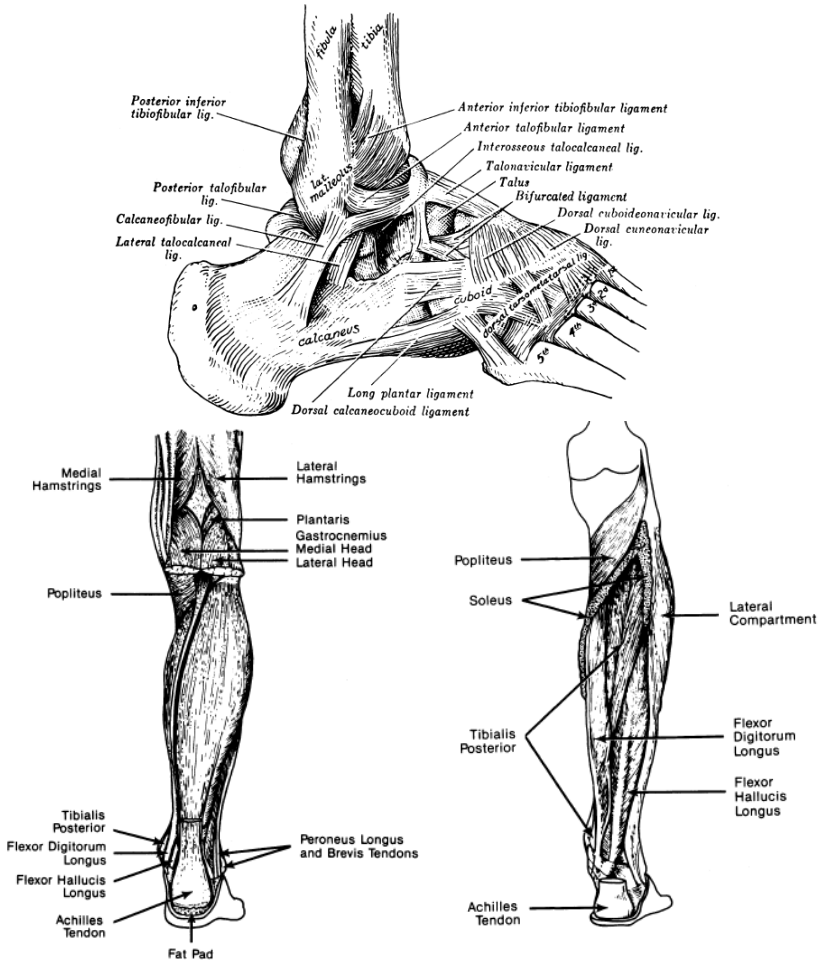

Figure 15. Anatomy of the ankle and shank, reproduced from [57].

The subtalar and tibiofibular joints allow inversion and eversion of the ankle. Typical range of motion for the talocrural joint is 20° dorsiflexion and 50° plantarflexion, and the subtalar joint can achieve roughly 5° eversion (rotation primarily in the coronal plane laterally) and 5° inversion (rotation primarily in the coronal plane medially). The major muscles that enable eversion and plantarflexion of the ankle are the gastrocnemius and the soleus, collectively called the triceps surae, or calf muscle, while the tibialis anterior enables inversion and dorsiflexion.

The knee joint, frequently modeled as a hinge, though it is capable of slight rotation, is a complex synovial joint that comprises several bones and ligaments. Flexion and extension of the knee occur by means of articulation between the femur and the tibia, known as the tibiofemoral joint, and between the femur and the patella, called the patellofemoral joint. The anterior and posterior cruciate ligaments, situated in the intercondylar area between the proximal end of the tibia and distal end of the femur, connect said bones to prevent translation and rotation of the femur relative to the tibia and vice versa.

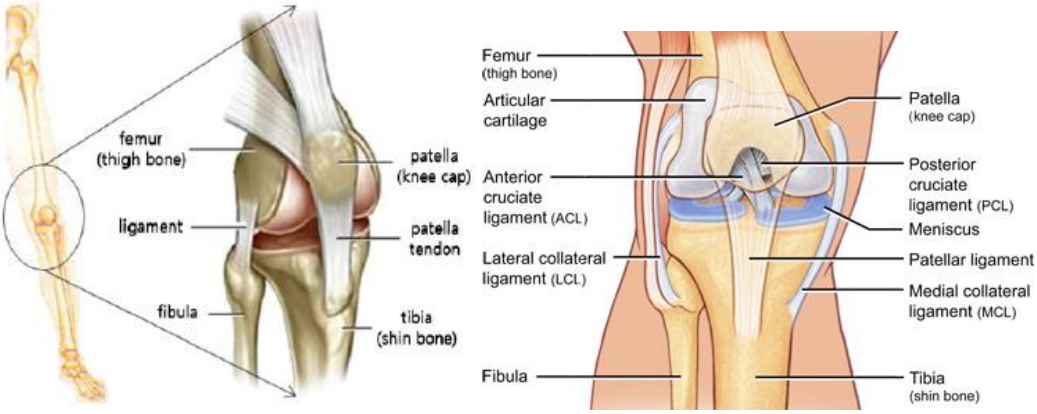

Figure 16. Anatomy of the knee joint, reproduced from [58], [59].

Connecting the medial sides and lateral sides of the ends of the tibia and femur are the medial collateral ligament and the lateral collateral ligament, respectively. These ligaments guard against sagittal displacements of the tibia and femur relative to one another. The patella, or kneecap, connects to the tibia to the quadriceps muscle via the patellar tendon, distally, and the quadriceps tendon, proximally. The knee joint has a range of motion of roughly 0° to 160° of flexion. Musculature in the thigh, which controls flexion and extension and contribute to the dynamic stability of the knee,

comprises several powerful muscles that are among the largest in the body. The biceps femoris, semitendinosus, and semimembranosus, collectively referred to as the hamstrings, are located on the posterior of the thigh and are responsible for flexion of the knee. On the anterior, the vastus lateralis, vastus medialis, vastus intermedius, and rectus femoris—collectively called the quadriceps femoris or, commonly, simply the quadriceps—allow for extension at the knee.

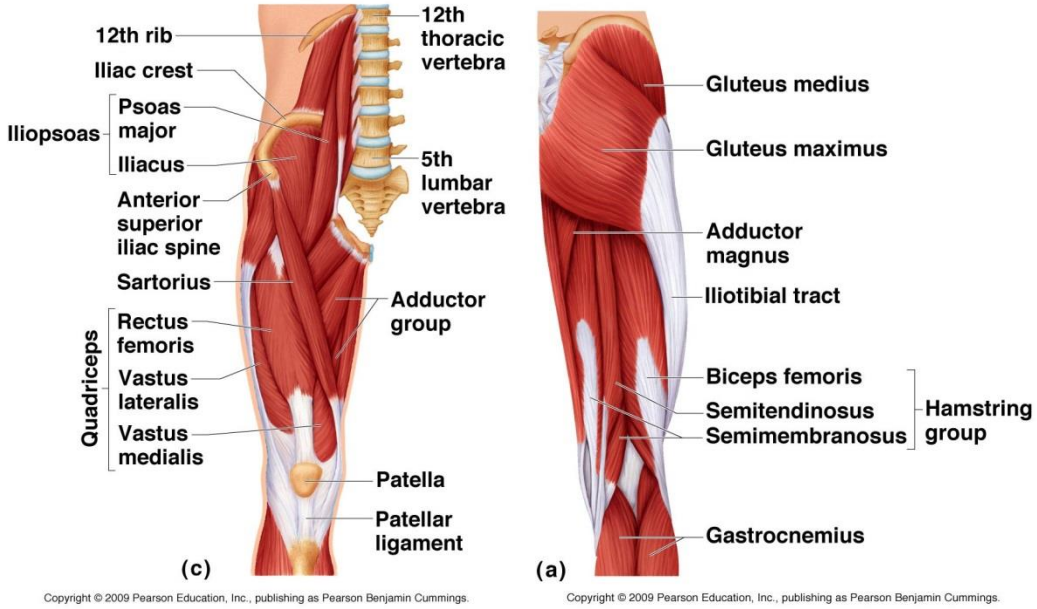

Figure 17. Musculature of the thigh.

During the eccentric, or descending, phase of the squat, the quadriceps act antagonistically to the flexor moment at the knee that results from the action of the hamstrings and the center of mass of the torso and thigh, and during the concentric, or ascending, phase, the quadriceps serve to extend the knee. As for the hamstrings, although one would expect the agonist—the quadriceps and knee extensors—to play the primary role in knee extension during the concentric phase, it turns out that the

hamstrings co-contract with the quadriceps in closed kinetic chain exercises like the squat. It is believed that this co-contraction mediates stability of the knee by counteracting shear forces that the quadriceps exerts on the anterior tibiofemoral joint, ultimately reducing stresses on the ACL.

Finally, we arrive at the hip joint, which is a ball-and-socket joint that functions via articulation of the rounded proximal head of the femur with the acetabulum, a concave cavity in the pelvis. The average range of hip flexion during a typical squatting motion is 95° ± 27°. Hip extension is achieved by contraction mainly of the gluteus maximus and hamstring muscles. During the eccentric phase of the squat, the gluteus maximus acts to stabilize the leg and hip as hip flexion occurs, and during the concentric phase of the squat, it serves as the primary agonist and hip extensor. The hip flexor muscles include the psoas major and iliacus, situated against the anterior of the pelvis. [60].

The joints of the ankle, knee, and hip give each leg six degrees of freedom for a total of twelve degrees of freedom between the two legs, allowing for a wide range of possible squat kinematics. Consequently, the squat can be performed many different ways and under a host of loading conditions, and there exist myriad variations of the squat. The squat may be performed as an athletic exercise or for other functional purposes.

The squat as an athletic exercise is common in fitness regimens, bodybuilding, powerlifting, and for rehabilitation. A standard body weight squat begins by planting the feet roughly shoulder width apart, toes angled slightly outward. The arms may be fully extended anterior to the body and parallel to the ground, or they may be held at the sides,

behind the head, or across the chest. The trunk is then lowered by flexion of the ankles, knees, and hips while maintaining a rigid posture in the spine, then rising to return to the initial position. Additional weight may be added by any of several means, most commonly with a barbell. Barbell back squats are performed by holding the barbell behind the neck against the scapulae, or, more precisely, the musculature of the scapulae—the trapezius muscles and the posterior deltoids—at or just below the horizontal axis formed by the acromion processes of the scapulae. Descent and ascent are then performed as described for standard squats. The barbell can also be placed anterior to the body, in what is termed a barbell front squat. In such a squat, the barbell rests against the clavicle and the anterior deltoids while any of several different grips can be used to stabilize the bar. The remainder of the squat is performed as previously described. Weighted squats can also be performed with dumbbells or kettlebells.

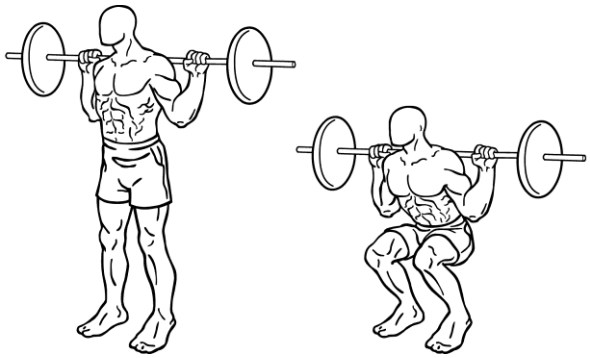

Figure 18. Barbell back squat, reproduced from [61].

In addition to its use as an athletic or rehabilitative exercise, the squatting motion and motions similar to it are employed in activities of daily living. In many parts of the world, individuals may squat above a toilet or latrine while urinating or defecating, and in other cases may squat for hours at a time when performing work on or near the floor, like

eating meals or washing household items or clothing. Some individuals may employ a squatting or squat-like motion for prayer or traditional ceremonies. In many Asian countries, deep or full range of motion squats are common for such activities [12], [13], [62].

Although there is no authoritative or standardized definition of levels of squat depth, squats are generally divided into three categories: partial squats (~45° knee flexion), half squats (~90° knee flexion), and deep squats or full squats (>100° knee flexion). Squats can be further classified by the stance width of the feet. A study by Escamilla, et al., considered the effect of narrow, medium, and wide stance widths on joint kinematics and joint kinetics during the squatting motion in a cohort of competitive powerlifters. Increased magnitudes of knee and hip moments were found in wider stances compared to narrower ones. It has also been suggested, based on electromyographic data, that activity of the ankle plantarflexors, namely the gastrocnemius, is higher with narrow stance widths, and that ankle dorsiflexors are recruited to a higher degree in medium and wide stances [63].

Squats may be performed with the heels up or the heels down. The heels down approach is generally used in the world of exercise, including by bodybuilders and powerlifters. The typical aforementioned “Asian squat” is commonly performed with the heels down for activities of daily living in many Asian and Middle Eastern countries [12]–[15]. It has been found that squatting with the heels up may significantly increase the peak tibiofemoral joint contact force—according to one study, by nearly 40% [62]. Another study, by Toutoungi, et al., suggested that forces in the ACL were nearly four times higher during the descent phase of the squat and nearly two times higher during the

ascent phase when the heels were up versus when they were flat on the ground [64]. Decreased range of motion of the ankle joint and weak ankle dorsiflexor musculature tend to cause individuals to raise the heels while squatting, and have been linked to higher rates of ankle injury and medial knee displacement [65]. These findings indicate that squatting with the heels down may be desirable to reduce forces in the shank and at the knee.

CHAPTER 3. MATERIALS AND METHODS

The aim of this experiment was to collect data on unsupported squatting as well as squatting with two levels of weight support, 20% BW and 35% BW. This was accomplished by having subjects perform squats on a forceplate instrumented treadmill to obtain CoP and GRF data, while infrared (IR) reflective markers placed on the subject's body were tracked by a Vicon (Vicon, Centennial, CO) camera system to obtain kinematic data. Forces and moments at the joints were then characterized by inverse dynamics based on the CoP, GRF, and kinematic data. The experimental results were compared to a simple dynamic model of the squat.

In this experiment, we were primarily concerned with the ascending (concentric) phase of the squat, like numerous other studies have done, as this phase of the squat represents a "worst case scenario" of sorts, as the individual must work against gravity to lift the weight of the body and potentially additional load if lifting an object [66]–[70]. Moreover, with a number of motions, such as the stand-to-sit transition or the lowering of a heavy object, the individual often has the advantage of descending onto a surface such as a chair or of setting a heavy object on the floor, which may not necessarily be the case with the ascending phase of the motion.

For trials with BW support, an apparatus was designed to provide a desired amount of vertical load applied at the hip. The apparatus integrated pneumatic valves, actuators, and load cells using rope, pulleys, and a primarily aluminum frame. The

apparatus interfaced with the subjects by means of a modified rock climbing harness, which the subjects wore while the apparatus applied the vertical load.

The following sections discuss the design of the apparatus, the experimental protocol, and data analysis procedures.

3.1 Design of the Apparatus

Several constraints and requirements were placed upon the design of the apparatus to provide the desired load support. These constraints were as follows:

1) The apparatus had to be able to provide a selectable, consistent, and measurable vertical load.
2) This vertical load had to be applied at the subject's hips through a significant portion of the subject's range of motion over the course of the squat.
3) The apparatus had to be built into or around the existing architecture of the Bertec treadmill and its assorted surrounding components. Among these was an overhead frame that could be fixed to the supports adjacent the treadmill. Due to the extremely sensitive nature of the forceplates, the apparatus could not, in any way, be in contact with the treadmill or the forceplates.
4) The apparatus had to interface with the person in a noninvasive fashion, and in as unobtrusive a manner as possible, so as not to interfere with or affect the person's natural squatting motion and kinematics.
5) The apparatus and system had to be safe enough for a person to use without fear of harm or injury, and safe enough to use without risk of damaging the treadmill or its various components.

Based on these constraints, we designed an apparatus that would utilize pneumatic actuators to apply force via a rope connected to a harness worn by the person. The design

consisted of a pair of pneumatic actuators, one on either side, fixed to a set of 80/20 aluminum extrusions that spanned the width of the Bertec treadmill and sat approximately 1.5 inches above its surface. The end of the cylinder of each pneumatic actuator was secured to a lever arm whose proportions provided a mechanical advantage while maximizing the potential displacement of the rope to achieve the largest possible range of supported motion for the person. Dimensions and angles of the components of the apparatus were chosen based on the outputs of a custom optimization routine in Matlab (MathWorks, Natick, MA). The lever arm's proportions provided a mechanical advantage of 2.4375; this dimension was based on the limitations of the CNC machine, vis-à-vis length of material, used to fabricate the components.

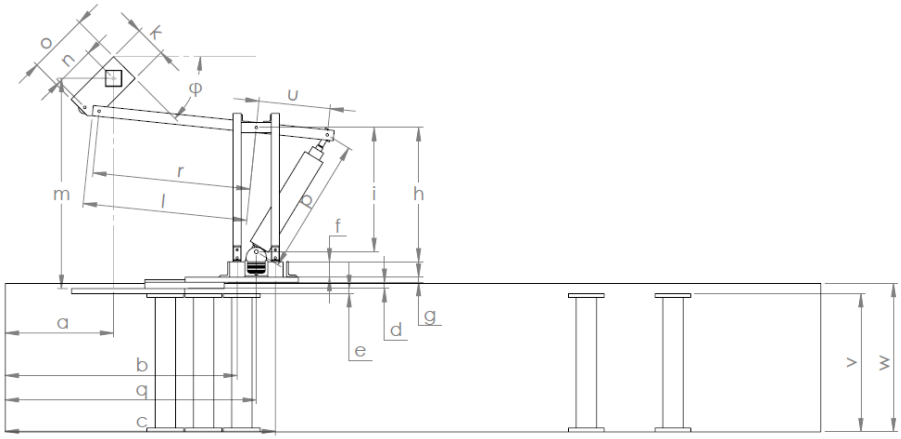

Figure 19. Early CAD drawing of the actuator portion of the apparatus, displaying a number of known (i.e., fixed) and variable dimensions. The values for variable dimensions were chosen based on the results of a Matlab optimization script to maximize the displacement of the rope end of the lever arm.

The short end of the lever arm was attached to the end of the piston of the pneumatic actuator by means of a machined clevis piece. Rope was tied to the long end of the lever arm. The height of the lever arm pivot point and the dimensions of the lever arm were

selected to maximize the arc length that could be achieved based on 6 in of stroke at the piston end. This translated to roughly 18 in of vertical displacement at the harness end of the rope, sufficient to provide support through most or all of the squatting motion, depending on the subject's height and leg segment lengths. One end of the rope was connected to the far end of the lever arm, and the other end was attached to the harness. The rope was routed through a pulley attached to the overhead frame, then down to the harness and person. Angled pulley blocks were added to the design, and the rope on either side routed through them, after it was found that they would increase the maximum possible displacement of the rope through the range of pneumatic cylinder stroke.

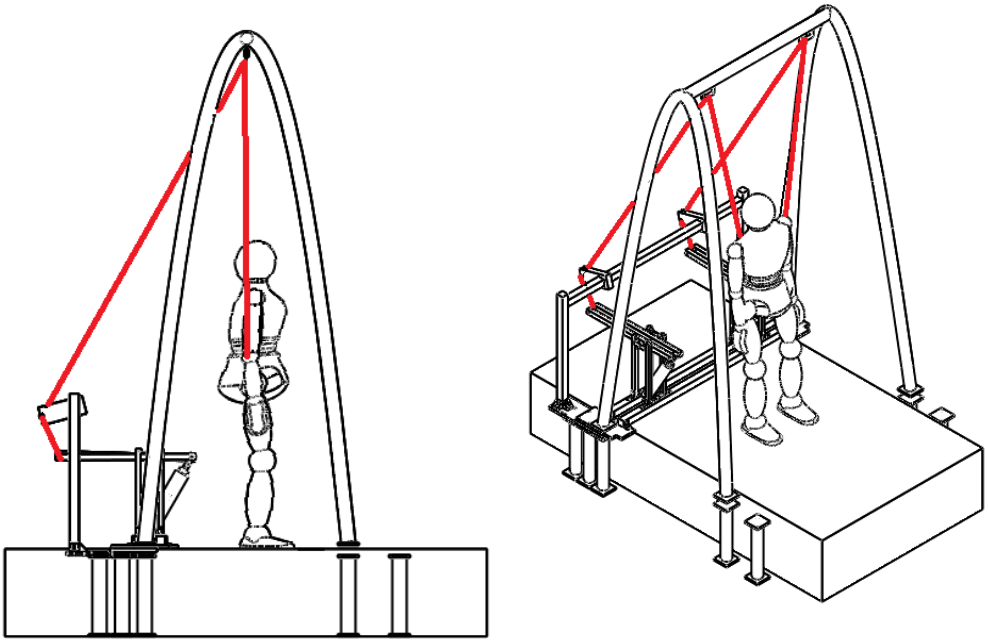

Figure 20. Diagram of the apparatus on the treadmill. Each pneumatic actuator, attached by a shaft and bearings to its lever arm, causes the lever arm to turn about the pivot point when the piston extends. This exerts tension in the rope, which is shown in red, causing displacement of the rope and applying a vertical force to the user.

Enfield pneumatic actuators and Enfield pneumatic valves (Enfield Technologies, Shelton, CT) were used to provide force. A steady supply of air at a pressure of approximately 80 psig was available. The amount of force a pneumatic actuator can deliver is based on the characteristics of the valve and the actuator. The outlet pressure of the valve depends on a number of variables. For choked flow—when the ratio of the outlet pressure to the inlet pressure is less than the critical pressure ratio, and critical pressure ratio depends on the fluid and the characteristics of the valve—the mass flow rate can be approximated with the following equation:

$$Q = p_{in} C \rho_0 \sqrt{\frac{T_{out}}{T_{in}}} \quad , \quad \text{for} \quad \frac{p_{out}}{p_{in}} \leq b \tag{1}$$

where Q is the mass flow rate in kg/s, p_{in} is the pressure upstream of the inlet in Pa, p_{out} is the pressure downstream of the outlet in Pa, C is the sonic conductance of the fluid in $m^3/s \cdot Pa$, ρ_0 is the density of air in kg/m^3, T_{out} is the fluid temperature downstream of the outlet in K, T_{in} is the fluid temperature upstream of the inlet in K, and b is the critical pressure ratio [71]. The pneumatic actuator, a double acting cylinder, had a bore diameter of 2.00 in and a piston rod diameter of 0.5 in. The available pressure of 80 psig was well below the actuator's maximum pressure limit of 250 psig. The inlet pressure and force provided for both piston instroke and outstroke are related by the effective area as follows:

$$F_{outstroke} = P \frac{\pi d^2}{4} \tag{2}$$

$$F_{instroke} = P \frac{\pi}{4} (d_1^2 - d_2^2) \tag{3}$$

where P is the pressure on the piston, d and d_1 are the diameter of the piston, and d_2 is the diameter of the piston rod. Based on these, at the maximum flow rate and assuming miniscule pressure drop across the valve from the upstream 80 psig, each piston could theoretically provide up to 251 lbs of force on an outstroke and up to 236 lbs on an instroke. Considering only the relevant piston motion, i.e., the outstroke, approximately 500 lbs of axial force could be provided between two pneumatic actuators. Although the actual tension in the rope would vary with the mechanical advantage of the lever arms, the angle of the piston to the lever arms, and the angle of the ropes to the lever arms, the magnitude of force made these actuators suitable for the task. The rope, which was to be attached at one end to the lever arm and at the other end to the load cells and harness, was tested in an Instron (Instron, Norwood, MA) device to ensure it would suffice under relatively high tensile load. Its force-strain curve may be found in Appendix A.

The combination of valves and actuators was chosen due to the high level of controllability they conferred upon the system and the apparatus. The pneumatic actuators were equipped with potentiometers that provided position feedback, allowing for accurate and precise position control of each actuator. Similarly, the load cells provided force feedback regarding tension in the rope, allowing for force control. The valves, each of which was controlled independently and possessed a frequency response of 110 Hz, were able to achieve accurate and precise position control, demonstrated by their success in tracking a position-based sine curve at high frequencies relative to the frequency of the squatting motion. The valves were able to achieve accurate and precise force control, as indicated by tension in the rope measured by the load cells, when the ropes were tied to a static load such as a 45 lb weight plate.

A CAD model of the apparatus and its components was created in SolidWorks (Dassault Systèmes). Stress analysis was performed on the components, based on the aforementioned expected potential loads, with the aid of the finite element stress analysis feature in the SolidWorks software (see Appendix A). The frame of the apparatus was machined and fabricated primarily from 80/20 slotted aluminum extrusions and lengths of square aluminum tubing. Steel shafts, bearings, and thrust washers at the pivot points of the lever arms ensured smooth, relatively frictionless rotation of the components. The components of the frame of the apparatus were fixed above the treadmill via machined adapter plates attached to the support struts on the sides of the treadmill, guaranteeing that the apparatus would, at no point, touch the treadmill. On either side, a Futek LSB-302 load cell (FUTEK, Irvine, CA) was placed in series between the rope end of the lever arm and the harness. These load cells had a working limit of 300 pounds. Extension springs from Century Spring Corp. (Century Spring Corp., Los Angeles, CA) with k = 34 lbs/in and initial length of 6.5 in were placed in series between the load cell and harness; it was found that the addition of springs stabilized the transient response of the system during the initial application of load.

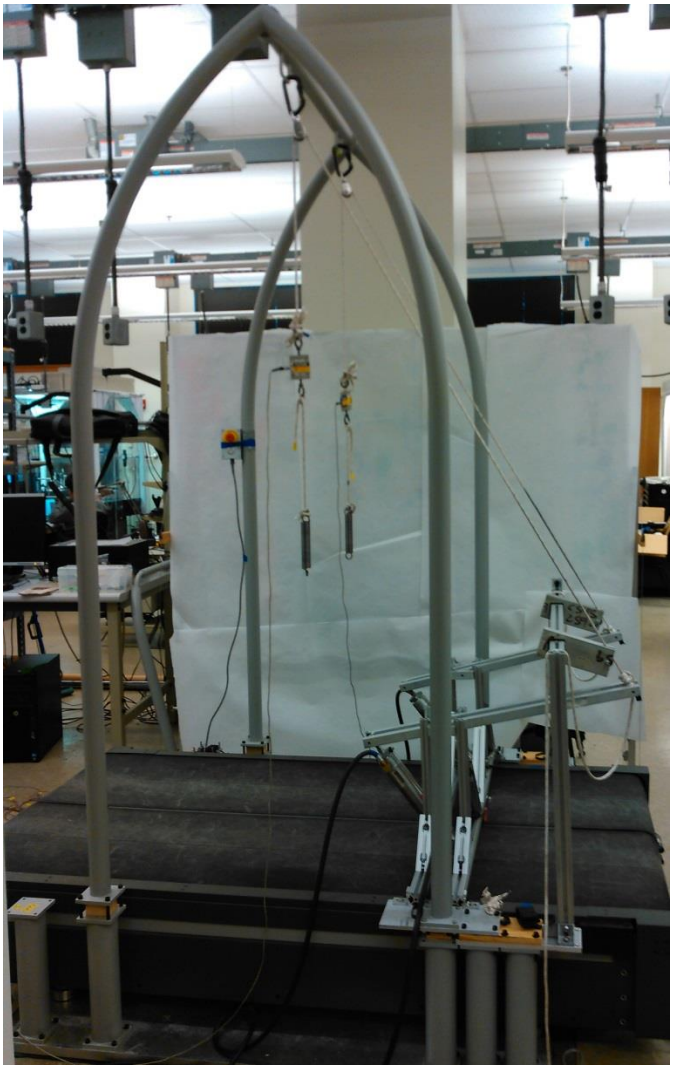

Figure 21. The pneumatic actuators, built into the aluminum frame of the apparatus, and the ropes.

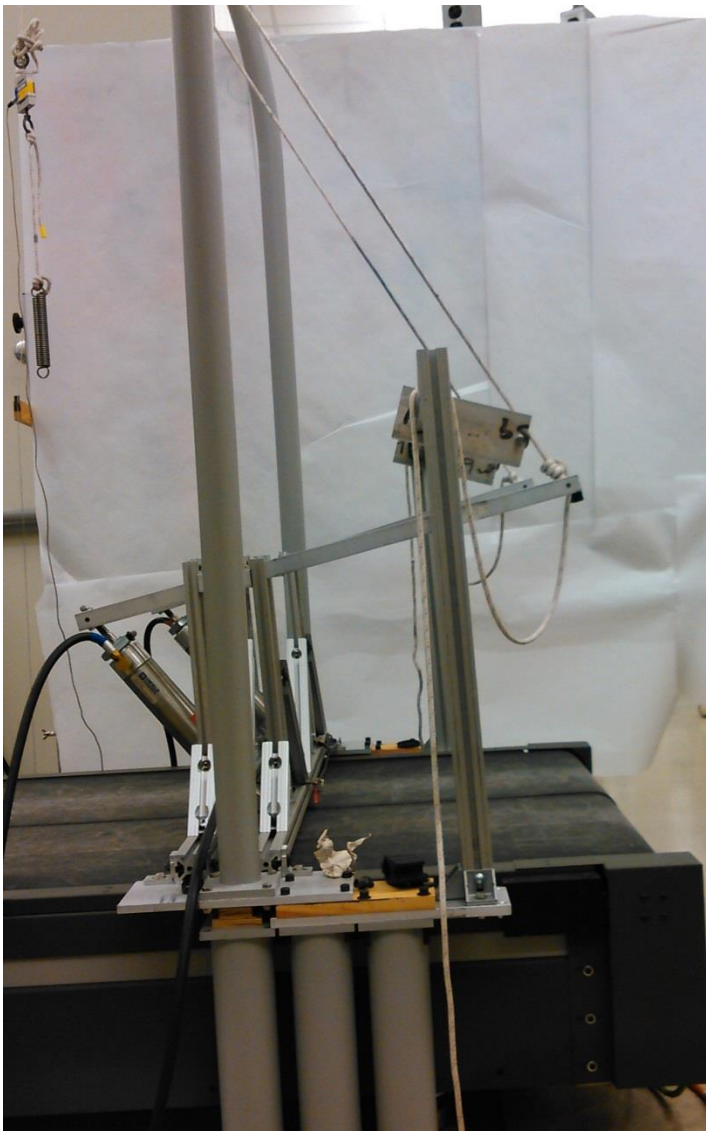

Figure 21. Continued.

Several options for harnessing were available, including a modified rock climbing harness, a modified hip orthotic, and a modified bicycle seat. Ultimately, the rock climbing harness was chosen because it was soft and, unlike rigid harnesses, did not significantly artificially constrain the wearer's movement.

Figure 22. The standard rock climbing harness, on the left, and the modified harness attached to the apparatus, on the right.

The commercially available rock climbing harness was modified by sewing additional straps into it, and by sewing segments of elastic material into the thigh straps to provide better fit, comfort, and stability for the user. The additional straps served to secure the harness on the user even when load was applied by the apparatus. On either side, a metal buckle was incorporated to allow attachment of the harness to the apparatus by means of the spring and rope. The harness itself weighed approximately 0.68 kg (1.5 pounds).

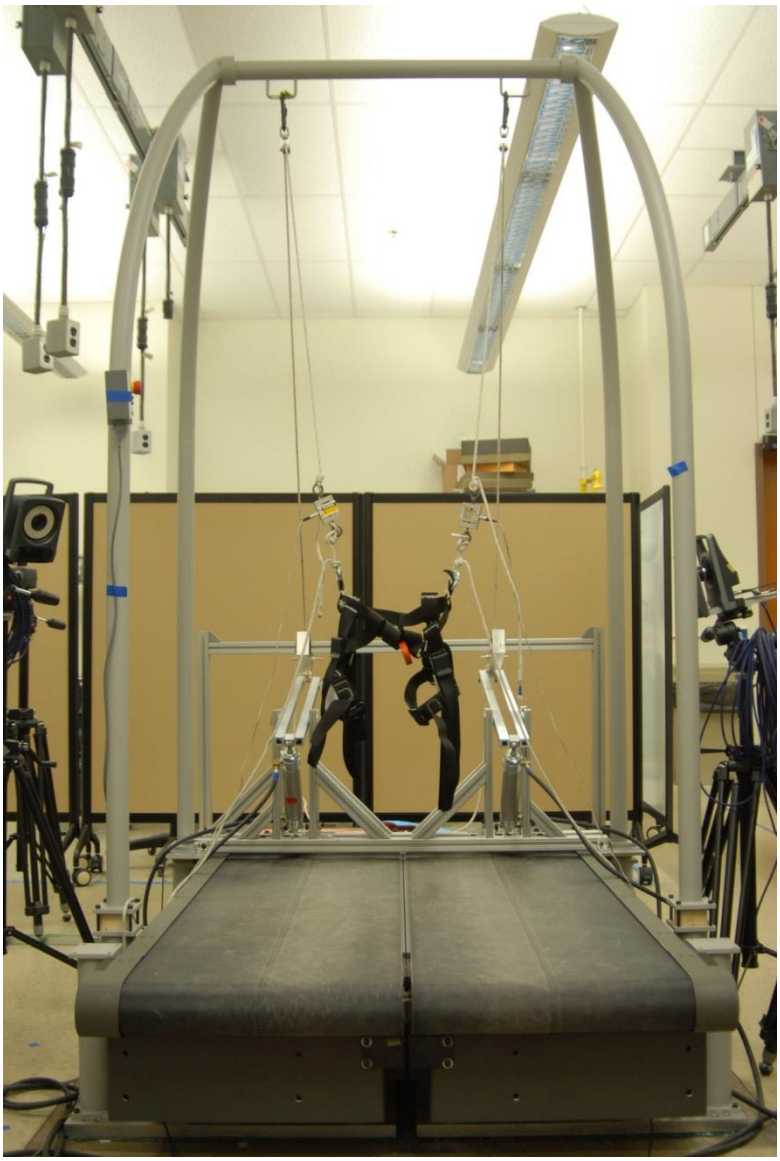

Figure 23. The experimental setup.

The outputs and/or inputs of the pneumatic valves, pneumatic actuators, and load cells were run to a National Instruments (National Instruments, Austin, TX) compact RIO (cRIO) module. Real-time control of the system was accomplished via PD controller in a custom LabVIEW program (see Appendix B). Load cell and piston stroke data for the load cells and pistons was logged and exported by the LabVIEW program. This overall

setup, with a vertically hanging rope connected to a harness above an instrumented treadmill, was similar to setups used in other studies. The major advantage of the apparatus we have developed and manufactured lies in its use of two independently controlled pneumatic actuators. This feature confers some flexibility in the potential applications of the apparatus. Because each side is controlled independently of the other, future experiments could utilize the same apparatus, or a slightly modified version, to study the effect of variable and alternately applied force during squatting or during locomotion. By attaching one side to one limb and the other side to the other limb, force could be applied to or removed from each leg as desired based on the phases of the gait cycle.

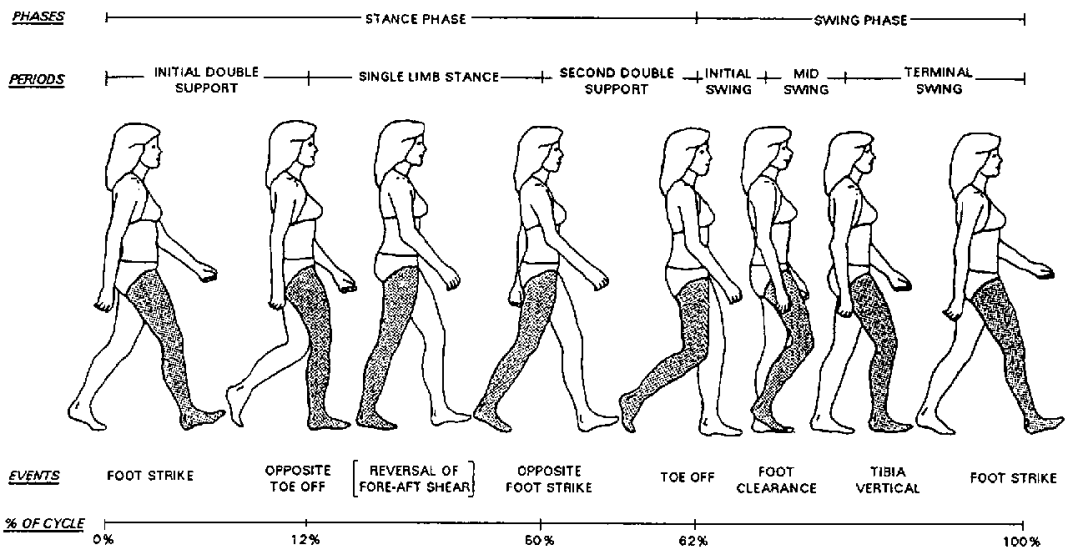

Figure 24. The gait cycle; reproduced from [72].

For instance, force could be applied at or just before the beginning of the swing phase to assist in accelerating the leg, then removed upon heel strike and transition to stance

phase. Such a control scheme would closely mimic the selectively applied, variable, bilaterally independent forces applied by a number of exoskeletons and assistive or augmentative devices.

3.2 Data Collection and Trial Protocol

Kinematic data was obtained by means of six Vicon motion capture cameras, which tracked the positions of infrared markers attached to the subject's body. Twenty markers were placed on the body according to a modified version of the Helen Hayes marker set.

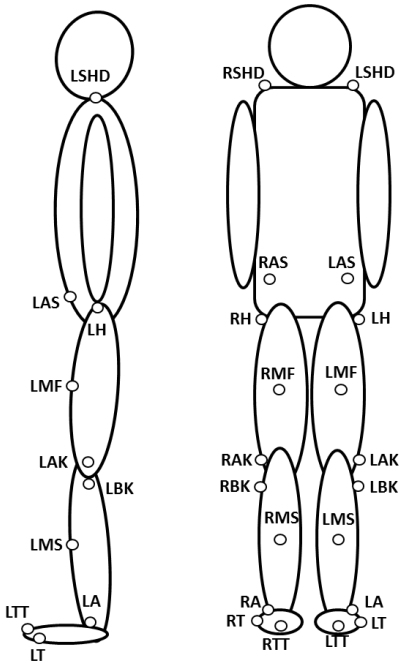

Figure 25. Marker placement.

where the markers are as follows:

LT/RT: Base of the left/right pinky toe.

LTT/RTT: Base of the left/right third (middle) toe.

LA/RA: Left/right ankle, on the lateral malleolus.

LMS/RMS: Left/right mid-shank, on the anterior part of the tibia.

LBK/RBK: Left/right below knee.

LAK/RAK: Left/right above knee.

LMF/RMF: Left/right mid-femur.

LH/RH: Left/right hip, at the greater trochanter.

LAS/RAS: Left/right anterior superior iliac spine (ASIS).

LSHD/RSHD: Left/right shoulder, atop the acromion.

GRF data and information on the center of pressure were obtained from the Bertec instrumented treadmill (Bertec, Columbus, OH), which contained two separate three-axis forceplates.

Eight subjects were recruited for the study, 5 male and 3 female, with an average age of 25.1 ± 1.7 years (mean ± SD), an average body mass of 66.8 ± 8.9 kg (mean ± SD), and an average height of 170.8 ± 6.6 cm (mean ± SD). Inclusion criteria for the study required that subjects be healthy, at least moderately fit adults physically able to perform consecutive squats, aged 18 to 35, with no musculoskeletal or neurological impairments that would prevent them from squatting. Participants in the study were neither excluded nor selected on the basis of sex or ethnic background.

Before the start of the session, subjects were outfitted with IR markers as described above. Before beginning any trials, they were given the opportunity to warm up by squatting several times. The first part of the experiment involved squatting without load support. During this part, subjects were asked to perform 3 sets of 3 to 5 squats, unharnessed, on the instrumented treadmill while the Vicon cameras captured kinematic data. To perform each squat, the subjects were instructed to stand with their feet roughly shoulder width apart, toes angled outward at an abduction angle of approximately 20°,

and their arms held fully extended anterior to their body and parallel to the ground. Having subjects position their arms this way prevented the hip markers from being obscured. The subjects were then instructed to squat, keeping their heels down, descending until their thighs were roughly parallel to the ground, then slowly ascending until returning to the initial standing position. Subjects were given the opportunity to rest for up to 3 minutes between each set, if needed. The second part of the experiment involved squatting with load support. Subjects donned the harness, then performed 3 sets of 3 to 5 squats as for the previous part while the apparatus applied a vertical load during the rising phase of the squat. The load was applied and removed gradually, which may reduce discomfort in the user by avoiding jerking motions and impulsive forces, and may avoid unnatural or awkward movements by the user. This ramp up and ramp down was consistent with previous studies that provided BW support via pneumatic actuation, which applied and removed load gradually [73], [74]. Two levels of load support (maximum applied force) were chosen: 20% of the subject's body weight and 35% of the subject's body weight. Subjects were instructed to adopt the fully flexed squatting position prior to the application of load support. The pneumatic actuators were then cued to begin applying gradually increasing load support.

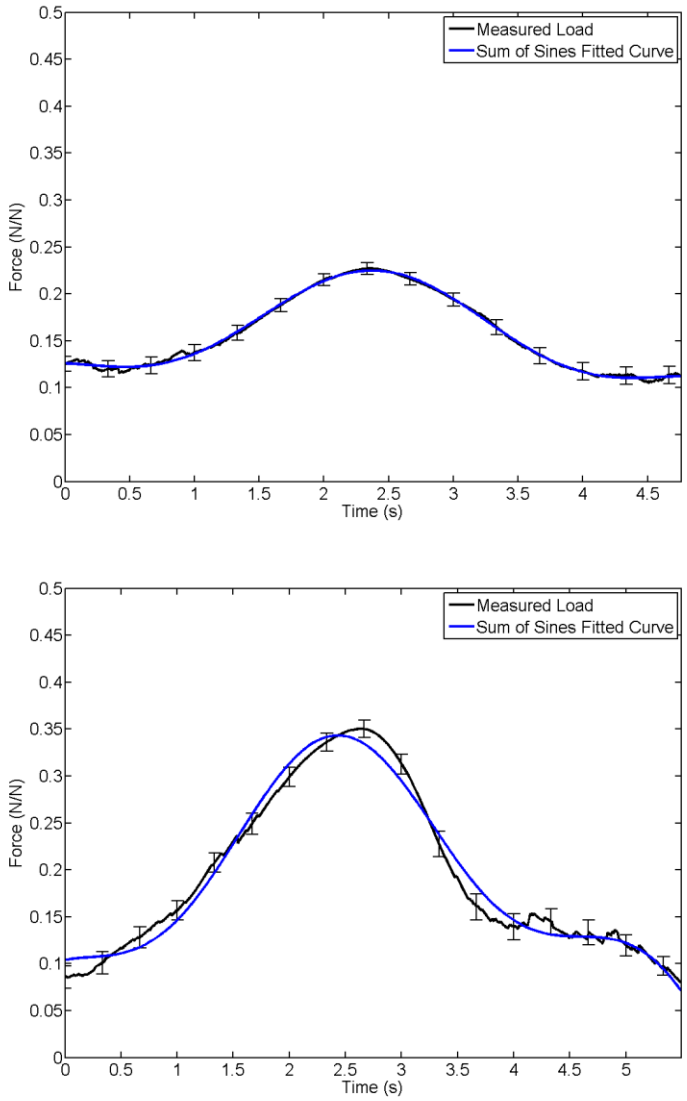

Figure 26. The mean measured applied load for the 20% BWS case (top) and 35% BWS case (bottom) plotted alongside a sum of sines curve fitted to the actual measured load, obtained from Matlab's curve fitting tool function. Load has been normalized to BW. The corresponding equations for the fitted curves are $F_{20}(t) = 0.192\sin(0.395t + 0.67) - 0.033\sin(2.06t - 0.21)$ for the 20% BWS case and $F_{35}(t) = 0.284\sin(0.510t + 0.298) + 0.06\sin(2.1t + 2.784)$ for the 35% BWS case.

The subjects were instructed to wait until the applied load was near the target maximum value, which was indicated to them by a color-changing indicator on a nearby computer monitor, before beginning to ascend. The apparatus stopped applying load support after

the piston stroke length passed a predetermined stroke length limit, which was implemented to prevent the lever arms of the apparatus from striking the surface of the treadmill. The length of the vertically hanging segment of the rope, to which the user was attached, was adjusted based on subject height such that the force control would be switched off roughly when the subject had completed the squat and achieved the standing position. Parameters, such as the time between subsequent squats and the PD controller gains were adjusted as necessary based on verbal feedback from the subjects, to allow them to squat in a manner that felt natural to them. The average time to ramp up to the maximum level of load support was approximately 2.36 s at the 20% BWS level and approximately 2.64 s at the 35% BWS level. The subjects performed 3 sets of 3 to 5 squats at the first level of load support, then 3 sets of 3 to 5 squats at the second level of load support, with up to 3 minutes of rest between sets if necessary.

Although subjects were instructed to begin squatting once the apparatus had ramped up to the target load support (and received visual feedback in the form of an indicator), subjects tended to begin the ascent, on average, when the applied load reached 12.3% ± 9% BW (mean ± SD) at the 20% BWS level, and 14.1% ± 10% BW (mean ± SD) at the 35% BWS level. On average, when the subjects completed the motion and achieved the standing position, the applied load was 10.8% ± 7.2% BW (mean ± SD) at the 20% BWS level, and 9.9% ± 9.2% BW (mean ± SD) at the 35% BWS level. As a result of these differences, the applied load profile over the course of the actual squatting motion was fairly constant at the 20% BWS level, but somewhat more sinusoidal at the 35% BWS level (see Figure 27).

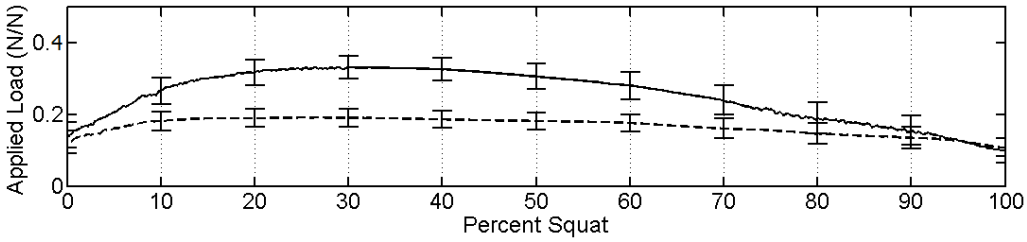

Figure 27. Applied load profile for the experimental data at the 20% BWS level (dashed line) and the 35% BWS level (solid line). Applied load has been normalized to BW. Time series over the course of the squatting motion has been normalized to percent squat phase based on the knee joint angles (see Section 3.4).

At the conclusion of the experiment, subjects were asked to complete a qualitative questionnaire regarding the experience and the harness (please see Appendix J for a copy of the questionnaire).

3.3 Data Processing and Analysis

The Vicon camera data and Bertec forceplate GRF data were captured and synchronized by a Vicon analog-digital converter, then reconstructed and labeled in the Vicon Nexus software. Forceplate GRF data was downsampled from 1200 Hz to 120 Hz to match the sample rate of the Vicon camera data. A fourth order, zero phase shift, lowpass Butterworth filter with a cutoff frequency of 3 Hz was applied to the Vicon data. A second order, zero phase shift, lowpass Butterworth filter with a cutoff frequency of 1 Hz was applied to the load cell data recorded by the LabVIEW VI. The low frequency of the squatting motion relative to activities such as walking, running, and jumping necessitated the use of low cutoff frequencies. The load cell data was synchronized with the forceplate and marker data by placing markers on one of the pneumatic actuators during the trials. By attaching one marker to any point on the cylinder and another marker to a point on the piston rod, the piston stroke, or the change and the rate of change of the piston stroke, could be compared against the piston stroke data recorded by the LabVIEW VI from the potentiometers in the pneumatic actuators.

An inverse dynamic approach was employed to compute joint reaction forces and moments. The inverse dynamic link-segment model makes several key assumptions: that the joints are frictionless, that body segments are rigid, that the mass of each body segment is concentrated at its center of mass, and that drag and air friction are negligible.

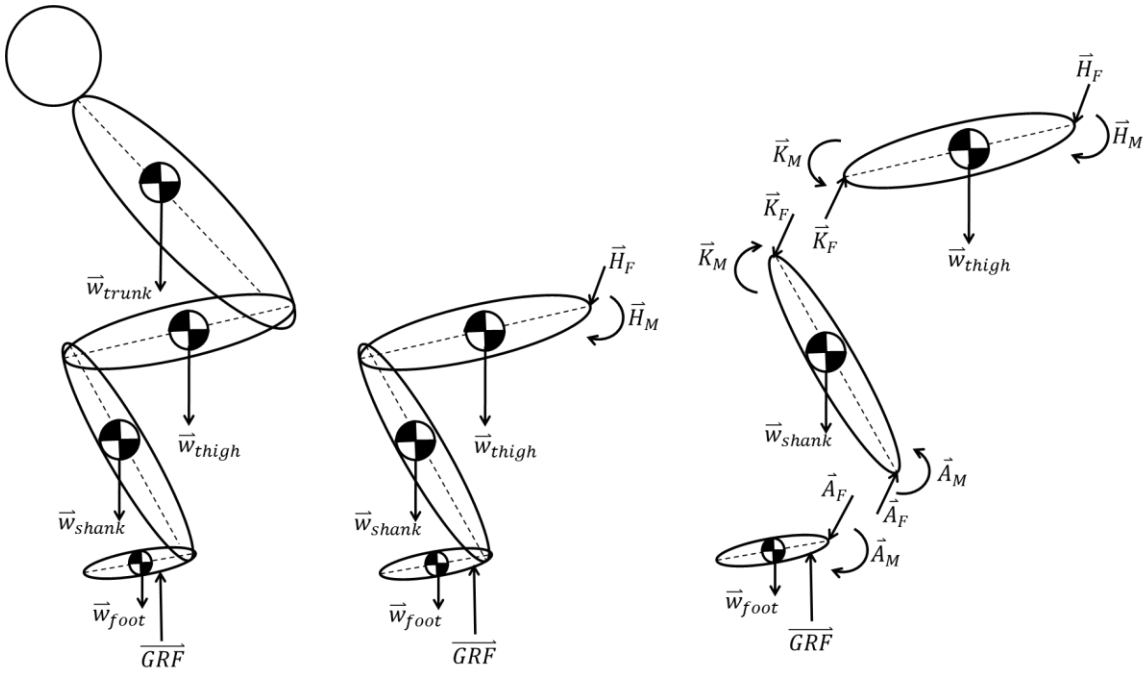

Figure 28. The inverse dynamic link-segment model. The figure on the left depicts the entire system, i.e., the whole person, with the weight of each segment counterbalanced by the ground reaction force. The figure in the center sections this free body diagram at the trunk and considers only the lower limbs, exposing the internal forces and moments of reaction at the hip. The figure on the right sections the lower limbs into the respective segments, exposing the internal forces and moments of reaction at each joint.

The dynamics of the system can be determined by deriving the Newton-Euler equations for each segment, then solving for the joint reactions. In this way, the reaction forces and moments at each joint can be back calculated from the GRF and the CoP at which said force acts. Free body diagrams and the sets of Newton-Euler vector equations for a three-dimensional inverse dynamic analysis are illustrated below.

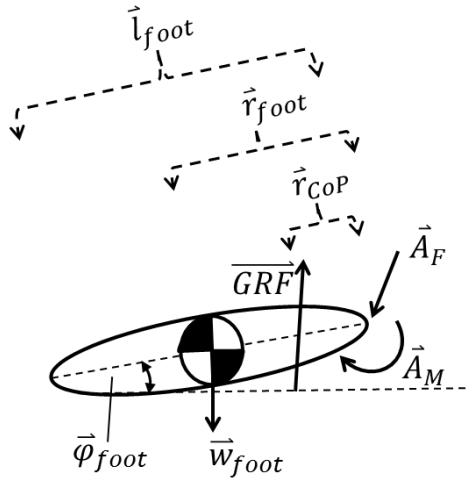

Figure 29. Link segment model FBD of the foot.

The Newton-Euler equations for the foot are as follows:

$$\sum \vec{F}_{foot} = m_{foot}\vec{a}_{foot} = \overrightarrow{GRF} + \vec{w}_{foot} - \vec{A}_F \tag{4}$$

$$\sum \vec{M}_{/A} = I_{foot}\ddot{\vec{\varphi}}_{foot} = \left(\vec{r}_{foot} \times \vec{w}_{foot}\right) + \left(\vec{r}_{CoP} \times \overrightarrow{GRF}\right) - \vec{A}_M \tag{5}$$

where:

$\vec{A}_F$ = reaction force at the ankle joint
$\vec{a}_{foot}$ = acceleration of center of mass of foot
$\vec{A}_M$ = ankle joint reaction moment
$\overrightarrow{GRF}$ = ground reaction force
I_{foot} = mass moment of inertia of the foot
$\vec{l}_{foot}$ = position vector from ankle to end of foot
m_{foot} = mass of the foot
$\vec{r}_{foot}$ = position vector from ankle to center of mass of foot
$\vec{r}_{CoP}$ = position vector from ankle to center of pressure
$\vec{w}_{foot}$ = weight of the foot
$\vec{\varphi}_{foot}$ = angle of foot with respect to the horizontal
$\ddot{\vec{\varphi}}_{foot}$ = angular acceleration of the foot

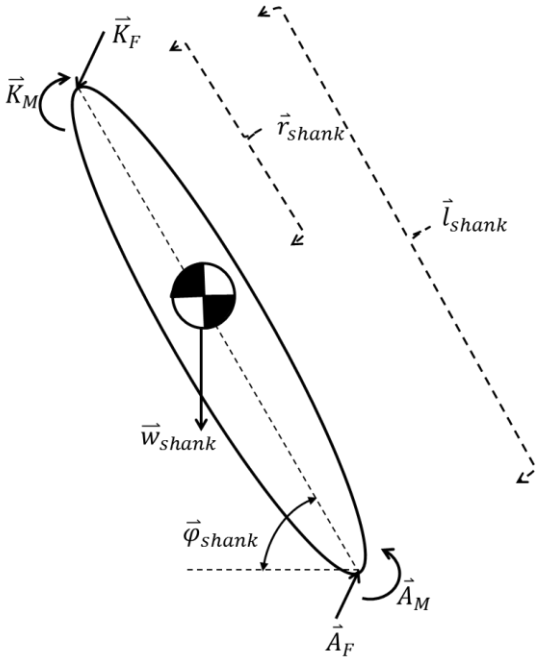

Figure 30. Link segment model FBD of the shank.

The Newton-Euler equations for the shank are:

$$\sum \vec{F}_{shank} = m_{shank}\vec{a}_{shank} = \vec{A}_F + \vec{w}_{shank} - \vec{K}_F \tag{6}$$

$$\sum \vec{M}_{/K} = I_{shank}\ddot{\vec{\varphi}}_{shank} = \vec{A}_M + (\vec{r}_{shank} \times \vec{w}_{shank}) + \left(\vec{l}_{shank} \times \vec{A}_F\right) - \vec{K}_M \tag{7}$$

where:

$\vec{A}_F$ = reaction force at the ankle joint
$\vec{a}_{shank}$ = acceleration of the center of mass of the shank
$\vec{A}_M$ = reaction moment at the ankle joint
I_{shank} = mass moment of inertia of the shank
$\vec{K}_F$ = reaction force at the knee joint
$\vec{K}_M$ = reaction moment at the knee joint
$\vec{l}_{shank}$ = position vector from knee to ankle
m_{shank} = mass of the shank
$\vec{r}_{shank}$ = position vector from knee to center of mass of shank
$\vec{w}_{shank}$ = weight of the shank
$\vec{\varphi}_{shank}$ = angle of shank with respect to the horizontal
$\ddot{\vec{\varphi}}_{shank}$ = angular acceleration of the shank

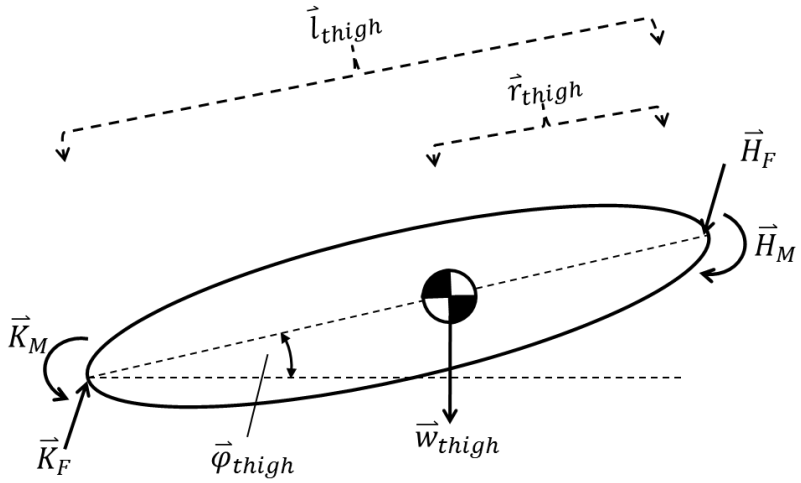

Figure 31. Link segment model FBD of the thigh.

The Newton-Euler equations of motion for the thigh are:

$$\sum \vec{F}_{thigh} = m_{thigh}\vec{a}_{thigh} = \vec{K}_F + \vec{w}_{thigh} - \vec{H}_F \tag{8}$$

$$\sum \vec{M}_{/H} = I_{thigh}\ddot{\vec{\varphi}}_{thigh} = \vec{K}_M + \left(\vec{r}_{thigh} \times \vec{w}_{thigh}\right) + \left(\vec{l}_{thigh} \times \vec{K}_F\right) - \vec{H}_M \tag{9}$$

where:

$\vec{a}_{thigh}$ = acceleration of the center of mass of the thigh
$\vec{H}_F$ = reaction force at the hip joint
$\vec{H}_M$ = reaction moment at the hip joint
I_{thigh} = mass moment of inertia of the thigh
$\vec{K}_F$ = reaction force at the knee joint
$\vec{K}_M$ = reaction moment at the knee joint
$\vec{l}_{thigh}$ = position vector from hip to knee
m_{thigh} = mass of the thigh
$\vec{r}_{thigh}$ = position vector from hip to center of mass of thigh
$\vec{w}_{thigh}$ = weight of the thigh
$\vec{\varphi}_{thigh}$ = angle of thigh with respect to the horizontal
$\ddot{\vec{\varphi}}_{thigh}$ = angular acceleration of the thigh

The lengths of limb segments were measured directly from the IR markers placed on the body. The locations of the centers of mass of each limb segment, the relative weight or mass of each segment, and the mass moments of inertia (calculated from the segment radii of gyration) were obtained from previous studies on body segment parameters [75]. These body segment parameters may be found in Table 7 in Appendix A.

The various joint angles, GRF, and CoP were obtained from the kinematic marker data and forceplate data. Linear and angular accelerations were computed by two forward-difference numerical differentiations of the kinematic data. The remaining joint reactions were computed as illustrated in the figures above. Because the subjects were told to maintain a relatively narrow stance, most of the relevant motion occurred in the sagittal plane. Thus, a bilateral two-dimensional analysis was conducted instead of a three-dimensional analysis by considering only those relevant terms in the sagittal plane and moments about the transverse axis.

The literature shows that a two-dimensional analysis produces results relatively similar to three-dimensional analysis for a narrow-stance squat, which was the stance subjects in this study were instructed to adopt [63]. A two-dimensional analysis presupposes that most of the relevant kinetic phenomena occur in the two-dimensional plane of interest—the sagittal plane. Prior studies have found that peak coronal plane moments during the squat are significantly lower than sagittal plane moments, according to one study by a factor of up to 86% [76]. One simple way to evaluate the potential kinetic effects in other planes is to consider the components of the GRF along the sagittal and transverse axes relative to the longitudinal (vertical) component of the GRF. Examination of the average components of the GRF along the various axes in the current

experiment were consistent with previous studies (please see Appendix D for GRF component data), and supported the validity of a two-dimensional analysis.

It should be noted that the use of inverse dynamic analysis in biomechanics is not without its limitations, one being that, although it allows calculation of total joint reaction moments, it reveals nothing about the contraction or co-contraction of the agonistic and antagonistic muscle groups in any given limb segment—it only tells us the net reaction moment. A comprehensive analysis of muscle activity at and around the joints would require additional tools to gather such information, like electromyography. Such an analysis was not the aim of the current study, which sought to characterize the net impact of load support on magnitudes and profiles of forces and moments in the lower limbs.

From the net reaction force acting at each joint, the shear and compressive forces in the limb segments were computed by resolving the force into its parallel and perpendicular components along the longitudinal axis of the segment [77].

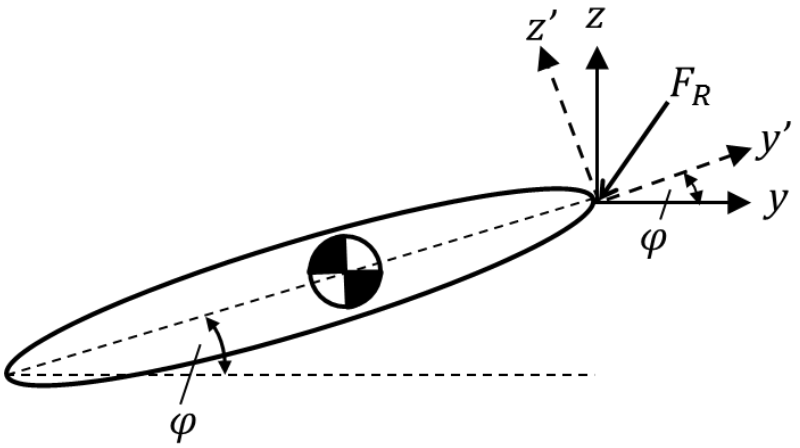

Figure 32. Coordinate transformation from the space-fixed xyz laboratory coordinate system to the segment-fixed x'y'z' coordinate system, where φ is the angle that the segment makes with the horizontal (i.e., with the xy plane) and F_R is the net reaction force at the proximal joint, with its components known in the xyz coordinate system.

This can be accomplished by a coordinate transformation of the reaction force for a given joint and limb segment from the space-fixed xyz-coordinate system to the limb-fixed x'y'z'-coordinate system for each limb segment, where y' lies along the longitudinal axis of the limb segment and z' is aligned perpendicular to it. The component of the reaction along each of these axes then represents the axial (compressive) and shear forces, respectively. This may be done by premultiplying the space-fixed coordinates by the appropriate rotation matrix for a rotation about the x axis, where $x = x'$.

$$\vec{X}' = R\vec{X} \tag{10}$$

The terms in Equation (10) may be written in their full form, which is:

$$\begin{pmatrix} x' \\ y' \\ z' \end{pmatrix} = \begin{bmatrix} 1 & 0 & 0 \\ 0 & \cos\varphi & \sin\varphi \\ 0 & -\sin\varphi & \cos\varphi \end{bmatrix} \begin{pmatrix} x \\ y \\ z \end{pmatrix} \tag{11}$$

From the moments acting at the joints and the angular velocities of the segments, mechanical power at the joints was computed based on the following equation:

$$P = \tau \cdot \omega \tag{12}$$

where P is the mechanical power, τ is the joint torque (moment), and ω is the angular velocity of the segment.

Differences between the three levels of load support (unsupported, 20%, and 35%) for the computed metrics were quantified by two-way, repeated measures ANOVA and post-hoc paired t-tests. Data are plotted as mean ± SEM, based on the number of subjects (8), unless noted otherwise.

All computations were performed using custom scripts in Matlab. Statistical calculations were performed in Matlab using functions from the Statistics and Machine Learning Toolbox.

3.4 Normalization of Results

Although the procedure encouraged subjects to squat in relatively consistent patterns, there tended to be slight differences in preferred squatting speed and squatting kinematics from subject to subject. To allow for direct comparisons, the activity is generally normalized by temporal or kinematic parameters. The former is accomplished by normalizing based on the beginning and end of the activity [67], [78]. Normalizing by kinematic parameters usually relies on measures such as joint angles or, as in one study on lifting, the height of the knee above the ground [68], [79]. For this experiment, the latter was performed, normalizing squats based on knee joint angle to a "percent squat phase," where zero percent squat phase is defined as the joint angle at the initial position—squatted and fully flexed—and one-hundred percent squat phase is defined as the joint angle at the final position—standing.

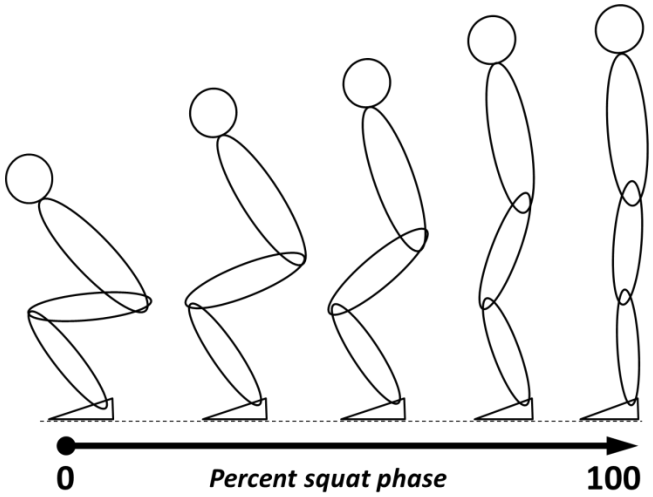

Figure 33. Normalization to "percent squat phase" based on joint angles, where 0% corresponds to the lowest portion of the squat and 100% to the highest (standing). Note that this diagram is for illustration purposes only—actual joint angles for a given squat vary between squats and between subjects.

If data on the knee angle was not available during any given frame, due to one or more of the knee markers being obscured or lost by the cameras, the hip angle was used for that frame.

The various computed reactions were normalized to body weight, body height, or both. Reaction moments were normalized to body weight and height. GRF, applied load, and reaction forces were normalized to body weight. Mechanical power was normalized to body weight. The position of the CoP relative to the trunk COM was normalized to body height. The position of the CoP along the foot was normalized to the distance along the sagittal axis from ankle marker to middle toe marker. Three squats from each trial were used for analysis, for a total of 72 squats per level of load support, corresponding to 3 squats per trial, 3 trials per subject, and 8 subjects at each level of load support.

3.5 Dynamic Model

A simplified dynamic model of the squatting motion was developed to predict the effect of varying levels of vertical load support, applied at the hip, on joint moments and forces. Body segment parameters and the locations of limb segment centers of mass were based on anthropometric studies by de Leva, et al., and Zatsiorsky, et al. [75]. Values for the range of motion of the several joints were obtained from previous studies on squat kinematics [60], [63]. Several simplifying assumptions were made for the model:

1) That joint angles vary linearly over the course of the squat.
2) That GRF acts purely along the body's longitudinal axis, i.e., vertically.
3) That the basic squat kinematics remain consistent regardless of limb dimensions and different loading conditions.
4) That any applied force acts precisely at the hip and in a purely vertical direction.
5) That the weight of each limb segment acts exclusively at the segment's center of mass.
6) That all relevant forces and moments occur in the body's sagittal plane and about the transverse axis, respectively, permitting a two-dimensional analysis.

Based on these assumptions, the location of the CoP was computed over the course of the squat by summing moments about an arbitrary point in space and solving for the moment arm of the GRF. For cases involving BW support, a load profile

consistent with the previously discussed scheme was applied. Inverse computations were then performed as previously described. The predictions based on the simplified model are presented alongside the experimental results in the following sections.

CHAPTER 4. EXPERIMENTAL RESULTS

4.1 Joint Reaction Moments with and without Support

Here we present and compare both model predictions of joint moments as well as the experimentally determined joint moments for the supported and unsupported cases. A positive joint moment is defined as a moment that induces joint extension, and a negative joint moment as one that induces joint flexion. Loads and moments consider one side of the body, and the values presented should be doubled to find the overall loads and moments acting on both sides of the body.

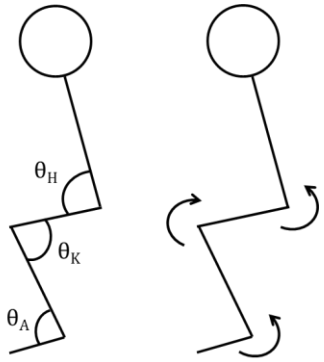

Figure 34. Definition of the joint angles and the positive senses of the several joint moments—a positive joint moment is defined as an extensor moment.

The simplified model (presented in Chapter 3 above) predicted that the ankle reaction moment would stay close to zero over the course of the squat, suggesting that,

during the prototypical unsupported squat, the GRF essentially remains in line with the ankle. The model also predicted that ankle reaction moment would increase slightly as the applied load increased. These hypotheses were largely borne out by the experimental data, which produced ankle moments of roughly the same magnitude (see Figure 36). Peak ankle moments increased with increasing support. Interestingly, the actual moments deviated sharply from the model around the 70% squat phase mark, at which point the previous trend—increasing ankle moment with increasing load support—essentially became inverted, and the moments in the supported cases overshot the moment in the unsupported case. Moreover, instead of converging to a common value, as predicted by the model, the moments in the unsupported cases continued to diverge as they approached the end of the squat. As a result, the minimum ankle moments decreased with increasing support—the total range of ankle moment over the course of the squat was about threefold larger at 35% BWS than in the unsupported case

The knee moments showed a similar pattern. The model predicted that the peak knee moment would occur at the beginning of the squat—a logical notion which follows from the fact that, at the beginning of the squat, the ankle is at its most flexed position, and the moment arms of the ankle reaction force and shank center of mass are maximized, producing a relatively large moment about the knee. The model also predicted increasingly reduced knee moments in the supported cases, corresponding to the overall reduction in GRF with load support. Again, the actual moments decreased over the course of the squat in a manner similar to the predicted moments (see Figure 37). As with the ankle moment, a noticeable deviation occurred at 70% percent squat phase, at which point the knee moment curves for the supported cases crossed the curve for the

unsupported case and considerably overshot said curve. Consequently, peak knee moments were diminished with increasing support, and the minimum knee moments increased.

Finally, the hip moment curves also revealed similar overall changes as the ankle and knee moments (see Figure 38). The model predicted that the hip moment would not change, regardless of support—a result that can be understood intuitively if one considers that the support is applied, at least in the idealized model, precisely at the hip. Such a force would affect the moment about any arbitrary point—or joint—around the hip, but would not affect the moment at the hip, since the moment arm of the applied force would be zero at that point and, furthermore, since the location of the CoP shifts as support is applied and GRF is reduced so as to maintain the equilibrium of the system, including the equilibrium of the moment about any arbitrary point. The actual moments at the hip were slightly lower at the beginning of the squat in the supported cases than in the unsupported case. These curves then started to converge, roughly, with the unsupported curve, before splitting sharply from it at approximately 70% squat phase as with the ankle and knee moment curves. Peak hip moments were reduced with larger amounts of load support, as were the minimum moments.

Based on the results of two-way ANOVA and post-hoc paired t-tests between each pair of levels of load support, significant differences were found between the levels of load support at all joints ($p < 0.001$). Significant differences were also found within subjects at all joints for most subjects (please see Appendix E for within-subjects statistics).

Table 1. Peak joint moments (%BW*height). Data presented as mean ± SD.

	Unsupported	20% BWS	35% BWS
Ankle	1.196 ± 0.552	1.570 ± 0.619	1.942 ± 0.611
Knee	4.725 ± 0.747	3.707 ± 1.018	3.660 ± 1.010
Hip	3.433 ± 0.755	2.561 ± 1.043	2.627 ± 0.815

Table 2. Minimum joint moments (%BW*height). Data presented as mean ± SD.

	Unsupported	20% BWS	35% BWS
Ankle	0.424 ± 0.721	0.249 ± 0.959	-0.421 ± 1.739
Knee	-1.037 ± 0.475	0.227 ± 1.527	1.035 ± 0.865
Hip	1.342 ± 0.509	0.627 ± 1.230	-0.313 ± 2.367

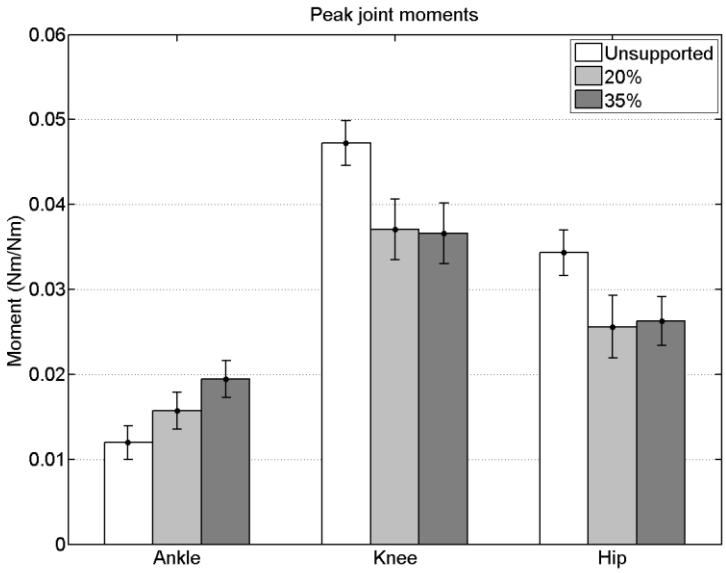

Figure 35. Changes in the peak moments at the joints at the different levels of load support, normalized by weight and height. Two-way ANOVA and paired t-tests showed significant differences ($p < 0.001$) at each joint between the different levels of load support.

Representative plots of a single subject may be found in Appendix F.

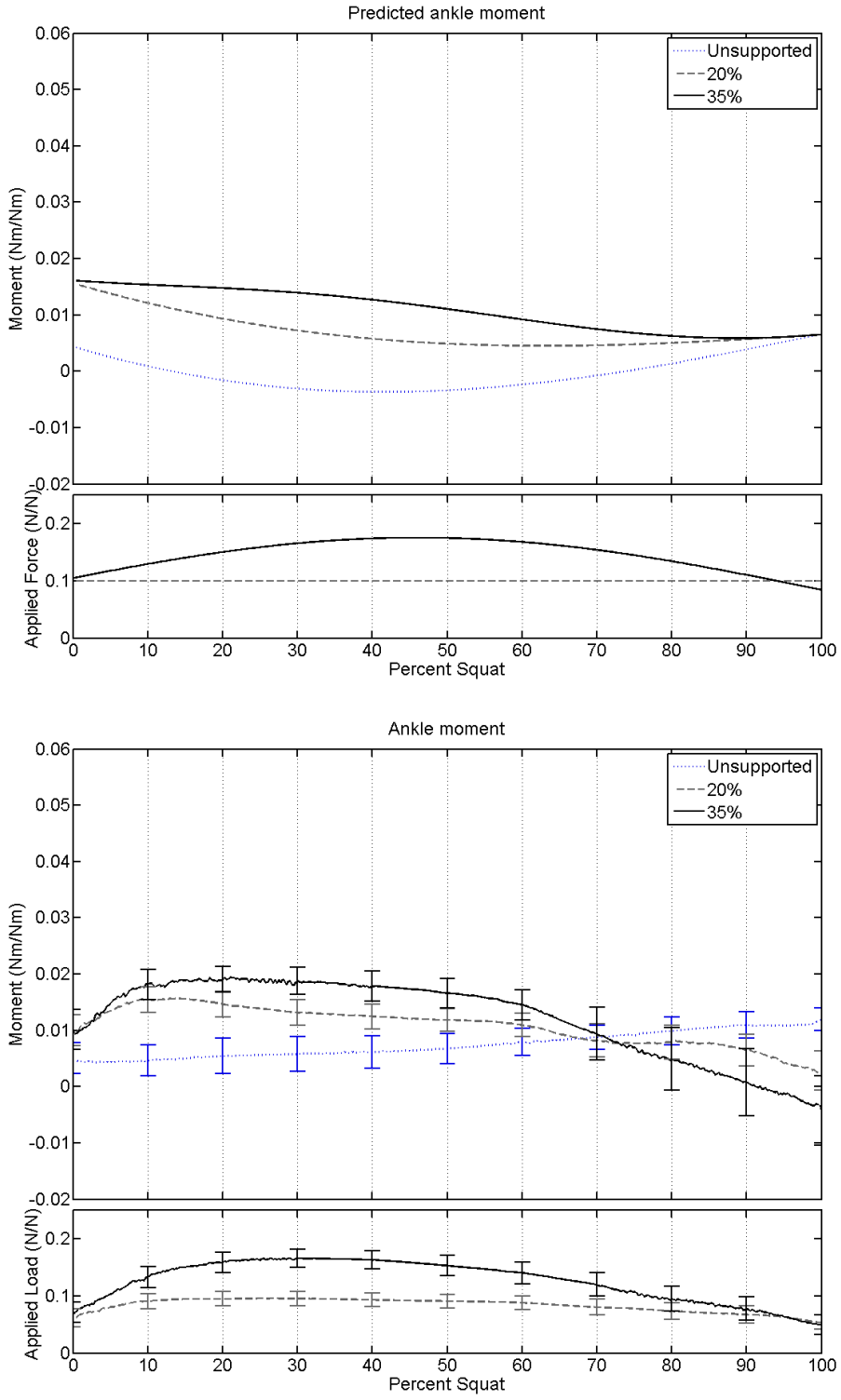

Figure 36. Predicted and actual ankle moments in the unsupported and supported cases. Moments have been normalized to body weight and height. Load has been normalized to body weight.

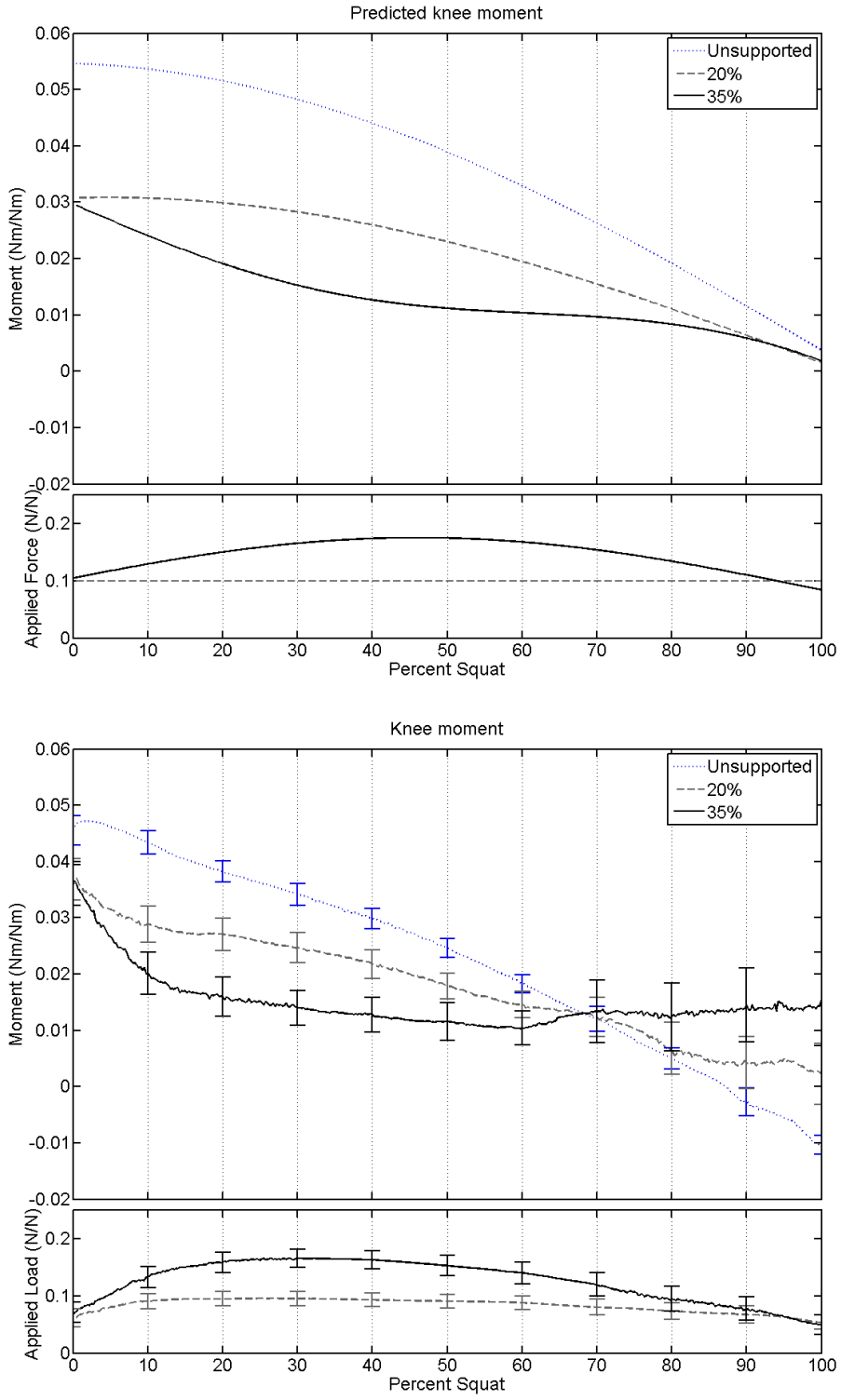

Figure 37. Predicted and actual knee moments in the unsupported and supported cases. Moments have been normalized to body weight and height. Load has been normalized to body weight.

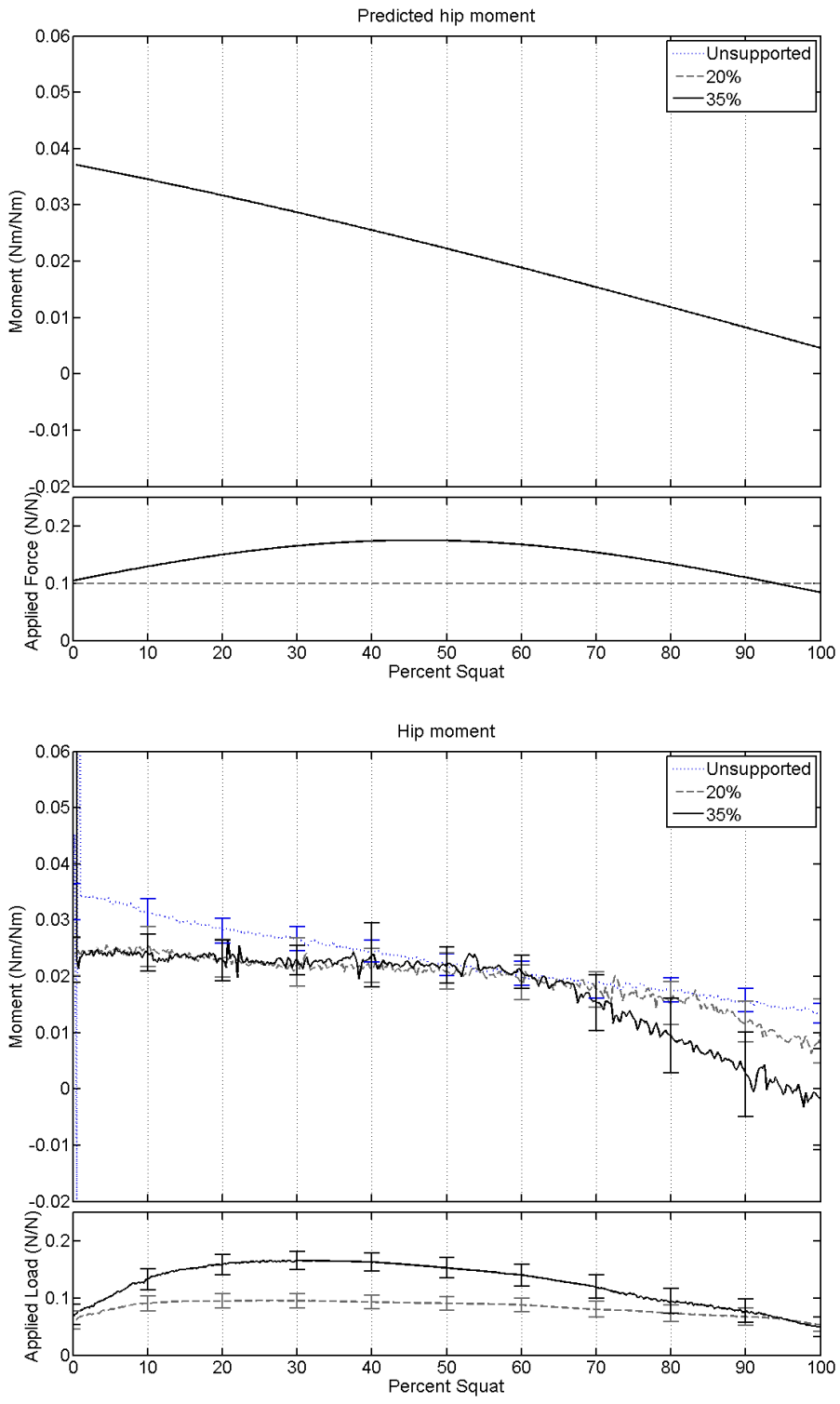

Figure 38. Predicted and actual hip moments in the unsupported and supported cases. Moments have been normalized to body weight and height. Load has been normalized to body weight.

4.2 Joint Reaction Forces with and without Support

The total joint reaction forces in the supported and unsupported cases were averaged over all subjects and trials to compare against the results predicted by the simplified model. As expected, the reaction forces at subsequent joints, beginning at the ankles and traveling proximally toward the trunk, decreased by a factor approximately equal to the weight of each intervening segment. In other words, the force at the ankle was roughly equal to the GRF, and the force at the hip to the weight of the head, arms, and torso. The model predicted that the inertial terms would not significantly alter the reaction force, a fact observed most clearly in the predicted unsupported force curves, which are visibly constant and linear. The actual reaction forces varied somewhat, though they did not stray far from the predicted values. The reaction force in the supported cases deviated from the predicted values at about 60% to 70% squat phase, at which point the curves for the supported cases intersected or crossed the curve for the unsupported case.

At all joints, both peak and minimum joint forces were reduced when load support was applied (see Tables 3 and 4). Significant differences were found between the three levels of load support at the ankle ($p < 0.001$), knee ($p < 0.001$), and hip ($p < 0.001$).

The forces in the following tables and plots consider one side of the body, and the values should be doubled to find the overall loads acting on both sides of the body.

Table 3. Peak joint forces (%BW). Data presented as mean ± SD.

	Unsupported	20% BWS	35% BWS
Ankle	53.83 ± 3.22	44.57 ± 4.84	46.39 ± 6.19
Knee	49.43 ± 3.31	40.30 ± 5.69	42.06 ± 6.28
Hip	36.03 ± 3.73	26.58 ± 8.15	28.73 ± 8.49

Table 4. Minimum joint forces (%BW). Data presented as mean ± SD.

	Unsupported	20% BWS	35% BWS
Ankle	45.14 ± 3.22	41.32 ± 4.58	33.85 ± 4.50
Knee	40.63 ± 3.48	36.79 ± 3.48	29.38 ± 4.58
Hip	26.47 ± 8.15	22.22 ± 4.58	15.26 ± 4.58

Representative plots of the total joint reaction forces for a single subject may be found in Appendix F.

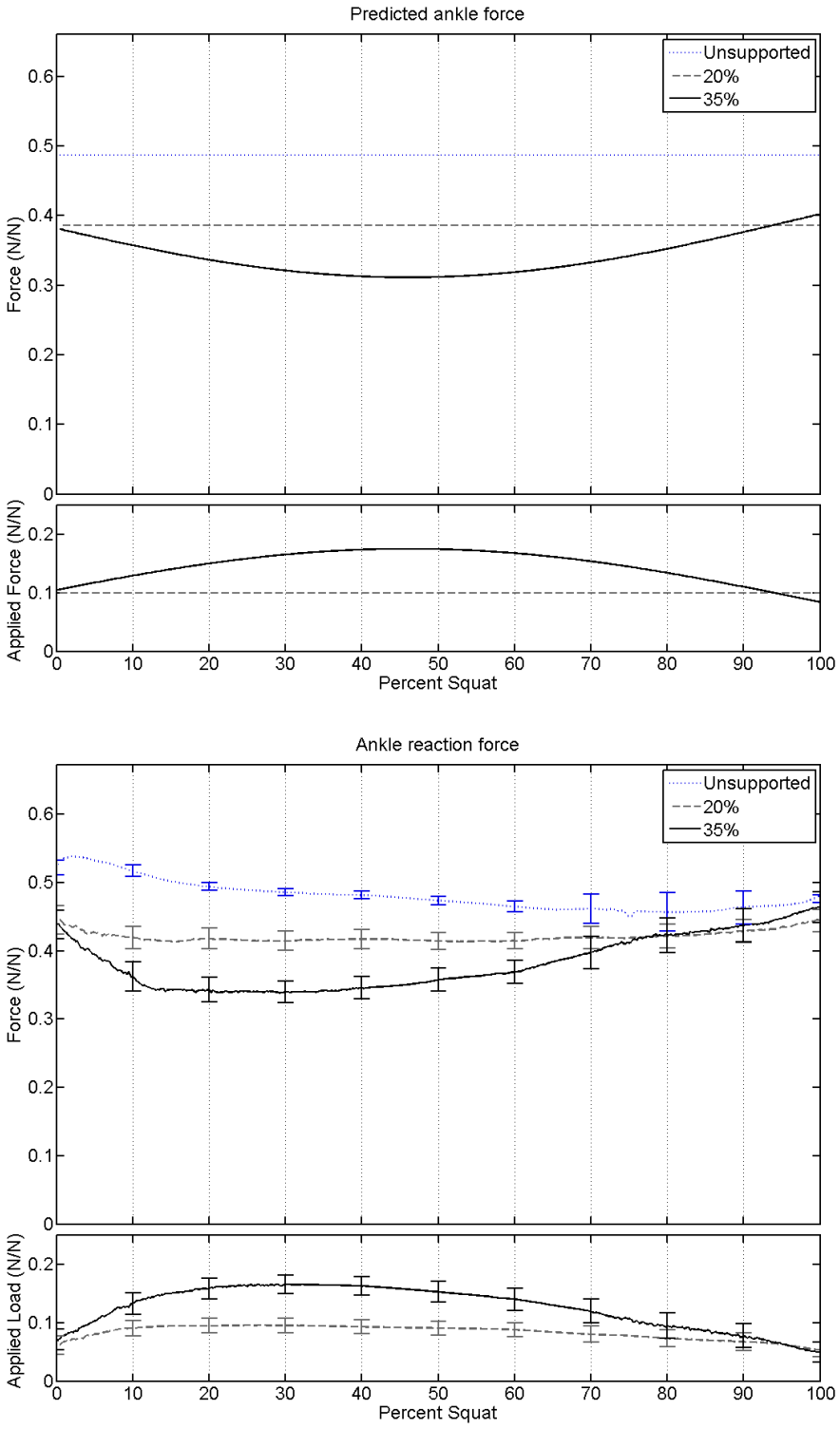

Figure 39. Predicted and actual total ankle reaction forces in the unsupported and supported cases. Forces and applied load have been normalized to body weight.

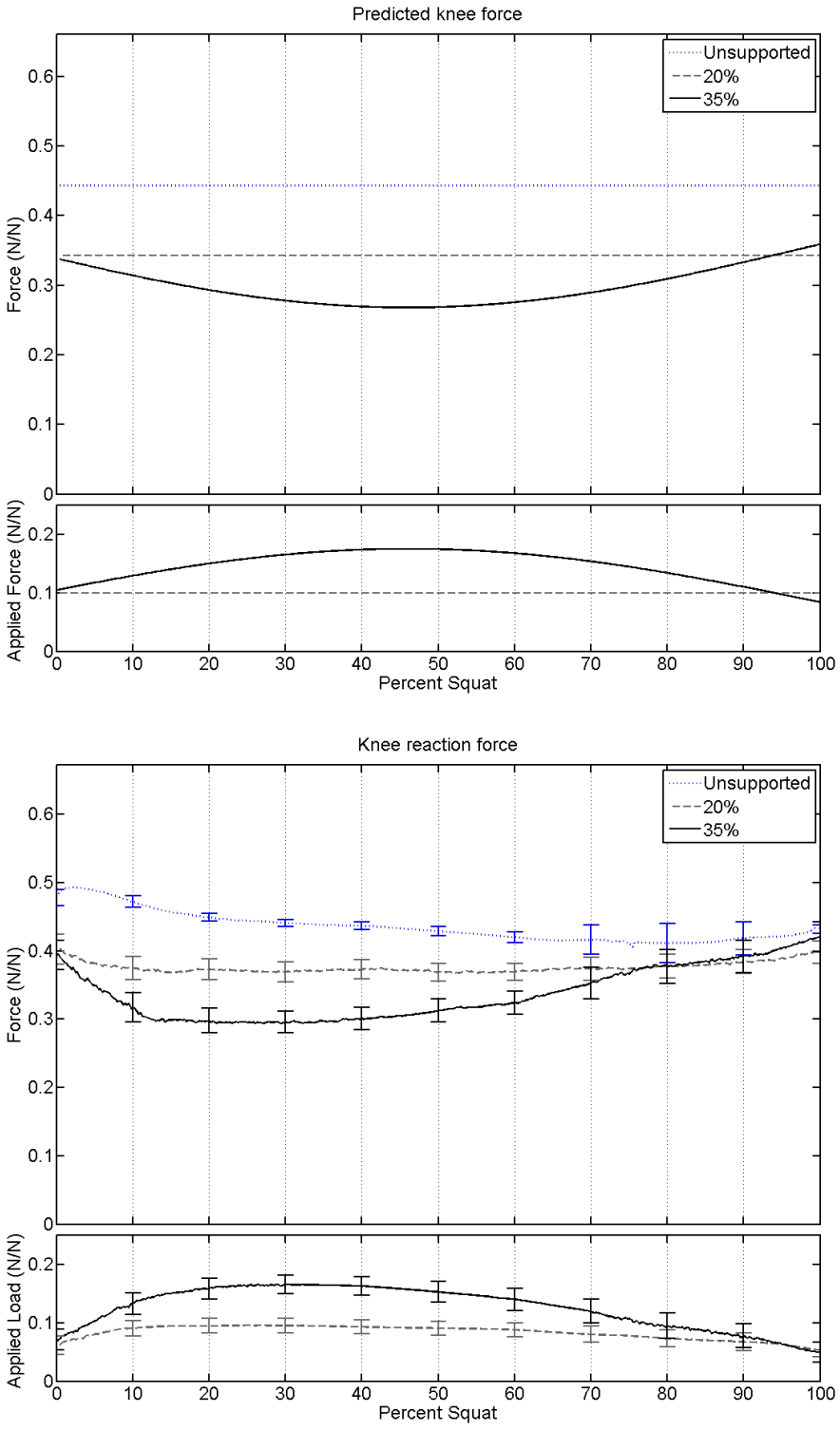

Figure 40. Predicted and actual total knee reaction forces in the unsupported and supported cases. Forces and applied load have been normalized to body weight.

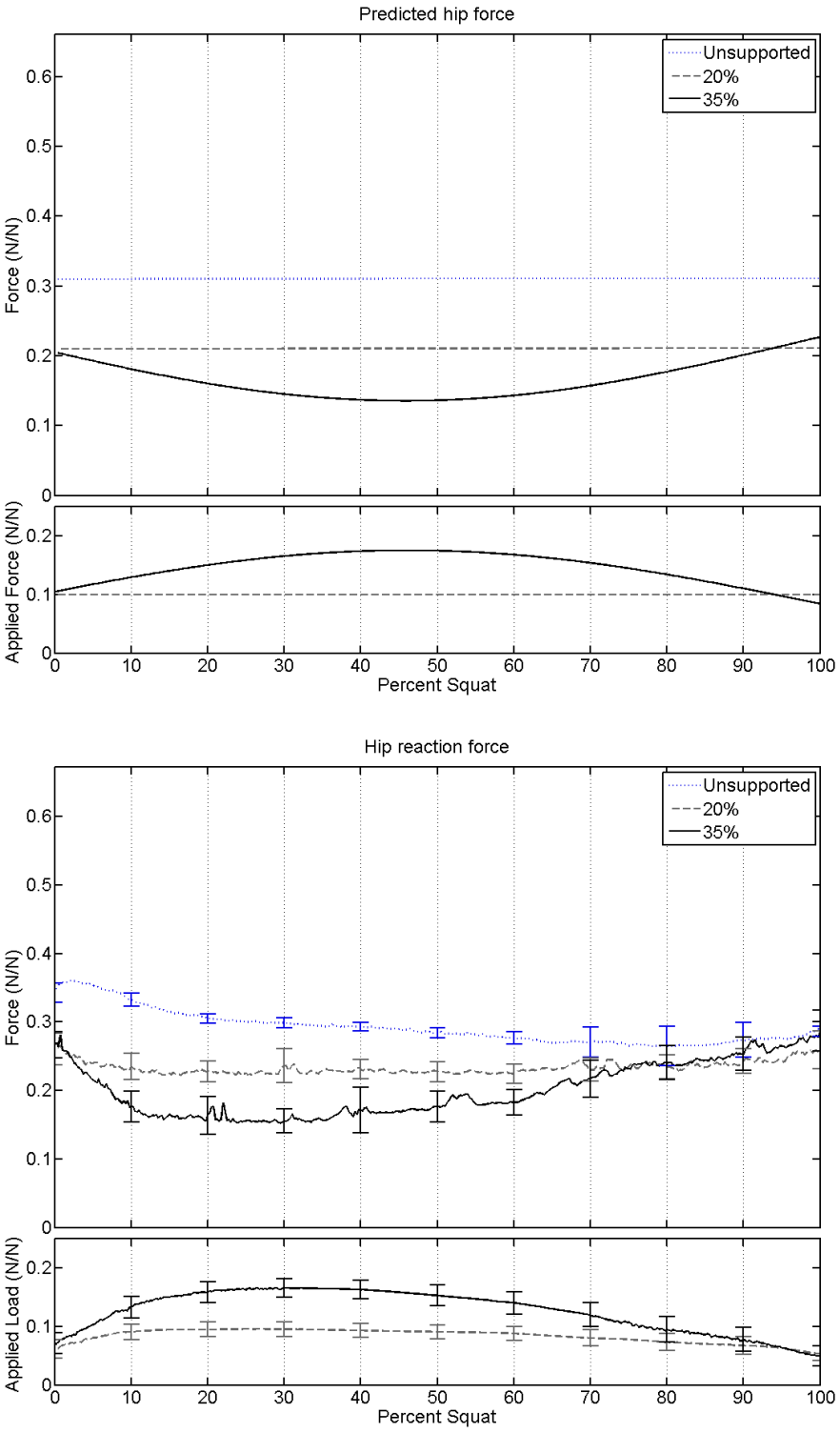

Figure 41. Predicted and actual total hip reaction forces in the unsupported and supported cases. Forces and applied load have been normalized to body weight.

4.3 Center of Pressure

The CoP, as measured by the Bertec forceplates, was compared against the predicted CoP based on the simplified dynamic model. The model predicted that CoP would shift anterior to the ankle, toward the toes, with increasing weight support, reaching roughly 40% of the distance spanned from ankle to the base of the middle toe with the highest level of load support, and staying centered relatively close to the ankle without load support. Though the actual CoP followed this basic trend, the values were exaggerated in comparison, with the CoP reaching nearly 80% of the distance from ankle to the base of the middle toe at the highest level of load support. In the unsupported case, the actual CoP started slightly anterior to the ankle joint and shifted slightly forward over the course of the squat, as predicted, though in a rather linear fashion relative to the predicted CoP.

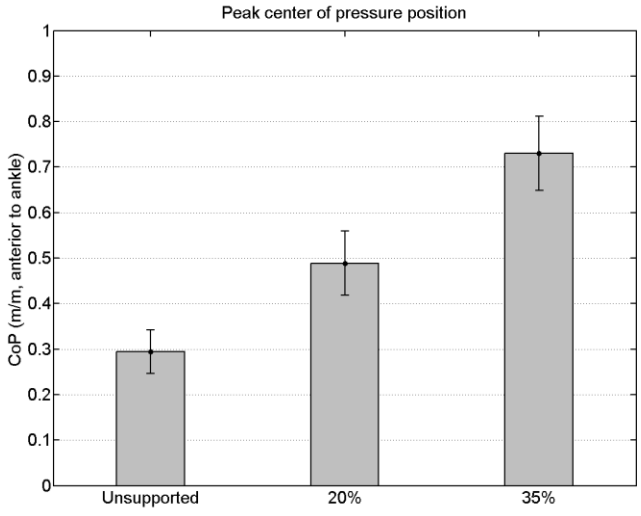

Figure 42. Peak CoP position along the sagittal axis of the foot at different levels of load support, normalized by the distance from the ankle joint to the base of the middle toe. Positive values are defined as anterior and distal to the ankle joint, toward the toes, and negative values are defined as posterior and distal to the ankle joint, toward the heel.

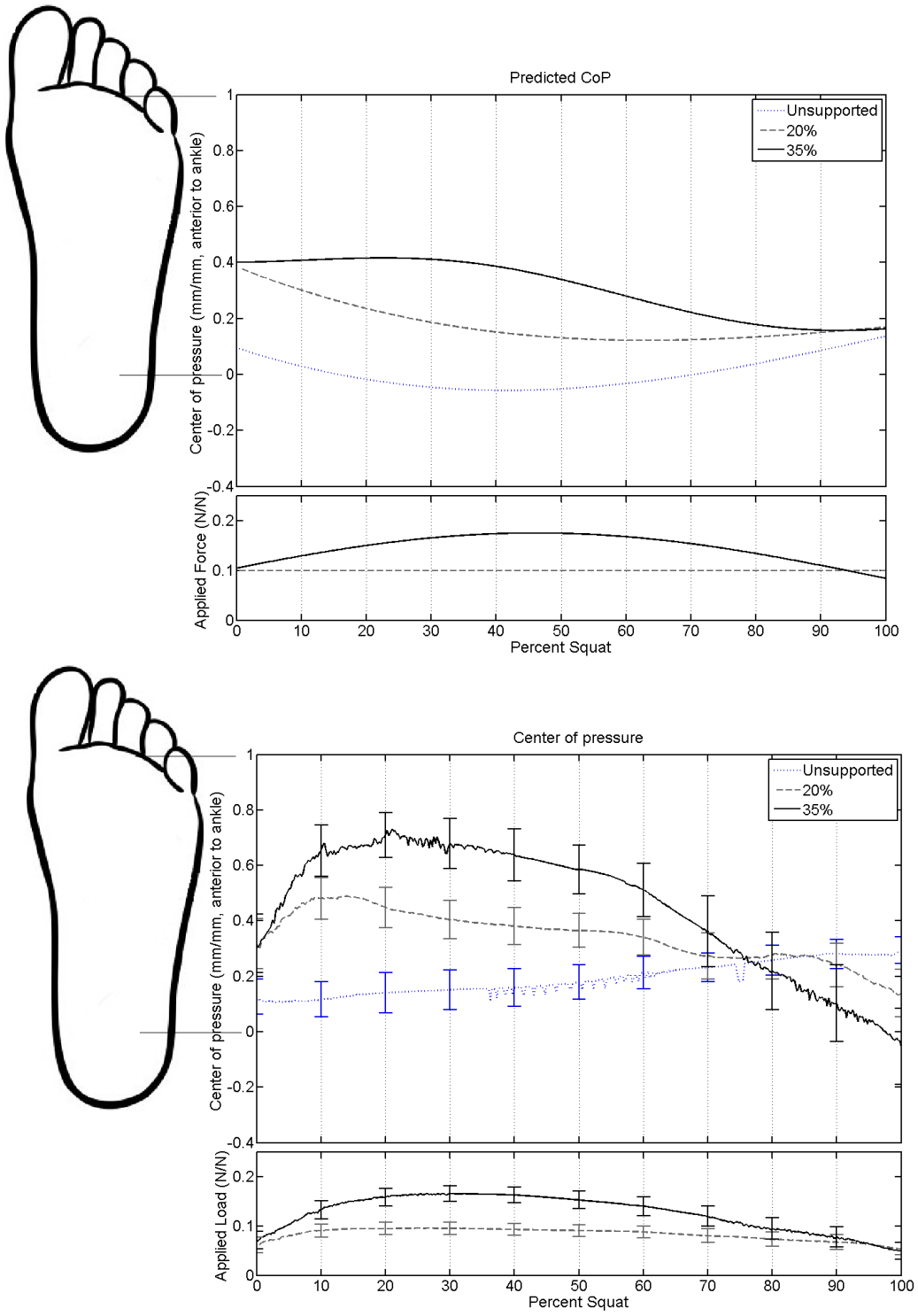

Figure 43. The predicted CoP (top) and actual CoP (bottom) along the sagittal axis of the foot. CoP has been normalized by the distance from the ankle joint to the base of the middle toe. The diagram of the foot corresponds approximately to the plots, where a positive value is defined as anterior and distal to the ankle joint, toward the toes, and a negative value is defined as posterior and distal to the ankle joint, toward the heel.

4.4 Trunk Inclination Angle and Trunk Center of Mass

The trunk inclination angle and trunk COM were measured and approximated, respectively, based on the hip and shoulder markers. The trunk inclination angle was defined as the angle of the trunk with the horizontal.

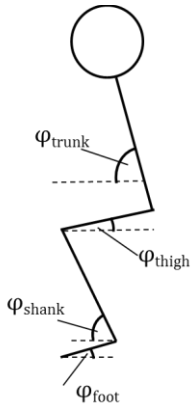

Figure 44. Definitions of the body segment angles. The angles are measured with respect to the horizontal.

As seen in Figure 45, the trunk tilt increased fairly steadily in the unsupported case from approximately 45°, at the initial position, to approximately 85° at the final standing position. In the supported cases, on the other hand, the initial trunk angle was roughly 55° and 58°, respectively, presumably due to a small amount of initial tension in the rope. This angle remained relatively constant, increasing slightly, until approximately 40% squat phase. From this point onward, the trunk inclination angle rose somewhat linearly to its final value of about 73°.

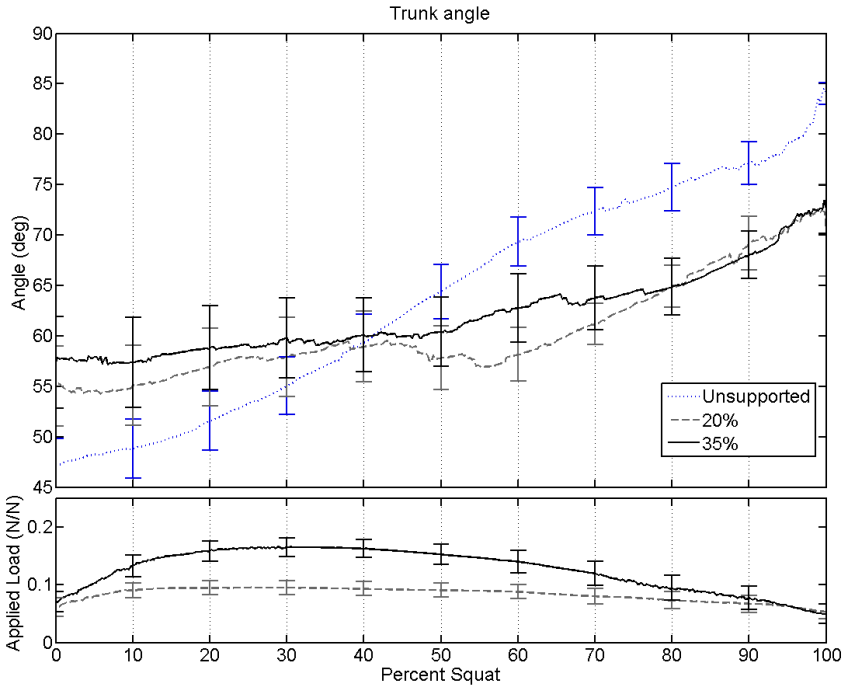

Figure 45. Trunk inclination angle, measured relative to the horizontal (i.e., relative to the transverse plane). Applied load has been normalized to body weight.

Figure 46 shows the position of the CoP, at which the GRF acts, relative to the trunk COM. In the unsupported case, the CoP remained centered almost directly beneath the trunk COM, implying that the trunk COM tends to remain largely in line with the body's COM under such conditions. In the supported cases, however, the position of the CoP shifted forward of the trunk COM. At about 70% to 80% squat phase, the CoP shifted until it was behind the trunk COM, toward the heels and posterior to the position of the CoP measured in the unsupported case.

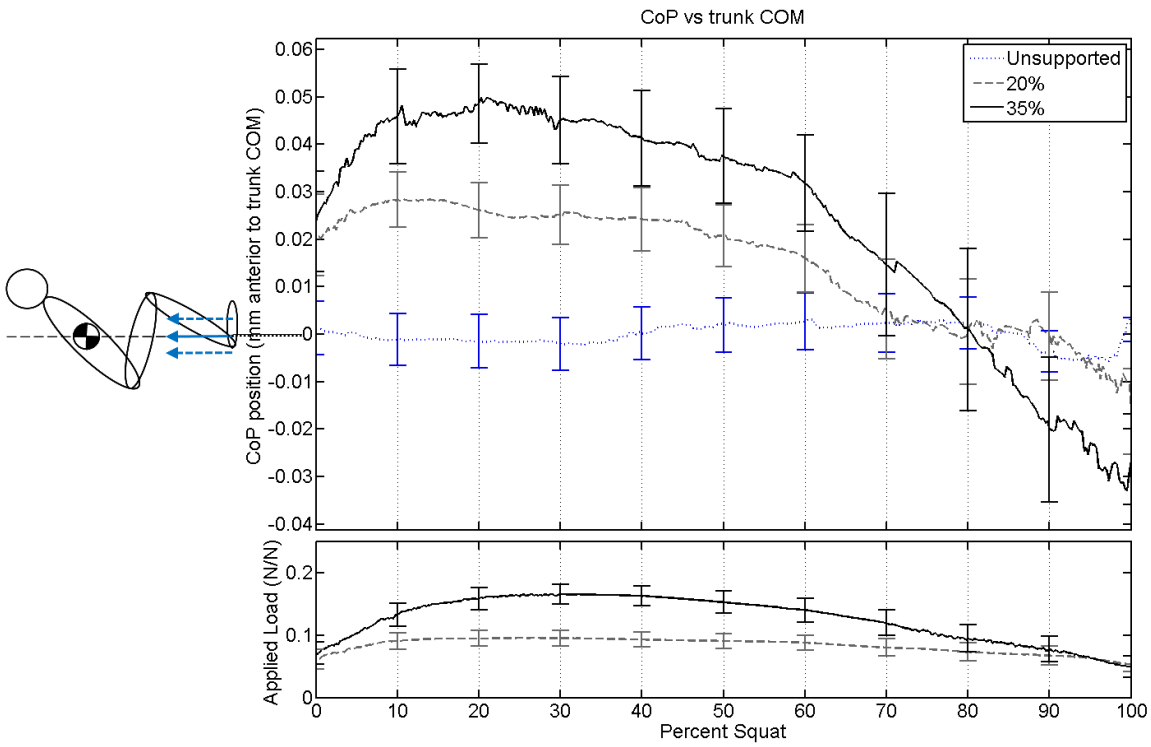

Figure 46. The position of the CoP relative to the trunk COM along the sagittal axis, where a positive value is defined as the CoP being anterior to the trunk COM and a negative value is defined as the CoP being posterior to the trunk COM. The distance has been normalized to body height. Applied load has been normalized to body weight. The diagram beside the y-axis is for illustration purposes and is not to scale.

4.5 Joint Mechanical Power

The mechanical power at the joints at each level of load support was quantified and compared. Since the kinematic data were numerically differentiated to obtain angular velocities, some of the resulting accelerations caused large spikes in the computations; these outliers were removed from the final analysis. The peak mechanical power produced by each joint under the different conditions is listed in Table 5. As would be expected for a heels down squat, the power at the ankle hovered relatively close to zero. The knee and hip generated positive power through most of the rising motion, with the hip generating less power in the supported cases than in the unsupported case. In the unsupported case, the concavity of the knee joint power curve changed around the third quartile of the rising motion, and the knee joint appeared to absorb power by the end of the squat as a result. With 20% BWS, this change was less pronounced, if not absent altogether. At 35% BWS, the power generated by the knee joint increased near the third quartile of the motion. It should be noted that, although subjects were instructed to and encouraged to squat at similar speeds for the supported as well as unsupported trials, some of the differences in power curves may be due to differences in squatting speed, as it was difficult to enforce complete control over the subjects' preferred squatting speeds.

Table 5. Peak mechanical power at the joints (%BW). Data presented as mean ± SD.

	Unsupported	20% BWS	35% BWS
Ankle	0.066 ± 0.670	0.014 ± 0.068	0.117 ± 0.365
Knee	1.640 ± 0.679	1.066 ± 0.636	1.019 ± 1.638
Hip	3.996 ± 2.300	1.722 ± 0.984	2.081 ± 1.290

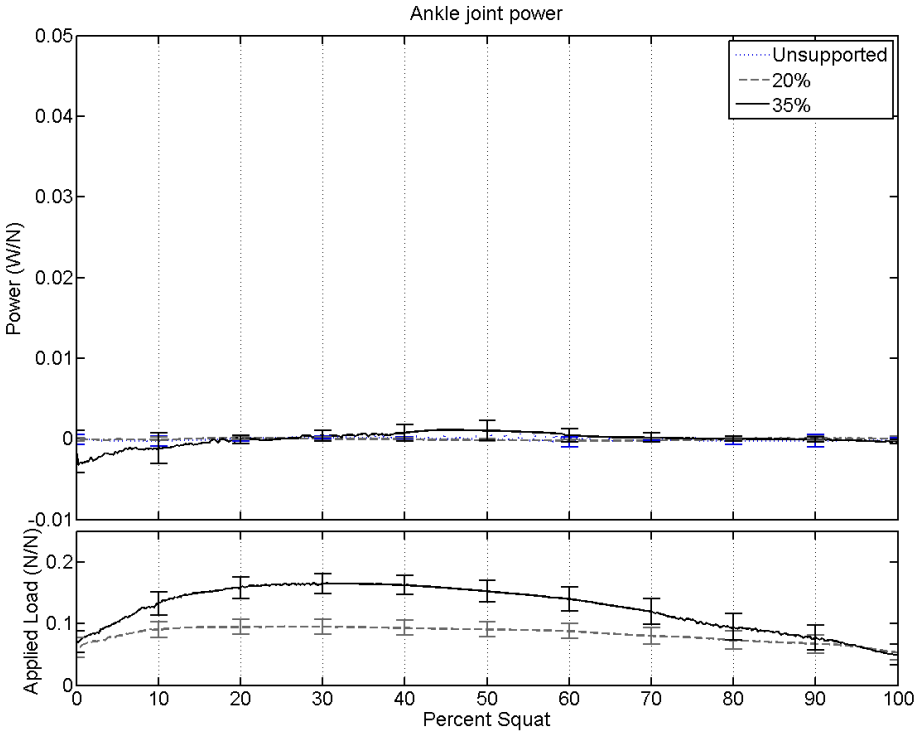

Figure 47. Ankle joint power. Power and applied load are normalized to body weight.

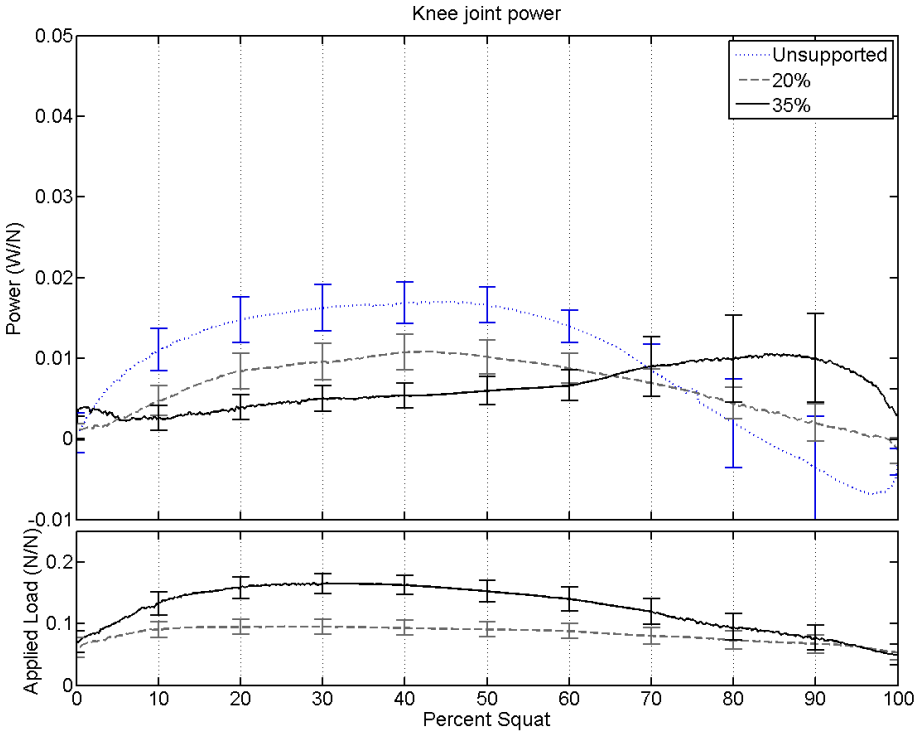

Figure 48. Knee joint power. Power and applied load are normalized to body weight.

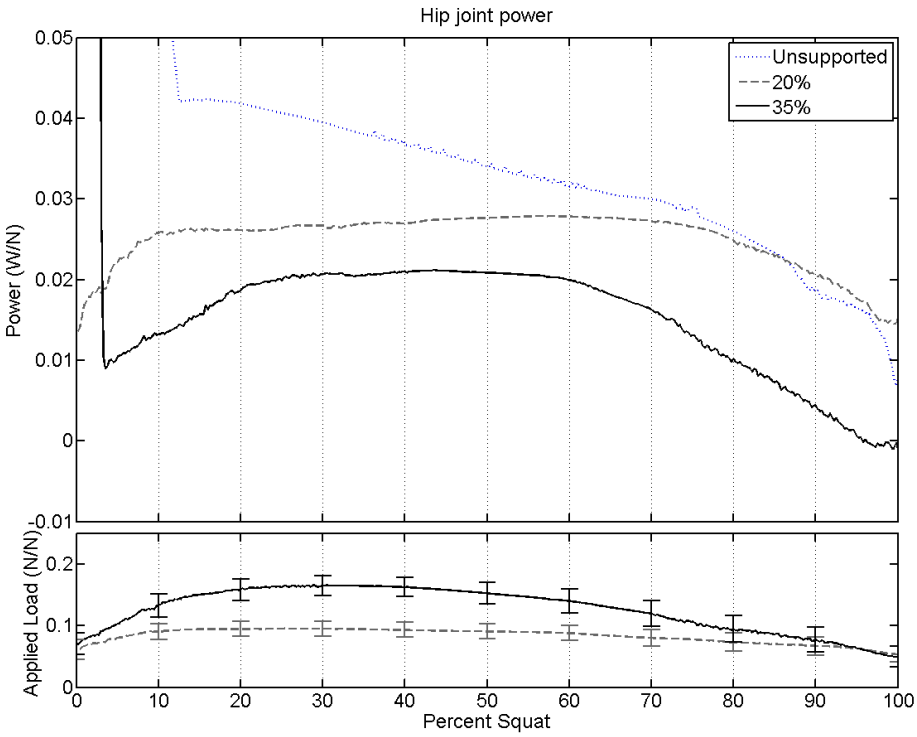

Figure 49. Hip joint power. Power and applied load are normalized to body weight.

Table 6. Hip joint power and standard error (W/N) at selected intervals. Presented as mean ± SEM.

Percent Squat	Unsupported	20% BWS	35% BWS
0	— —	0.0131 ± 0.0217	— —
10	— —	0.0258 ± 0.025	0.0132 ± 0.0034
20	0.0418 ± 0.0085	0.0261 ± 0.025	0.0186 ± 0.0046
30	0.0394 ± 0.0084	0.0267 ± 0.025	0.0207 ± 0.0049
40	0.0367 ± 0.0077	0.027 ± 0.0249	0.021 ± 0.0045
50	0.034 ± 0.0069	0.0276 ± 0.0248	0.0209 ± 0.0041
60	0.0315 ± 0.0064	0.0278 ± 0.0248	0.0199 ± 0.0045
70	0.030 ± 0.006	0.0272 ± 0.0248	0.0163 ± 0.0056
80	0.026 ± 0.0049	0.0249 ± 0.0249	0.0101 ± 0.0068
90	0.0188 ± 0.0039	0.0207 ± 0.0251	0.0044 ± 0.0084
100	0.008 ± 0.0032	0.0153 ± 0.0261	-0.001 ± 0.0061

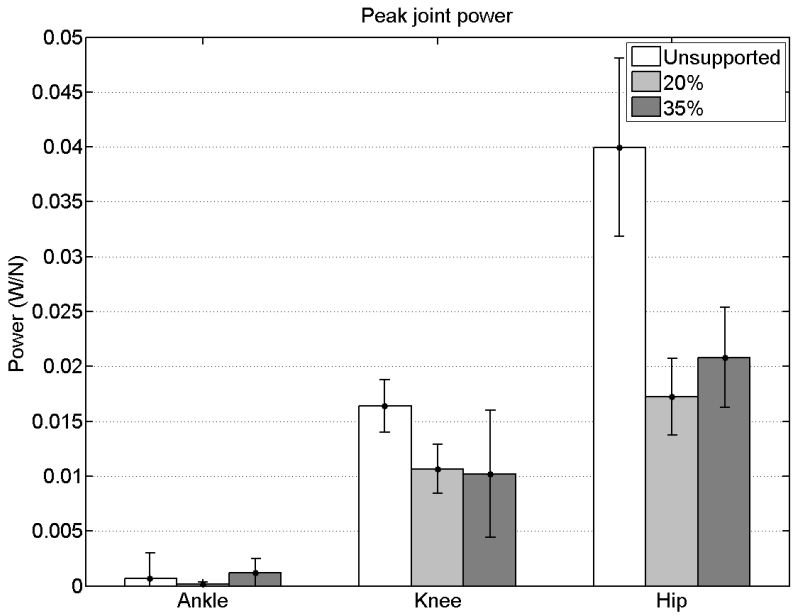

Figure 50. Changes in the peak power at the joints at the different levels of load support, normalized by weight. Two-way ANOVA showed significant differences ($p < 0.001$) at each joint between the different levels of load support.

4.6 Qualitative Participant Feedback

Subjects were asked to complete a questionnaire at the end of the experiment regarding both the harness and the load supported squatting (please see a copy of the survey in Appendix J). Nearly all participants reported that the modified rock climbing harness did not hinder their ability to squat. A couple suggested that the harness could, at times, be awkward to wear, and that multiple harness sizes could be useful for different body types instead of a single, one-size-fits-all harness. The majority of participants said they felt most comfortable in the standing position and least comfortable in the squatted position while wearing the harness. Some users reported that the fit of the harness grew looser over the course of the experiment, while others reported it grew tighter. Similarly, some reported that the harness did not ride up their waist, hips, or thighs to the point of being uncomfortable at any stage of the experiment, while others felt the opposite, especially at the higher level of load support, suggesting that the fit of the harness may have to be tailored with more care for each user. Almost all subjects reported that they felt a noticeable difference between the two levels of load support, and that rising from the squat with increasing load support was easier than performing the motion with less or no load support. Most participants stated that donning the harness was “somewhat easy” or “acceptable,” and on average it took approximately 4.5 minutes to put the harness on and about 1 minute to remove it. The subjects unanimously agreed that tightening the harness and its various straps, as well as keeping them from growing loose, was the most difficult aspect of putting the harness on.

CHAPTER 5. DISCUSSION

Currently, literature on squatting with load support is insufficient to directly compare the results of this experiment to prior work. Furthermore, though there have been many studies on heels down squatting, few or none have examined the CoP during such activity, especially during the rising phase of the squat [12]–[17]. However, the results for load supported squatting can be understood by direct analysis of the measured variables, and the reaction forces and moments for unsupported squatting are easily compared to previous work on forces and moments during the squat. The joint moments obtained in this study for the unsupported case were found to be comparable to joint moments reported in the literature [45], [54], [60], [63], [67], [68], [78], [80].

A number of reductions in joint moments were found. The peak knee moment decreased from 4.725 ± 0.747 (%BW*height), in the unsupported case, to 3.660 ± 1.010 (%BW*height) at 35% BW support. This corresponds to roughly a 22.5% decrease in the knee moment. The peak hip moment declined from 3.433 ± 0.755 (%BW*height) without support to 2.627 ± 0.815 (%BW*height) at 35% BW support, which corresponds to a decrease of approximately 23.5% in the hip moment. On the other hand, peak ankle moments increased from 1.196 ± 0.552 (%BW*height) without support to 1.942 ± 0.611 (%BW*height) with 35% BW support. This translates to an increase of about 62.4% in the ankle moment. These data suggest that load support eases the kinetic demands on the knee and hip to similar degrees while disproportionately increasing the moments at the

ankle. Assuming these trends hold across different populations, the utility of load supported squatting motions depends on whether the increase in ankle moment is an acceptable tradeoff for reduced knee and hip moments. Increased ankle joint moment is an indicator for various lower limb injuries, not only to the ankle but also to the tibia and knee complex, including knee valgus and ACL injuries. However, such injuries generally occur under higher loading conditions, such as those experienced during running or competitive weightlifting. The moments experienced by subjects in the current study were, in some cases, an order of magnitude less than the moments that occur in the aforementioned activities, and the ankle joint angles did not approach the angles at which injuries are commonly seen [63], [81]–[83]. Although further study may be required, this would imply that joint moments during a relatively low frequency controlled motion like the load supported squatting increase but are unlikely to cause injury.

While, for the most part, the joint moments and forces did not deviate much from the predicted values, they did take a sharp turn near the end of the squatting motion in both supported cases, often overshooting the values to which they were expected to converge. Glancing at the CoP data indicates that the CoP shifted considerably forward of the ankle in the supported cases, particularly at the highest level of load support. The trunk angle with respect to the horizontal deviated significantly in the supported cases relative to the trunk angle in the unsupported case, whereas the angles of the foot, shank, and thigh with respect to the horizontal changed little, if at all (see Appendix I). It follows, then, that the trunk inclination angle and, by corollary, the change in position of the trunk COM, were largely responsible for the shift in CoP, since the kinematics of the other body segments and the positions of their respective centers of mass did not change

much when load support was applied. This supposition is supported by the data comparing the position of the CoP relative to the trunk COM, which shows that CoP moves forward of the trunk COM for most of the concentric phase of the squat before falling quickly behind it.

This suggests that squat kinematics with the load support are altered, perhaps due to the moment that results about the trunk COM as a result of the vertical force applied at the hip. Such a moment could induce the person to bend or lean farther forward at the hip than they might in the absence of load support. The marked change in inflection of the force, moment, and power curves with increasing load support may also be consistent with some sort of anticipatory braking effect. It is reasonable to assume that load support induces kinematic or physiological adaptations in the body while squatting, much as load support or added load induce changes during locomotion—for instance, in the preferred walk-run transition speed or metabolic rate or other metrics [4], [7], [11], [46].

The compressive and shear forces at the various joints have been relatively well characterized by previous studies [63], [84]. Compressive forces at the knee and tibiofemoral tendon in excess of 8,000 N have been reported [69], [85]. Forces of this magnitude only manifest in situations involving large amounts of excess load, such as in weightlifters performing barbell squats with several times their body weight. Although the forces in the tendons were not quantified as part of this study, the compressive and shear forces in the tibia (see Appendix G) were similar to those found in studies on kneeling and squatting without additional load [86]. The magnitudes of compressive and shear loading on the body segments experienced in this study were not high enough to test the limits of acute injury due to shear or compressive loading. However, the effect of

even higher levels of load support on such forces remains to be characterized, as does the long-term effect of repeated exposure to such loads.

The joint powers computed are similar, at least for the unsupported case, to previous studies which have quantified joint power [68]. The addition of load support resulted in reduced peak mechanical power at the joints. Peak mechanical power at the knee declined from 1.640 ± 0.679 (%BW) without support to 1.019 ± 1.638 (%BW) at 35% BW support, a reduction of nearly 38%. Peak mechanical power at the hip declined from 3.996 ± 2.300 (%BW) without support to 1.722 ± 0.984 (%BW) at 20% BW support, corresponding to a reduction of almost 57%. Since power is a function of velocity, further study on the speed of squatting versus applied load, or versus the rate at which the applied load is ramped up to its maximum value, is required.

It should also be noted that, on average, subjects began the ascent phase of the squat when the support reached about 12% to 14% BW, regardless of the target load or external cues to the contrary. This may suggest that this level of support is a sort of threshold of BWS at which individuals naturally lose the tendency to resist the motion and begin squatting.

CHAPTER 6. CONCLUSIONS

The results of this experiment and thesis aim to fill some of the apparent gaps in the current literature on squatting with load support and heels-down squatting.

Squatting with the heels down is utilized in activities of daily living in many Asian countries, among others. It is also commonly recommended as the proper form for performing an athletic squat in weightlifting settings, and with good reason—performing squats with the heels up, particularly with heavy loads, is associated with forces two to four times greater than squatting with the heels down, and is linked to higher rates of injury (and vice versa). While a number of studies have sought to characterize the kinetics and kinematics of heels down squatting, few have examined the CoP during said activity, and fewer still have examined the CoP during the rising phase of the squat. The descent phase of the squat is a valuable, to be sure—it does, after all, constitute half the squatting motion—but the rising phase of the squat is equally important. A proper understanding of the mechanics of all aspects of the motion are necessary for a better understanding of the effects of different types of squatting kinematics on the body, whether in a functional setting—squatting over a toilet, in some countries, for instance—or in a rehabilitative setting, or in weightlifting, or for manual materials handling by warehouse employees or military personnel. The current study found that the CoP stays centered below the trunk COM through most of the rising portion of the unsupported

squat—in terms of the foot, this translates to the CoP shifting slightly forward of the ankle over the course of the rising portion of the squat, approaching but not quite reaching the middle or the arch of the foot.

When vertical load support was applied, the CoP shifted considerably farther, past the mid-foot and toward the toes. This was consistent with the trunk COM and trunk inclination angle data, which indicated that the trunk remained tilted toward the horizontal for a larger portion of the rising phase of the squat, all of which suggests that higher levels of load support result in kinematic adaptations by the individual. The individual's stance at the higher levels of load support can potentially be explained by the moment exerted about the trunk COM by the applied load.

As one might expect, and consistent with our theoretical model prediction, most of the peak joint forces, moments, and powers at the knees and hips were reduced with load support. Peak moment at the knee decreased from 4.725 ± 0.747 (%BW*height), in the unsupported case, to 3.660 ± 1.010 (%BW*height) at 35% BW support at the beginning of the squat, when knee moments were highest. The peak hip moment declined from 3.433 ± 0.755 (%BW*height) without support, at the beginning of the squat, to 2.627 ± 0.815 (%BW*height) at 35% BW support, a value which was roughly maintained from the beginning of the squat until about the 60% squat phase mark, at which point the supported moments declined. Peak ankle moments increased from 1.196 ± 0.552 (%BW*height) without support, a value reached at the end of the unsupported squat, to 1.942 ± 0.611 (%BW*height) with 35% BW support, at approximately 20% squat phase. These values were also consistent with the model prediction. However, the joint forces, moments, and powers under the influence of load support deviated from the expected

values near the end of the squat—a symptom of the trunk tilt compensatory mechanism described above. The ankle moment in the 35% BW support case declined to its minimum value of -0.421 ± 1.739 (%BW*height) at the end of the squat instead of converging to the value from the unsupported case of 0.424 ± 0.721 (%BW*height) like the model predicted it would. Similarly, the knee moments diverged from the model near 70% squat phase, ultimately arriving at 0.227 ± 1.527 (%BW*height) and 1.550 ± 2.376 (%BW*height) at the end of the squat with 20% and 35% BW support, respectively, rather than declining to -1.037 ± 0.475 (%BW*height) as in the unsupported case. The hip moments diverged as well, reaching a minimum of -0.313 ± 2.367 (%BW*height) at the end of the squat in the 35% BW support case but 1.342 ± 0.509 (%BW*height) in the unsupported case. It is important to keep such effects in mind when developing or testing any BWS system, not only with respect to the kinematics of the user but also for the implications of injury to that user.

This work also utilized a relatively novel and versatile system for providing load support. While the use of pneumatic, hydraulic, and other electromechanical actuators is not new, previous systems and apparatuses have generally relied upon a single actuator to provide support. The current apparatus utilizes two independently controlled actuators, which may be useful for conducting future studies on locomotion, or squatting with bilaterally asymmetric loads.

LIST OF REFERENCES

LIST OF REFERENCES

[1] A. Gams, T. Petric, T. Debevec, and J. Babic, "Effects of Robotic Knee Exoskeleton on Human Energy Expenditure," *IEEE Transactions on Biomedical Engineering*, vol. 60, no. 6, pp. 1636–1644, Jun. 2013.

[2] T. Petrič, A. Gams, T. Debevec, L. Žlajpah, and J. Babič, "Control approaches for robotic knee exoskeleton and their effects on human motion," *Advanced Robotics*, vol. 27, no. 13, pp. 993–1002, Sep. 2013.

[3] C. T. Farley and T. A. McMahon, "Energetics of walking and running: insights from simulated reduced-gravity experiments," *Journal of Applied Physiology*, vol. 73, no. 6, pp. 2709–2712, Dec. 1992.

[4] S. R. Goldberg and S. J. Stanhope, "Sensitivity of joint moments to changes in walking speed and body-weight-support are interdependent and vary across joints," *Journal of Biomechanics*, vol. 46, no. 6, pp. 1176–1183, Apr. 2013.

[5] T. M. Griffin, N. A. Tolani, and R. Kram, "Walking in simulated reduced gravity: mechanical energy fluctuations and exchange," *Journal of Applied Physiology*, vol. 86, no. 1, pp. 383–390, Jan. 1999.

[6] M. D. Lewek, "The influence of body weight support on ankle mechanics during treadmill walking," *J Biomech*, vol. 44, no. 1, pp. 128–133, Jan. 2011.

[7] R. Kram, A. Domingo, and D. P. Ferris, "Effect of reduced gravity on the preferred walk-run transition speed.," *J Exp Biol*, vol. 200, no. 4, pp. 821–826, Feb. 1997.

[8] K. E. Norman, A. Pepin, M. Ladouceur, and H. Barbeau, "A treadmill apparatus and harness support for evaluation and rehabilitation of gait," *Archives of Physical Medicine and Rehabilitation*, vol. 76, no. 8, pp. 772–778, Aug. 1995.

[9] A. M. Grabowski and R. Kram, "Effects of velocity and weight support on ground reaction forces and metabolic power during running," *J Appl Biomech*, vol. 24, no. 3, pp. 288–297, Aug. 2008.

[10] L. P. J. Teunissen, A. Grabowski, and R. Kram, "Effects of independently altering body weight and body mass on the metabolic cost of running," *J. Exp. Biol.*, vol. 210, no. Pt 24, pp. 4418–4427, Dec. 2007.

[11] A. Grabowski, C. T. Farley, and R. Kram, "Independent metabolic costs of supporting body weight and accelerating body mass during walking," *Journal of Applied Physiology*, vol. 98, no. 2, pp. 579–583, Feb. 2005.

[12] A. Hemmerich, H. Brown, S. Smith, S. S. K. Marthandam, and U. P. Wyss, "Hip, knee, and ankle kinematics of high range of motion activities of daily living," *J. Orthop. Res.*, vol. 24, no. 4, pp. 770–781, Apr. 2006.

[13] A. Thambyah, "How critical are the tibiofemoral joint reaction forces during frequent squatting in Asian populations?," *The Knee*, vol. 15, no. 4, pp. 286–294, Aug. 2008.

[14] S. J. Mulholland and U. P. Wyss, "Activities of daily living in non-Western cultures: range of motion requirements for hip and knee joint implants," *Int J Rehabil Res*, vol. 24, no. 3, pp. 191–198, Sep. 2001.

[15] J. Zelle, M. Barink, M. De Waal Malefijt, and N. Verdonschot, "Thigh–calf contact: Does it affect the loading of the knee in the high-flexion range?," *Journal of Biomechanics*, vol. 42, no. 5, pp. 587–593, Mar. 2009.

[16] K. Hase, M. Sako, J. Ushiba, and N. Chino, "Motor strategies for initiating downward-oriented movements during standing in adults," *Exp Brain Res*, vol. 158, no. 1, pp. 18–27, Mar. 2004.

[17] V. C. Dionisio, G. L. Almeida, M. Duarte, and R. P. Hirata, "Kinematic, kinetic and EMG patterns during downward squatting," *Journal of Electromyography and Kinesiology*, vol. 18, no. 1, pp. 134–143, Feb. 2008.

[18] "Laborers and Freight, Stock, and Material Movers, Hand." [Online]. Available: http://www.bls.gov/oes/current/oes537062.htm. [Accessed: 08-Nov-2015].

[19] "Nonfatal occupational injuries and illnesses requiring days away from work, 2013," Bureau of Labor Statistics, Dec. 2014.

[20] J. F. Kraus, K. B. Schaffer, D. L. McArthur, and C. Peek-Asa, "Epidemiology of acute low back injury in employees of a large home improvement retail company," *Am. J. Epidemiol.*, vol. 146, no. 8, pp. 637–645, Oct. 1997.

[21] N. Yagn, "Apparatus for facilitating walking, running, and jumping," Patents 420 179 and 438 830, 1890.

[22] A. M. Dollar and H. Herr, "Lower Extremity Exoskeletons and Active Orthoses: Challenges and State-of-the-Art," *IEEE Transactions on Robotics*, vol. 24, no. 1, pp. 144–158, 2008.

[23] S. J. Zaroodny, *BUMPUSHER - A POWERED AID TO LOCOMOTION*. Defense Technical Information Center, 1963.

[24] J. A. Moore and L. A. N. Laboratory, *PITMAN, a Powered Exoskeletal Suit for the Infantryman*. Los Alamos National Laboratory, 1986.

[25] R. A. Heinlein, *Starship Troopers*. 1959.

[26] E. Garcia, J. Sater, and J. Main, "Exoskeletons for human performance augmentation (EHPA): A program summary," *Journal of the Robotics Society of Japan*, vol. 20, no. 8, pp. 822–826, 2002.

[27] US Army Center for Army Lessons Learned, “The Modern Warrior’s Combat Load,” US Army Center for Army Lessons Learned, 2003.

[28] J. Bachkosky, M. Andrews, R. Douglass, J. Feigley, L. Felton, F. Fernandez, P. Fratarangelo, A. Johnson-Winegar, R. Kohn, N. Polmar, and others, “Lightening the load,” DTIC Document, 2007.

[29] “Weight of War: Gear that protects troops also injures them,” *The Seattle Times*.

[30] S. P. Cohen, C. Brown, C. Kurihara, A. Plunkett, C. Nguyen, and S. A. Strassels, “Diagnoses and factors associated with medical evacuation and return to duty among nonmilitary personnel participating in military operations in Iraq and Afghanistan,” *CMAJ*, vol. 183, no. 5, pp. E289–E295, Mar. 2011.

[31] J. Knapik, E. Harman, and K. Reynolds, “Load carriage using packs: A review of physiological, biomechanical and medical aspects,” *Applied Ergonomics*, vol. 27, no. 3, pp. 207–216, Jun. 1996.

[32] J. J. Knapik, K. L. Reynolds, and E. Harman, “Soldier load carriage: historical, physiological, biomechanical, and medical aspects,” *Mil Med*, vol. 169, no. 1, pp. 45–56, Jan. 2004.

[33] S. Karlin, “Raytheon Sarcos’s Exoskeleton Nears Production,” 29-Jul-2011. [Online]. Available: http://spectrum.ieee.org/at-work/innovation/raytheon-sarcoss-exoskeleton-nears-production. [Accessed: 09-Nov-2015].

[34] “Raytheon’s Sarcos XOS 2 military exoskeleton just does the heavy lifting -- for now,” *Engadget*. [Online]. Available: http://www.engadget.com/2010/09/28/raytheons-sarcos-xos-2-military-exoskeleton-just-does-the-heavy/. [Accessed: 09-Nov-2015].

[35] “Raytheon XOS 2 Exoskeleton, Second-Generation Robotics Suit,” *Army Technology*. [Online]. Available: http://www.army-technology.com/projects/raytheon-xos-2-exoskeleton-us/. [Accessed: 09-Nov-2015].

[36] E. Guizzo and H. Goldstein, “The rise of the body bots [robotic exoskeletons],” *IEEE Spectrum*, vol. 42, no. 10, pp. 50–56, Oct. 2005.

[37] H. Herr, “Exoskeletons and orthoses: classification, design challenges and future directions,” *Journal of NeuroEngineering and Rehabilitation*, vol. 6, no. 1, p. 21, Jun. 2009.

[38] L. M. Mooney, E. J. Rouse, and H. M. Herr, “Autonomous exoskeleton reduces metabolic cost of human walking during load carriage,” *Journal of NeuroEngineering and Rehabilitation*, vol. 11, no. 1, p. 80, May 2014.

[39] A. Blaszczak-Boxe, “Bionic Exoskeleton Could Help Paralyzed Patients Walk,” *LiveScience.com*. [Online]. Available: http://www.livescience.com/47353-robot-exosuit-helps-paralyzed-move.html. [Accessed: 09-Nov-2015].

[40] S. Viteckova, P. Kutilek, and M. Jirina, “Wearable lower limb robotics: A review,” *Biocybernetics and Biomedical Engineering*, vol. 33, no. 2, pp. 96–105, 2013.

[41] A. Zoss, H. Kazerooni, and A. Chu, “On the mechanical design of the Berkeley Lower Extremity Exoskeleton (BLEEX),” in *2005 IEEE/RSJ International Conference on Intelligent Robots and Systems, 2005. (IROS 2005)*, 2005, pp. 3465–3472.

[42] H. Kazerooni, A. Zoss, “Architecture and Hydraulics of a Lower Extremity Exoskeleton,” 2005.

[43] “Kickstart by Cadence Biomedical,” *Kickstart Walking System*. [Online]. Available: http://www.cadencebiomedical.com/. [Accessed: 13-Oct-2013].

[44] “Cadence Biomedical Nets $1M, Loads of Press, for Walk-Assist Device,” *Xconomy*. [Online]. Available: http://www.xconomy.com/seattle/2013/05/30/cadence-biomedical-pulls-in-1m-from-military-for-walk-assist-device/. [Accessed: 13-Oct-2013].

[45] C. J. Walsh, K. Endo, and H. Herr, “A quasi-passive leg exoskeleton for load-carrying augmentation,” *International Journal of Humanoid Robotics*, vol. 4, no. 03, pp. 487–506, 2007.

[46] A. Danielsson and K. S. Sunnerhagen, “Oxygen consumption during treadmill walking with and without body weight support in patients with hemiparesis after stroke and in healthy subjects,” *Archives of Physical Medicine and Rehabilitation*, vol. 81, no. 7, pp. 953–957, Jul. 2000.

[47] J. S. Gottschall and R. Kram, “Energy cost and muscular activity required for propulsion during walking,” *Journal of Applied Physiology*, vol. 94, no. 5, pp. 1766–1772, May 2003.

[48] M. Frey, G. Colombo, M. Vaglio, R. Bucher, M. Jorg, and R. Riener, “A Novel Mechatronic Body Weight Support System,” *IEEE Transactions on Neural Systems and Rehabilitation Engineering*, vol. 14, no. 3, pp. 311–321, Sep. 2006.

[49] “Ortho Rehabilitation Treadmill with AlterG,” *AlterG*. [Online]. Available: http://www.alterg.com/products/anti-gravity-treadmills/m320-f320/professional-pt. [Accessed: 09-Nov-2015].

[50] M. A. Scott, A. E. Kilding, “A Kinematic Comparison of Deep Water Running and Overground Running in Endurance Runners,” *Journal of strength and conditioning research / National Strength & Conditioning Association*, vol. 21, no. 2, pp. 476–80, 2007.

[51] T. Reilly, C. N. Dowzer, and N. T. Cable, “The physiology of deep-water running,” *J Sports Sci*, vol. 21, no. 12, pp. 959–972, Dec. 2003.

[52] G. L. Killgore, “A biomechanical and physiological comparison of deep-water running styles,” Jul. 2003.

[53] M. Rutland, D. O’Connell, J.-M. Brismée, P. Sizer, G. Apte, and J. O’Connell, “Evidence-Supported Rehabilitation Of Patellar Tendinopathy,” *N Am J Sports Phys Ther*, vol. 5, no. 3, pp. 166–178, Sep. 2010.

[54] G. J. Salem, R. Salinas, and F. V. Harding, “Bilateral kinematic and kinetic analysis of the squat exercise after anterior cruciate ligament reconstruction1,” *Archives of Physical Medicine and Rehabilitation*, vol. 84, no. 8, pp. 1211–1216, Aug. 2003.

[55] CFCF, *Anatomical Planes*. 2014.

[56] Osteomyoamare, *English: Profile showing anatomical directions, made in microsoft word*. 21AD.

[57] C. L. Riegger, “Anatomy of the Ankle and Foot,” *PHYS THER*, vol. 68, no. 12, pp. 1802–1814, Dec. 1988.

[58] Y. Jun, “Morphological analysis of the human knee joint for creating custom-made implant models,” *Int J Adv Manuf Technol*, vol. 52, no. 9–12, pp. 841–853, Jun. 2010.

[59] “What is the ACL? | The Knee.” [Online]. Available: http://www.theknee.com/acl-anterior-cruciate-ligament/what-is-the-acl-anterior-cruciate-ligament/. [Accessed: 09-Nov-2015].

[60] B. J. Schoenfeld, “Squatting kinematics and kinetics and their application to exercise performance,” *J Strength Cond Res*, vol. 24, no. 12, pp. 3497–3506, Dec. 2010.

[61] Everkinetic, *parallel squat*. 2010.

[62] S. M. Smith, R. A. Cockburn, A. Hemmerich, R. M. Li, and U. P. Wyss, “Tibiofemoral joint contact forces and knee kinematics during squatting,” *Gait & Posture*, vol. 27, no. 3, pp. 376–386, Apr. 2008.

[63] R. F. Escamilla, G. S. Fleisig, T. M. Lowry, S. W. Barrentine, and J. R. Andrews, “A three-dimensional biomechanical analysis of the squat during varying stance widths,” *Med Sci Sports Exerc*, vol. 33, no. 6, pp. 984–998, Jun. 2001.

[64] D. E. Toutoungi, T. W. Lu, A. Leardini, F. Catani, and J. J. O’Connor, “Cruciate ligament forces in the human knee during rehabilitation exercises,” *Clinical Biomechanics*, vol. 15, no. 3, pp. 176–187, Mar. 2000.

[65] D. R. Bell, D. A. Padua, and M. A. Clark, “Muscle Strength and Flexibility Characteristics of People Displaying Excessive Medial Knee Displacement,” *Archives of Physical Medicine and Rehabilitation*, vol. 89, no. 7, pp. 1323–1328, Jul. 2008.

[66] R.-R. Lu, F. Li, Y. Wu, Y.-S. Hu, X.-L. Xu, R.-L. Zou, and X.-F. Hu, “Demonstration of posturographic parameters of squat-stand activity in hemiparetic patients on a new multi-utility balance assessing and training system,” *J Neuroeng Rehabil*, vol. 10, p. 37, Apr. 2013.

[67] P. Wretenberg, Y. Feng, F. Lindberg, and U. P. Arboreilus, “Joint moments of force and quadriceps muscle activity during squatting exercise,” *Scandinavian Journal of Medicine & Science in Sports*, vol. 3, no. 4, pp. 244–250, Dec. 1993.

[68] S. Hwang, Y. Kim, and Y. Kim, “Lower extremity joint kinetics and lumbar curvature during squat and stoop lifting,” *BMC Musculoskeletal Disorders*, vol. 10, no. 1, p. 15, Feb. 2009.

[69] A. C. Fry, J. C. Smith, and B. K. Schilling, “Effect of knee position on hip and knee torques during the barbell squat,” *J Strength Cond Res*, vol. 17, no. 4, pp. 629–633, Nov. 2003.

[70] G. Eom, J. Kim, B. Park, J. Hong, S. Chung, B. Lee, G. Tack, and Y. Kim, “Postural Sway of the Elderly Males and Females during Quiet Standing and Squat-and-Stand Movement,” in *13th International Conference on Biomedical Engineering*, C. T. Lim and J. C. H. Goh, Eds. Springer Berlin Heidelberg, 2009, pp. 1814–1816.

[71] P. Beater, *Pneumatic Drives*. Berlin, Heidelberg: Springer Berlin Heidelberg, 2007.

[72] J. Rose and J. G. Gamble, *Human walking*. Williams & Wilkins, 1994.

[73] Y. P. Ivanenko, R. Grasso, V. Macellari, and F. Lacquaniti, “Control of Foot Trajectory in Human Locomotion: Role of Ground Contact Forces in Simulated Reduced Gravity,” *Journal of Neurophysiology*, vol. 87, no. 6, pp. 3070–3089, Jun. 2002.

[74] R. af Klint, N. Mazzaro, J. B. Nielsen, T. Sinkjaer, and M. J. Grey, “Load Rather Than Length Sensitive Feedback Contributes to Soleus Muscle Activity During Human Treadmill Walking,” *Journal of Neurophysiology*, vol. 103, no. 5, pp. 2747–2756, May 2010.

[75] P. de Leva, “Adjustments to Zatsiorsky-Seluyanov’s segment inertia parameters,” *J Biomech*, vol. 29, no. 9, pp. 1223–1230, Sep. 1996.

[76] S. Flanagan, G. J. Salem, M.-Y. Wang, S. E. Sanker, and G. A. Greendale, “Squatting Exercises in Older Adults: Kinematic and Kinetic Comparisons,” *Med Sci Sports Exerc*, vol. 35, no. 4, pp. 635–643, Apr. 2003.

[77] J. W. Chow, W. Chae, “Tibiofemoral Joint Forces During The Landing Phase Of Different Types of Vertical Jump.”

[78] J. Ekholm, R. Nisell, U. P. Arborelius, C. Hammerberg, and G. Németh, “Load on knee joint structures and muscular activity during lifting,” *Scand J Rehabil Med*, vol. 16, no. 1, pp. 1–9, 1984.

[79] R. Nisell, “Mechanics of the knee. A study of joint and muscle load with clinical applications,” *Acta Orthop Scand Suppl*, vol. 216, pp. 1–42, 1985.

[80] S. Almosnino, D. Kingston, and R. B. Graham, “Three-dimensional knee joint moments during performance of the bodyweight squat: effects of stance width and foot rotation,” *J Appl Biomech*, vol. 29, no. 1, pp. 33–43, Feb. 2013.

[81] T. Grund, I. Reihl, T. Krosshaug, V. Senner, and K. Gruber, “Calculation of ankle and knee joint moments during ACL-injury situations in soccer,” *Procedia Engineering*, vol. 2, no. 2, pp. 3255–3261, Jun. 2010.

[82] J. Petersen, R. O. Nielsen, S. Rasmussen, and H. Sørensen, "Comparisons of increases in knee and ankle joint moments following an increase in running speed from 8 to 12 to 16 km·h− 1," *Clinical Biomechanics*, vol. 29, no. 9, pp. 959–964, Nov. 2014.

[83] B. T. Bates, K. J. Simpson, "The Effects of Running Speed on Lower Extremity Joint Moments Generated During the Support Phase," *Human Kinetics Journals*, 21-Apr-2010. [Online]. Available: http://journals.humankinetics.com/jab-back-issues/jabvolume6issue3august/theeffectsofrunningspeedonlowerextremityjointmomentsgeneratedduringthesupportphase. [Accessed: 24-Nov-2015].

[84] T. Nagura, C. O. Dyrby, E. J. Alexander, and T. P. Andriacchi, "Mechanical loads at the knee joint during deep flexion," *J. Orthop. Res.*, vol. 20, no. 4, pp. 881–886, Jul. 2002.

[85] R. F. Escamilla, "Knee biomechanics of the dynamic squat exercise," *Med Sci Sports Exerc*, vol. 33, no. 1, pp. 127–141, Jan. 2001.

[86] J. P. Pollard, W. L. Porter, and M. S. Redfern, "Forces and moments on the knee during kneeling and squatting," *J Appl Biomech*, vol. 27, no. 3, pp. 233–241, Aug. 2011.

APPENDICES

APPENDIX A. METHODS—ADDITIONAL MATERIAL

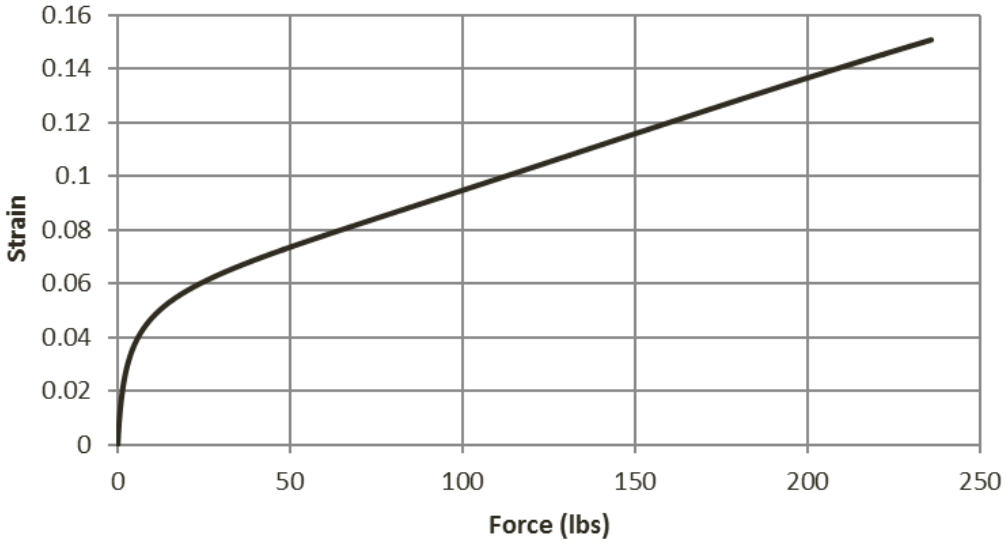

Figure 51. Force-strain curve of the rope used by the apparatus to apply tension to the harness worn by the user.

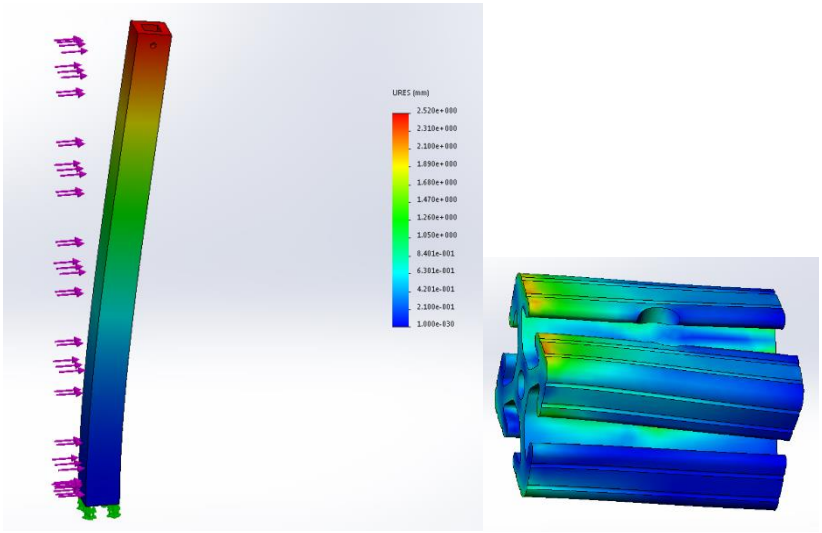

Figure 52. Stress analysis of apparatus components.

Table 7. Adjustments to Zatsiorsky, et al.'s body segment parameters by de Leva, adapted from [75].

	Endpoints		Longitudinal length (mm)		Mass* (%)		Longitudinal CM position (%)		Sagittal r (%)		Transverse r (%)		Longitudinal r (%)	
Segment	Origin	Other	F	M	F§	M¶	F	M	F	M	F	M	F	M
Head	VERT†	MIDG†	200.2	203.3	6.68	6.94	58.94	59.76	33.0	36.2	35.9	37.6	31.8	31.2
Trunk	SUPR†	MIDH‡	529.3	531.9	42.57	43.46	41.51	44.86	35.7	37.2	33.9	34.7	17.1	19.1
UPT	SUPR†	XYPH†	142.5	170.7	15.45	15.96	20.77	29.99	74.6	71.6	50.2	45.4	71.8	65.9
MPT*	XYPH†	OMPH†	205.3	215.5	14.65	16.33	45.12	45.02	43.3	48.2	35.4	38.3	41.5	46.8
LPT	OMPH†	MIDH‡	181.5	145.7	12.47	11.17	49.20	61.15	43.3	61.5	40.2	55.1	44.4	58.7
Upper arm	SJC‡	EJC‡	275.1	281.7	2.55	2.71	57.54	57.72	27.8	28.5	26.0	26.9	14.8	15.8
Forearm	EJC‡	WJC‡	264.3	268.9	1.38	1.62	45.59	45.74	26.1	27.6	25.7	26.5	9.4	12.1
Hand	WJC‡	MET3†	78.0	86.2	0.56	0.61	74.74	79.00	53.1	62.8	45.4	51.3	33.5	40.1
Thigh	HJC‡	KJC‡	368.5	422.2	14.78	14.16	36.12	40.95	36.9	32.9	36.4	32.9	16.2	14.9
Shank	KJC‡	LMAL†	432.3	434.0	4.81	4.33	44.16	44.59	27.1	25.5	26.7	24.9	9.3	10.3
Foot*	HEEL†	TTIP†	228.3	258.1	1.29	1.37	40.14	44.15	29.9	25.7	27.9	24.5	13.9	12.4
Using alternative endpoints:														
Head*	VERT†	CERV†	243.7	242.9	6.68	6.94	48.41	50.02	27.1	30.3	29.5	31.5	26.1	26.1
Trunk	CERV†	MIDH‡	614.8	603.3	42.57	43.46	49.64	51.38	30.7	32.8	29.2	30.6	14.7	16.9
Trunk	MIDS‡	MIDH‡	497.9	515.5	42.57	43.46	37.82	43.10	37.9	38.4	36.1	35.8	18.2	19.7
UPT*	CERV†	XYPH†	228.0	242.1	15.45	15.96	50.50	50.66	46.6	50.5	31.4	32.0	44.9	46.5
Forearm	EJC‡	STYL†	262.4	266.9	1.38	1.62	45.92	46.08	26.3	27.8	25.9	26.7	9.5	12.2
Hand	WJC†	DAC3†	170.1	187.9	0.56	0.61	34.27	36.24	24.4	28.8	20.8	23.5	15.4	18.4
Hand*	STYL†	DAC3‡	172.0	189.9	0.56	0.61	35.02	36.91	24.1	28.5	20.6	23.3	15.2	18.2
Hand	STYL†	MET3†	79.9	88.2	0.56	0.61	75.34	79.48	51.9	61.4	44.3	50.2	32.7	39.2
Shank	KJC‡	AJC‡	438.6	440.3	4.81	4.33	43.52	43.95	26.7	25.1	26.3	24.6	9.2	10.2
Shank	KJC‡	SPHY†	426.0	427.7	4.81	4.33	44.81	45.24	27.5	25.8	27.1	25.3	9.4	10.5

* Not adjusted values.
† Normal projection on the segment longitudinal axis.
‡ Assumed to lay on the segment longitudinal axis.
§ Zatsiorsky *et al.* (1990a).
¶ Zatsiorsky *et al.* (1990b, 1993).

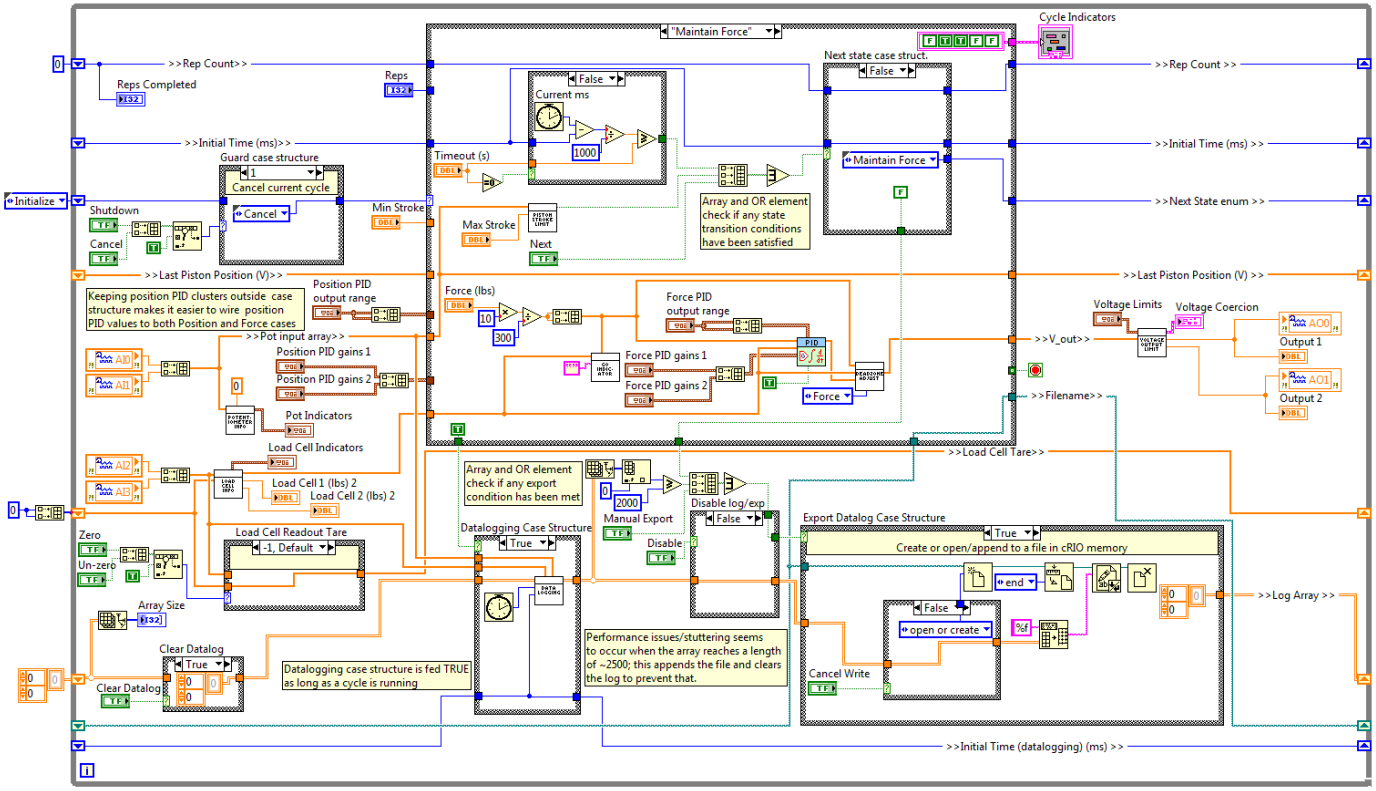

Figure 53. Block diagram of the main LabVIEW VI used to control the apparatus. The program utilized position feedback from potentiometers in the pneumatic cylinders to mediate position control, and force feedback from the load cells to achieve force control, with a PD control scheme. The program logged data from the potentiometers and load cells, providing information on piston stroke and applied load. The program also provided visual feedback to the user based on the measured load in the load cells.

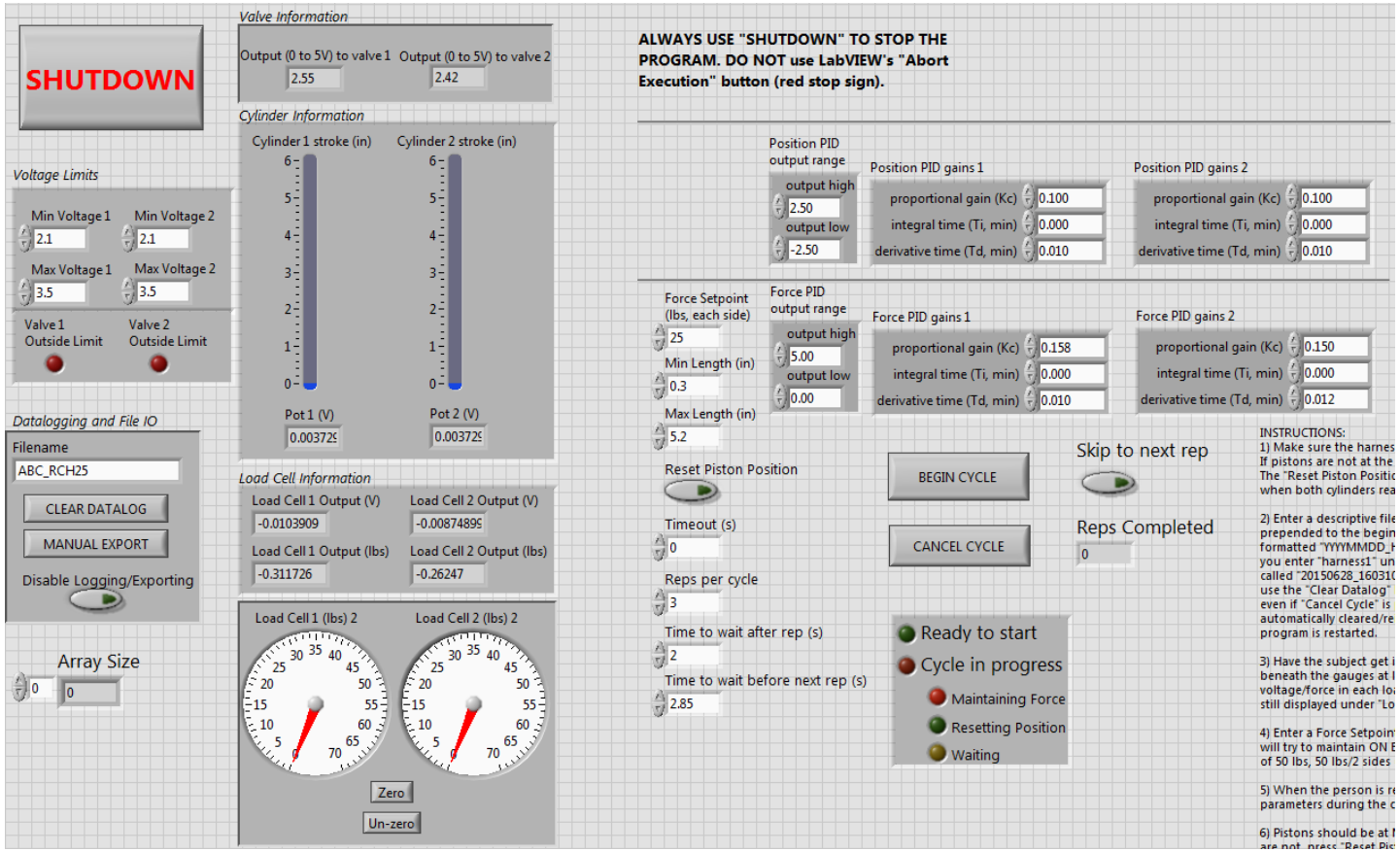

Figure 54. Front panel of the main LabVIEW VI used to control the apparatus. Controls are present enabling the adjustment of maximum force setpoint, PID gains, and other values directly or indirectly related to the speed of the application of force and various system limits.

APPENDIX C. VERIFYING THE FUNCTION OF THE APPARATUS

To ascertain that the apparatus did, in fact, provide vertical force as desired, the GRF was compared to the applied load as measured by the load cells.

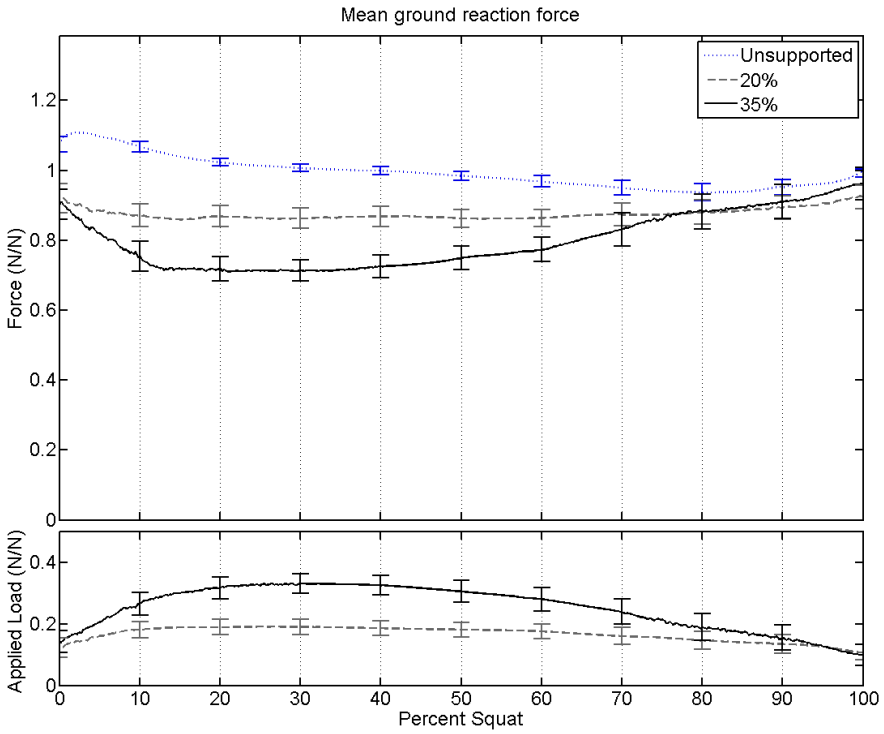

Figure 55. Average GRF and the measured applied load over the course of the squatting motion, normalized to body weight.

Any value recorded by the values ought to be balanced by a commensurate decrease in the GRF, relative to the GRF in the case where no load is applied. As seen in Figure 55, the GRF in the unsupported case was approximately equal to body weight throughout the squat, with some fluctuation due to dynamic effects. In the supported cases, the decrease in GRF was approximately equal to the applied load.

APPENDIX D. GRF AND SAGITTAL PLANE DYNAMICS

As Figure 56 and Table 8 illustrate, the average ground reaction forces across all subjects for both an unsupported and a supported squat act largely in the vertical direction. The components of the GRF along the transverse and sagittal axes translate to 12.9% and 1.2%, respectively, of the component of the GRF along the vertical axis, in line with previous studies on the topic. At the highest level of load support, the components along the transverse and sagittal axes were, similarly, about 13% and 3.3% of the vertical component. This, combined with the fairly small moment arms of body segment centers of mass relative to the CoP in the coronal plane compared to the moment arms in the sagittal plane, suggests that most of the relevant effects occur in the sagittal plane, supporting the validity of a two-dimensional, sagittal plane analysis of a narrow-stance squat.

Table 8. Components of GRF along the different axes with and without load support. Data presented as mean ± SD.

	Unsupported	35% BWS
Transverse axis	0.1267 ± 0.0189	0.1039 ± 0.0159
Sagittal axis	0.0119 ± 0.0018	0.0262 ± 0.0021
Longitudinal (vertical) axis	0.9836 ± 0.0480	0.7879 ± 0.0159

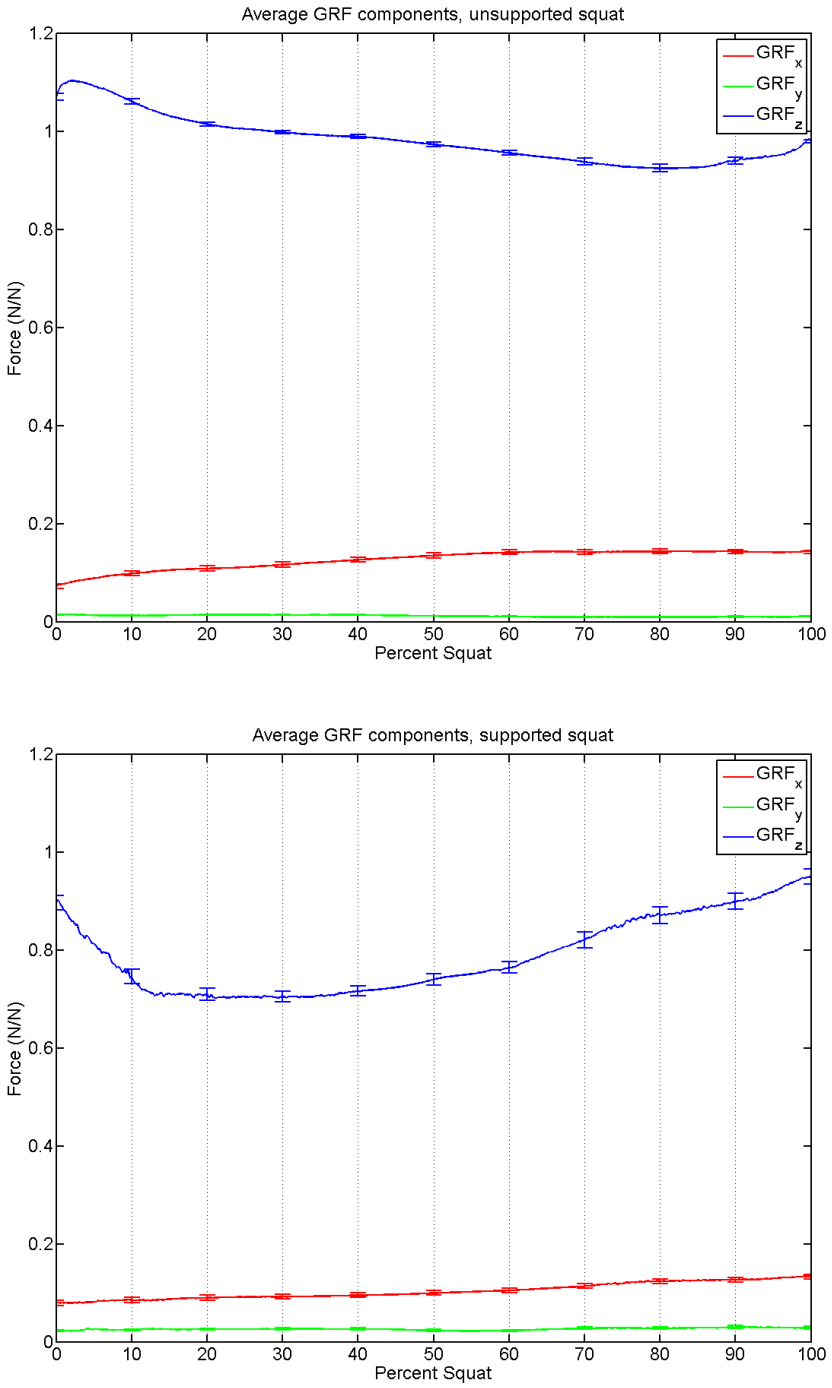

Figure 56. The average component of GRF over the course of the unsupported squat (top) and 35% BW supported squat (bottom) along the *x* (transverse), *y* (sagittal), and *z* (longitudinal/vertical) axes over the course of the squatting motion. Forces have been normalized to body weight.

APPENDIX E. WITHIN-SUBJECTS STATISTICS

Table 9. Results of two-way ANOVA and paired t-tests for ankle moments by subject.

	ANOVA	Paired t-tests		
Subject	All	Unsupported, 20%	Unsupported, 35%	20%, 35%
1	*	*	*	*
2	*	*	*	*
3	*	*	*	*
4	*	*	*	*
5	*	*	*	*
6	*	*	*	*
7	*	*	*	*
8	*	*	*	*

Table 10. Results of two-way ANOVA and paired t-tests for knee moments by subject.

	ANOVA	t-tests		
Subject	All	Unsupported, 20%	Unsupported, 35%	20%, 35%
1	*	*	*	*
2	*	*	*	*
3	*	*	*	*
4	*	†	*	*
5	*	*	*	p = 0.4375
6	*	*	*	*
7	*	*	*	*
8	*	*	*	*

Table 11. Results of two-way ANOVA and paired t-tests for hip moments by subject.

	ANOVA	t-tests		
Subject	All	Unsupported, 20%	Unsupported, 35%	20%, 35%
1	†	*	†	p = 0.2562
2	*	*	p = 0.1085	*
3	*	p = 0.6	*	*
4	*	*	†	*
5	*	*	*	*
6	*	*	*	*
7	*	*	*	†
8	*	*	*	*

** ($p < 0.001$)*
† ($p < 0.05$)

APPENDIX F. REPRESENTATIVE PLOTS OF MOMENTS AND FORCES

For a single representative subject, Figure 57 shows the mean ankle, knee, and hip moments as well as the applied load (these values should be doubled to find the overall moments and load applied to both sides of the body). The joint angles are also plotted to place the forces and moments in the context of the subject's stance. As might be expected, and based on previous studies of joint reaction moments, hip and knee reaction moments were greatest at the bottom of the squat, and declined as the standing position was approached. Also as might be expected, the addition of load support attenuated the peak joint moments. A clearer picture emerged when the concentric (rising) phases of the squats in each trial were isolated, normalized to percent squat phase based on the joint angles, and averaged together, as seen in Figure 58.

Representative plots of the magnitude of the joint reaction forces in supported and unsupported cases for a single subject over the course of a single trial are shown in Figure 59. Representative plots of the magnitude of the joint reaction forces in supported and unsupported cases for a single subject over the course of the concentric (rising) phase of the squat are shown in Figure 60. These figures display the mean of the two sides (these values should be doubled to obtain the total reaction forces and total applied load).

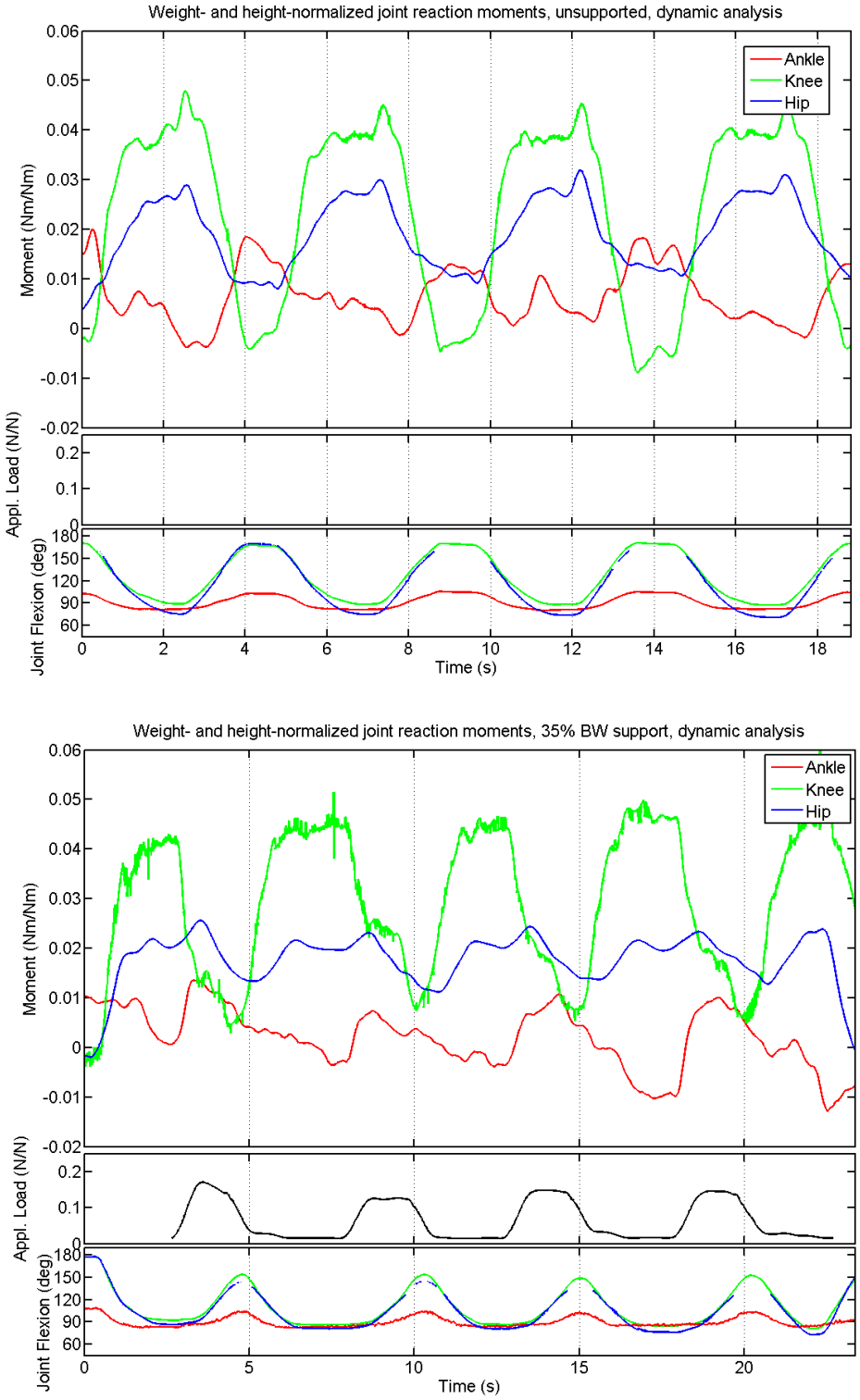

Figure 57. Representative plots of the joint moments, applied load, and joint angles versus time for an unsupported and a supported case for single trials of a single subject. Moments have been normalized by weight and height. Applied load has been normalized by weight.

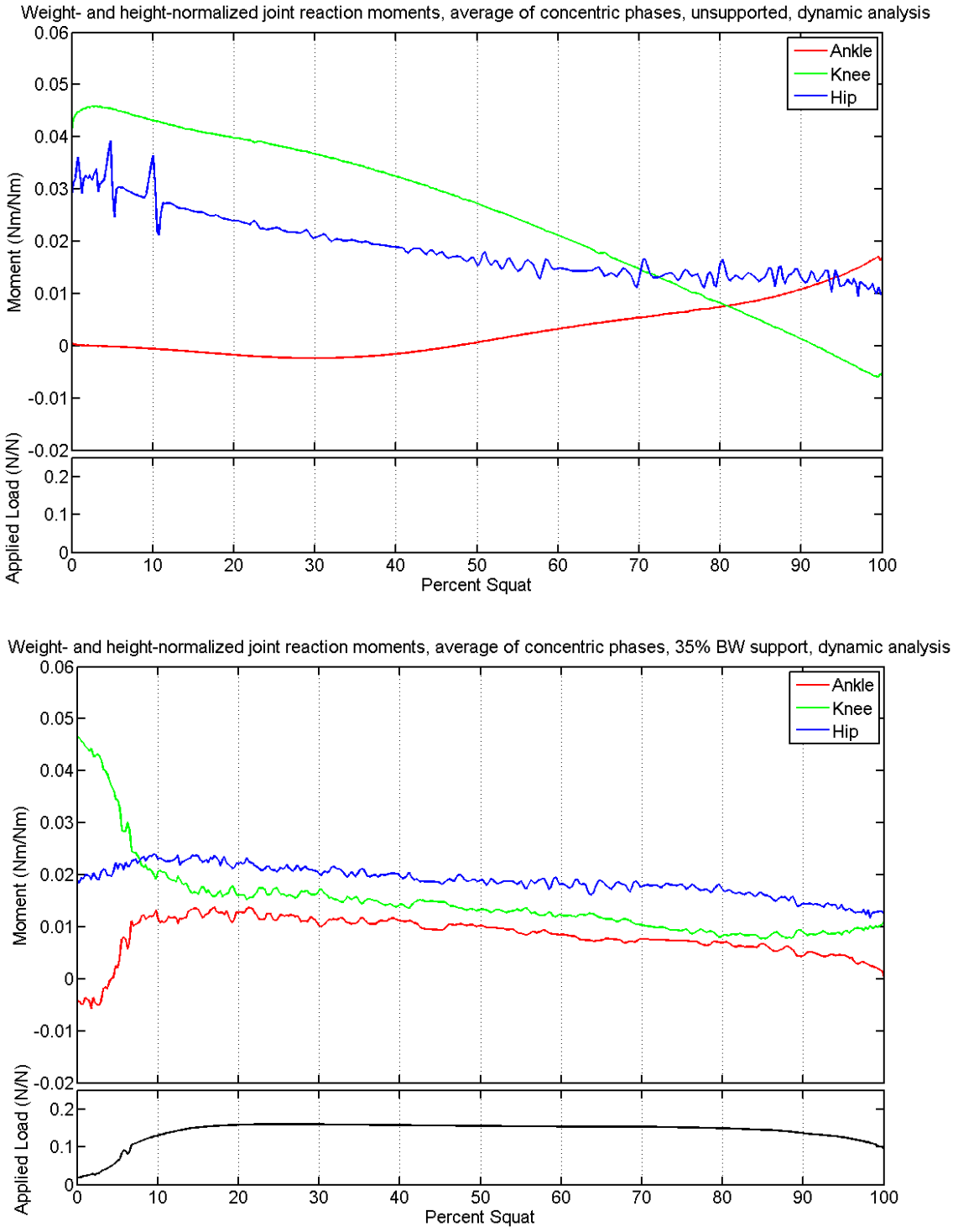

Figure 58. Representative plots of the mean joint moments over the course of the squatting motion without (top) and with (bottom) BWS for single trials of a single subject; to construct these plots, the rising portions of all squats in each respective trial were averaged. Moments have been normalized to body weight and height. Applied load has been normalized to body weight.

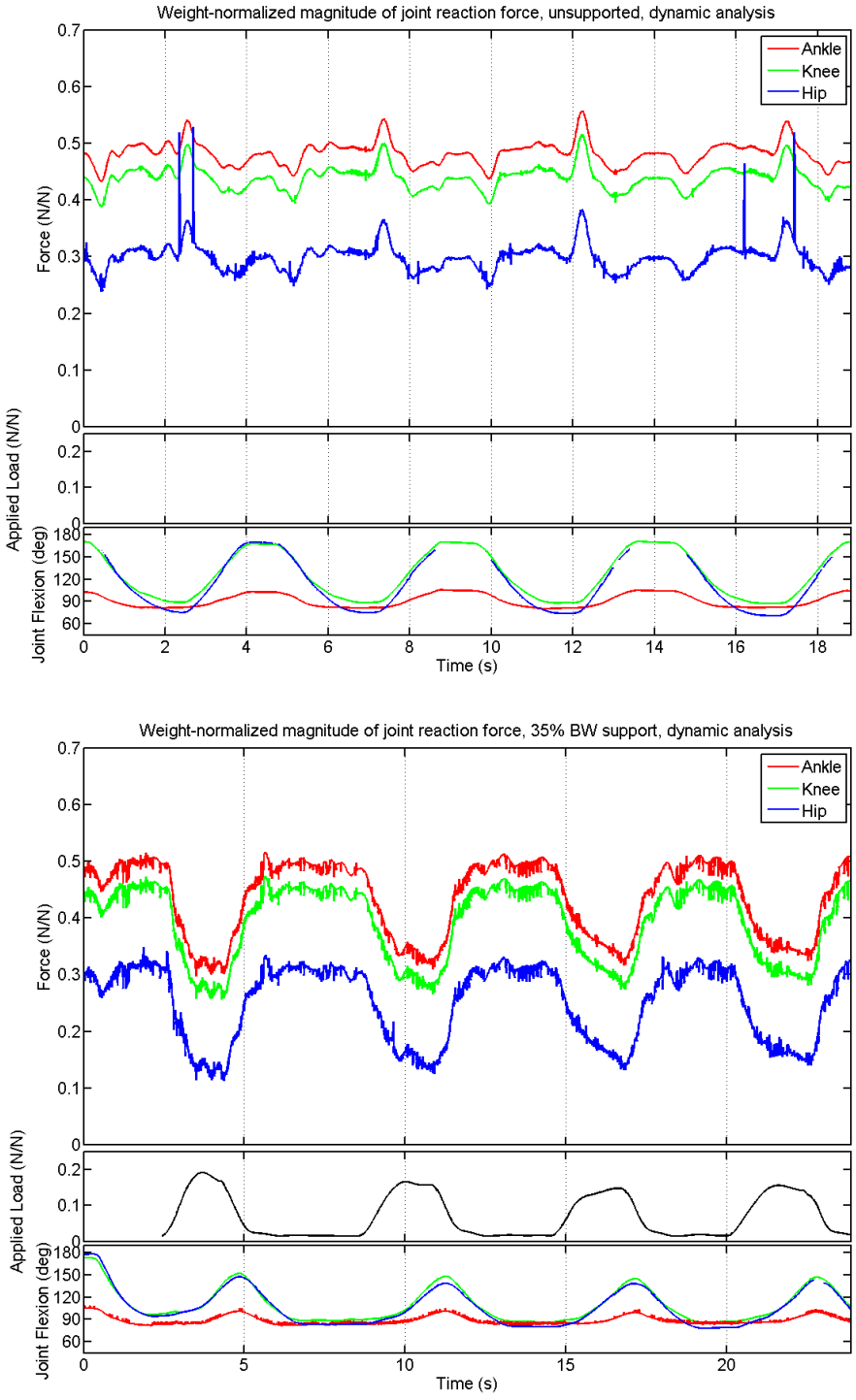

Figure 59. Representative plots of the joint forces, applied load, and joint angles versus time for an unsupported and a supported case for single trials of a single subject. Forces and applied load have been normalized by body weight.

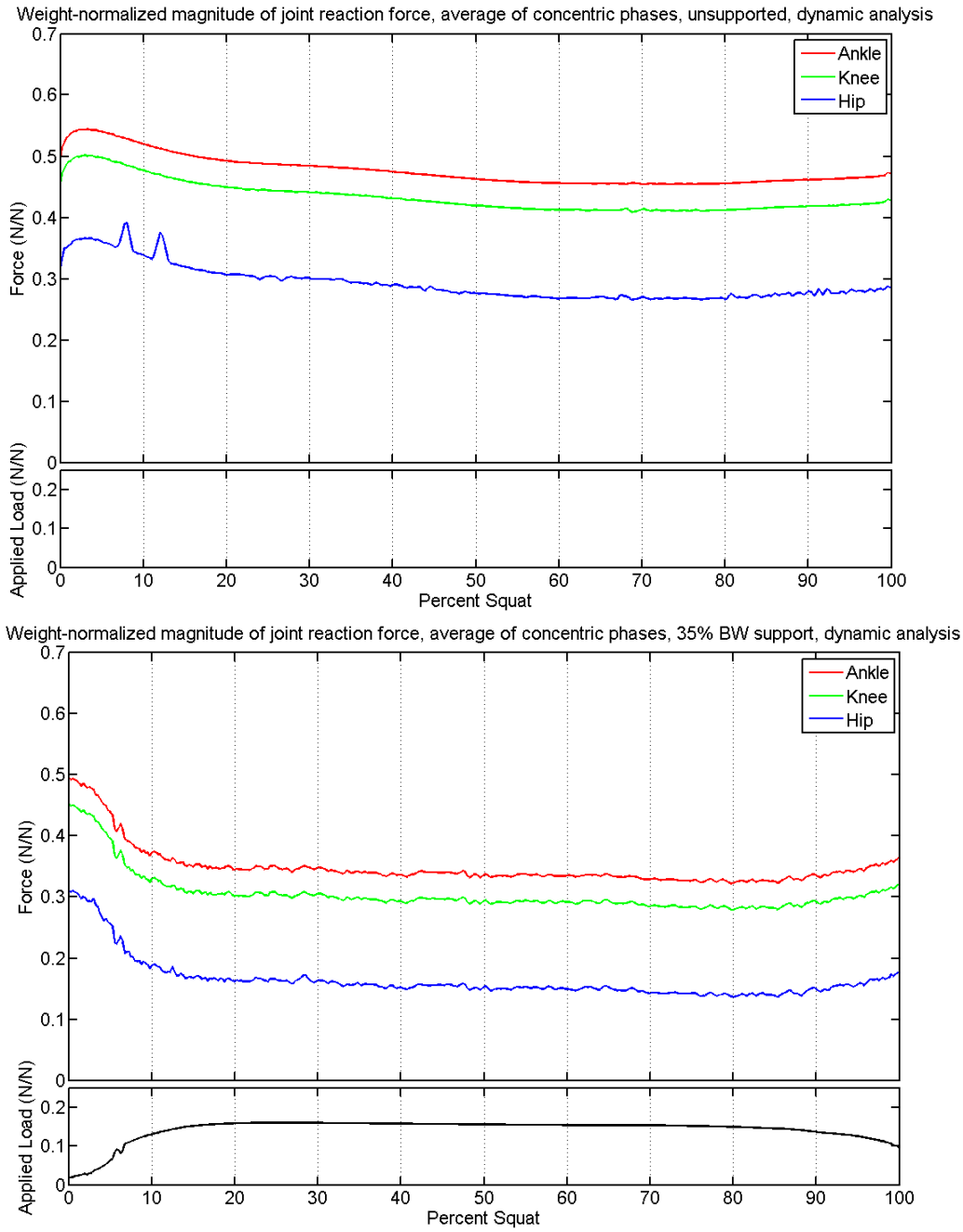

Figure 60. Representative plots of the mean joint forces over the course of the squatting motion without (top) and with (bottom) BWS for single trials of a single subject; to construct these plots, the rising portions of all squats in the respective trials were averaged. Forces and applied load have been normalized to body weight.

APPENDIX G. COMPRESSIVE AND SHEAR FORCES

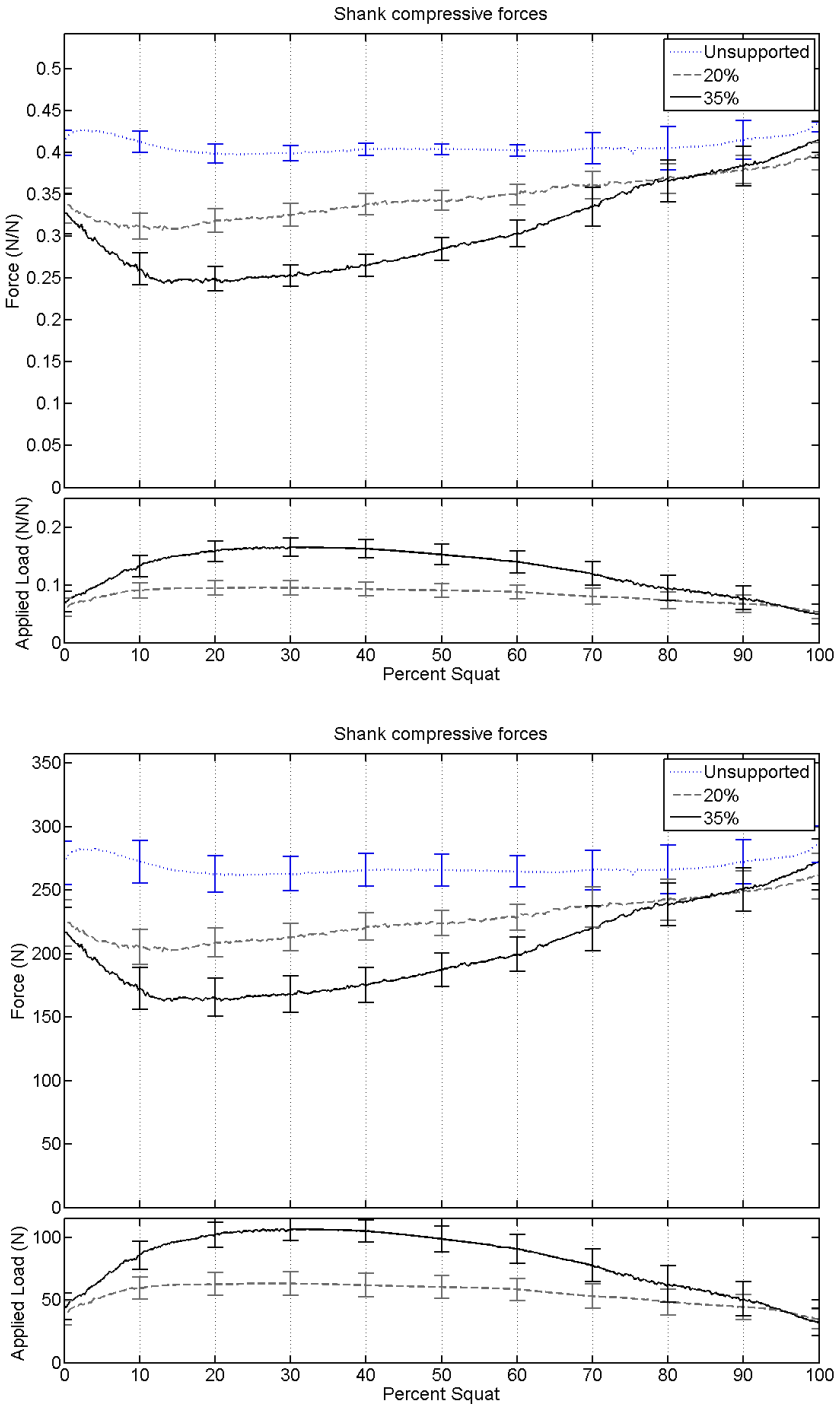

Figure 61. Compressive forces in the shank/tibia at different levels of load support. These plots show forces normalized to body weight (top) and unnormalized (bottom).

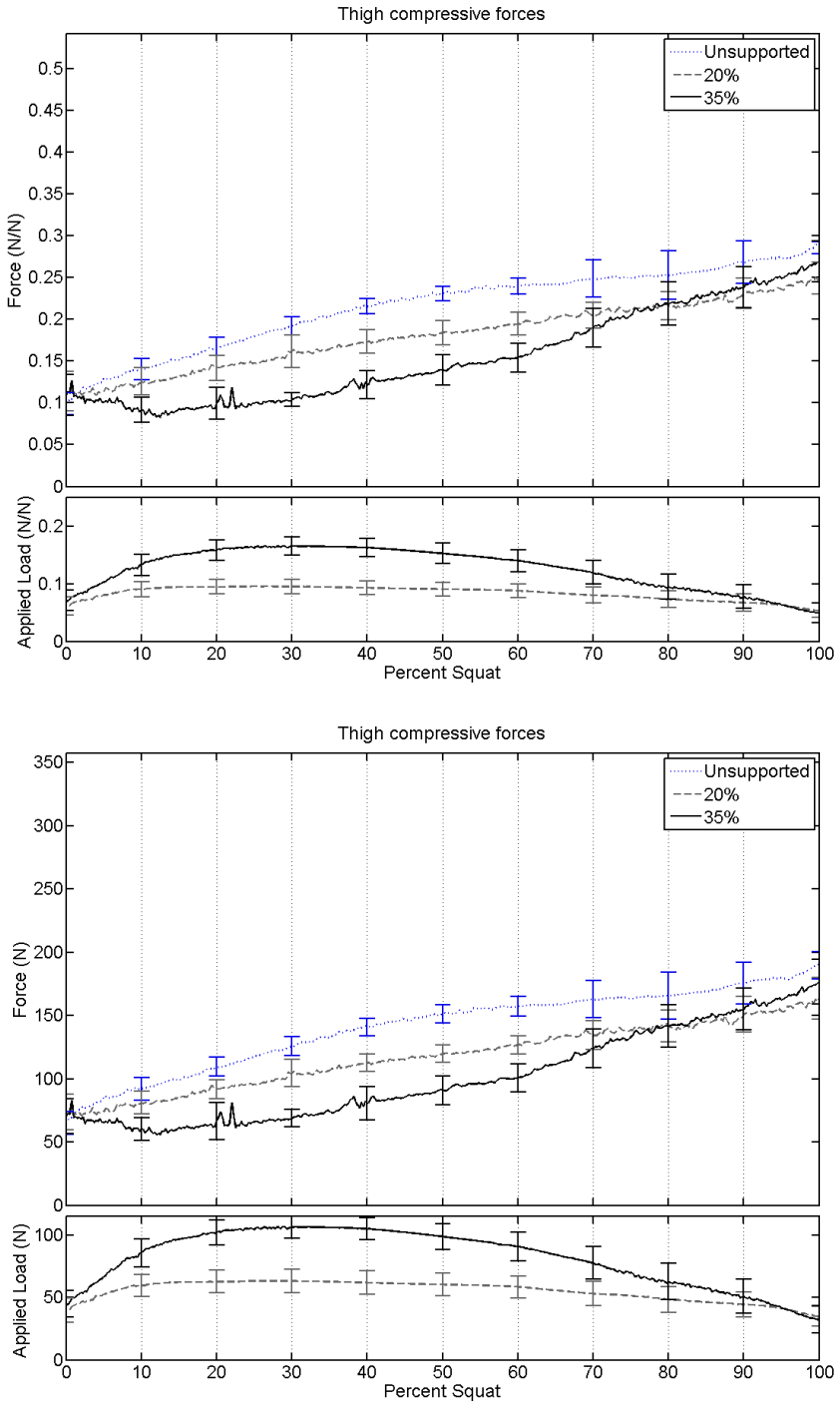

Figure 62. Compressive forces in the thigh/femur at different levels of load support. These plots show forces normalized to body weight (top) and unnormalized (bottom).

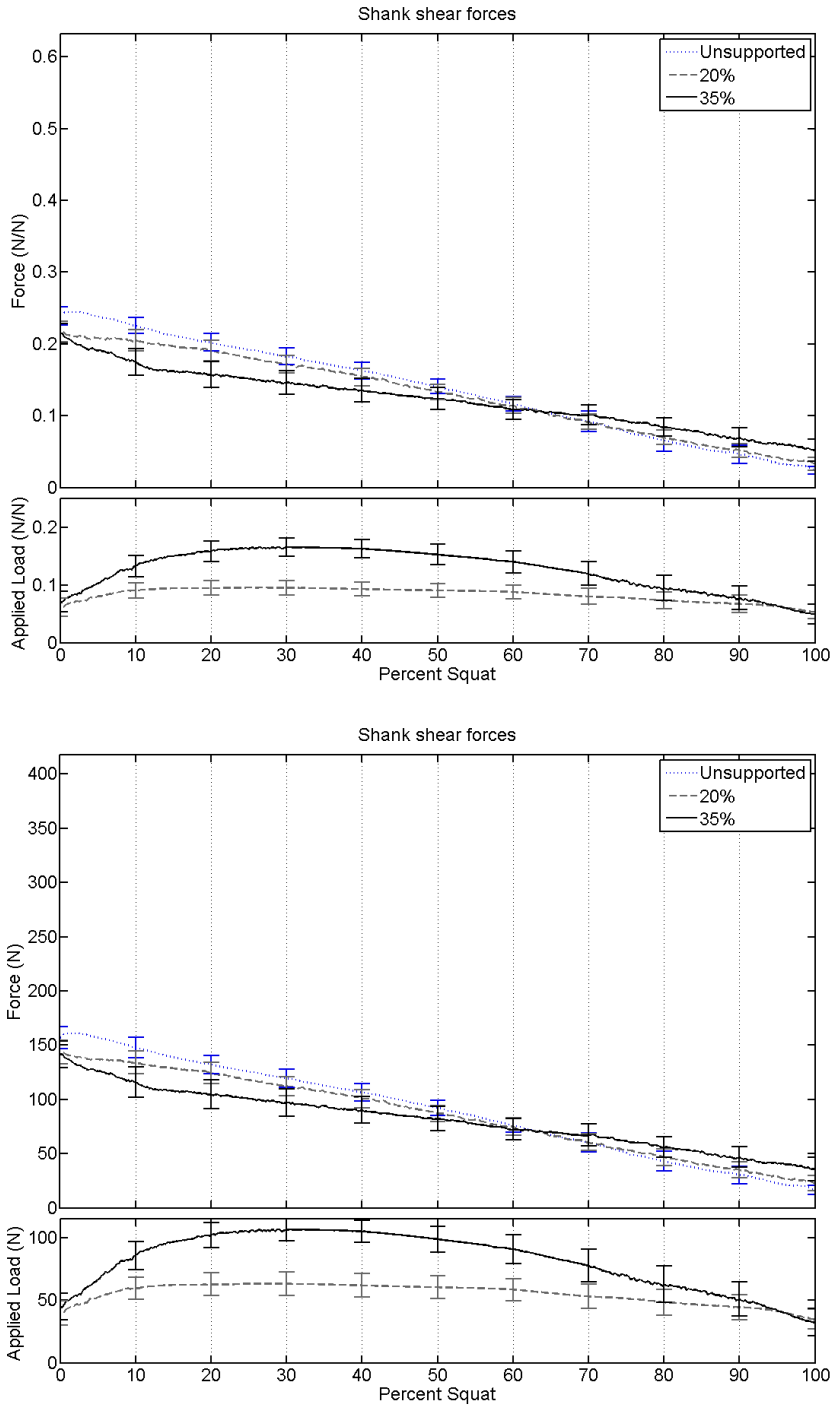

Figure 63. Shear forces in the shank/tibia at different levels of load support. These plots show forces normalized to body weight (top) and unnormalized (bottom).

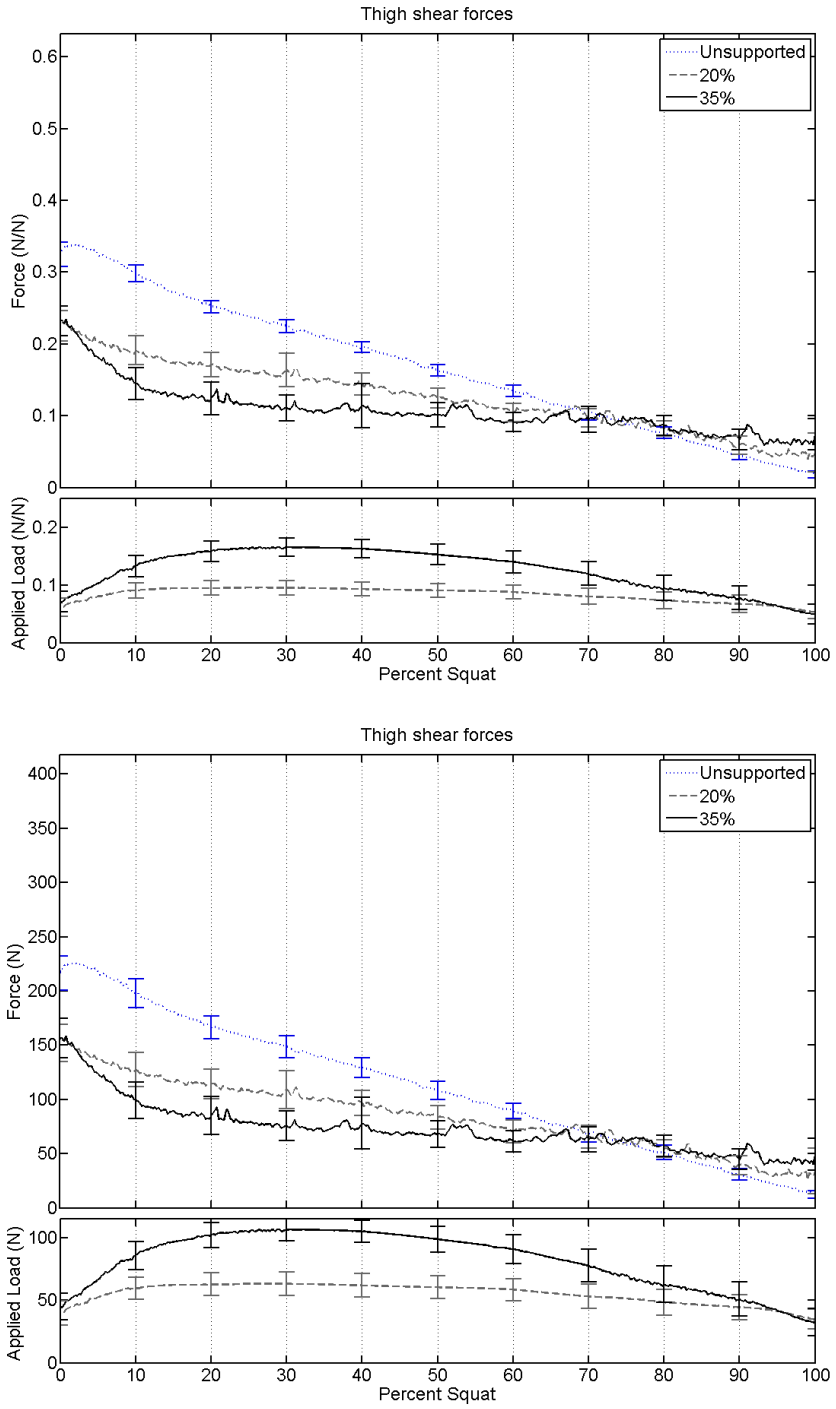

Figure 64. Shear forces in the thigh/femur at different levels of load support. These plots show forces normalized to body weight (top) and unnormalized (bottom).

APPENDIX H. UNNORMALIZED JOINT REACTION FORCES

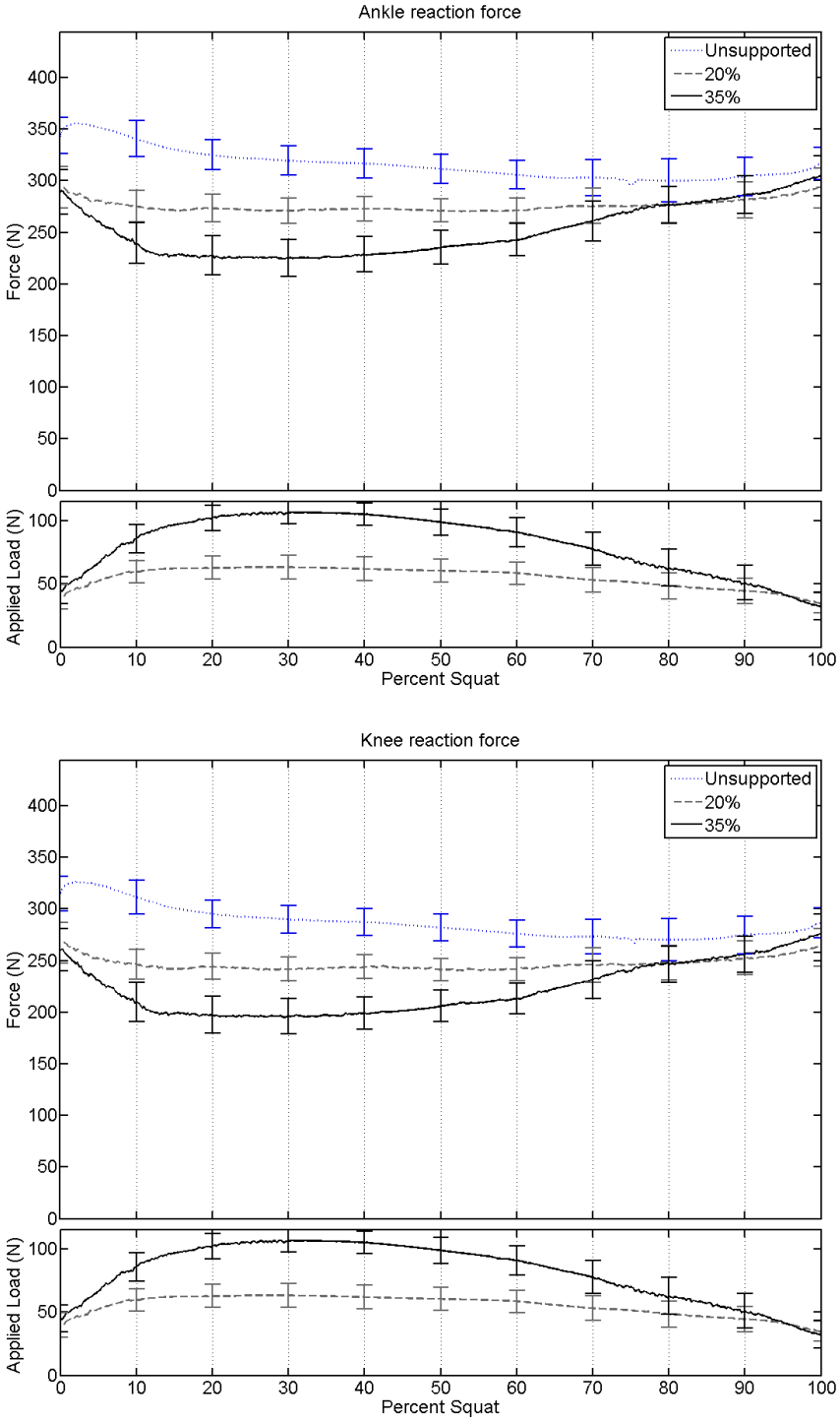

Figure 65. Unnormalized total joint reaction forces. These values were not normalized to subject body weights before being averaged together, and represent the mean magnitudes of the joint reaction forces at the various levels of load support.

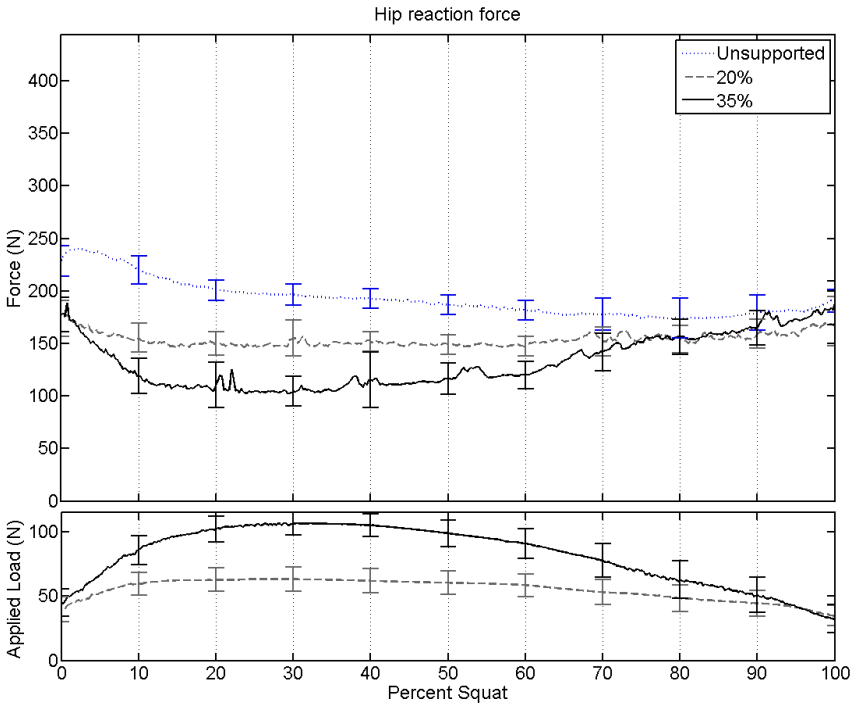

Figure 65. Continued.

APPENDIX I. JOINT AND SEGMENT ANGLES

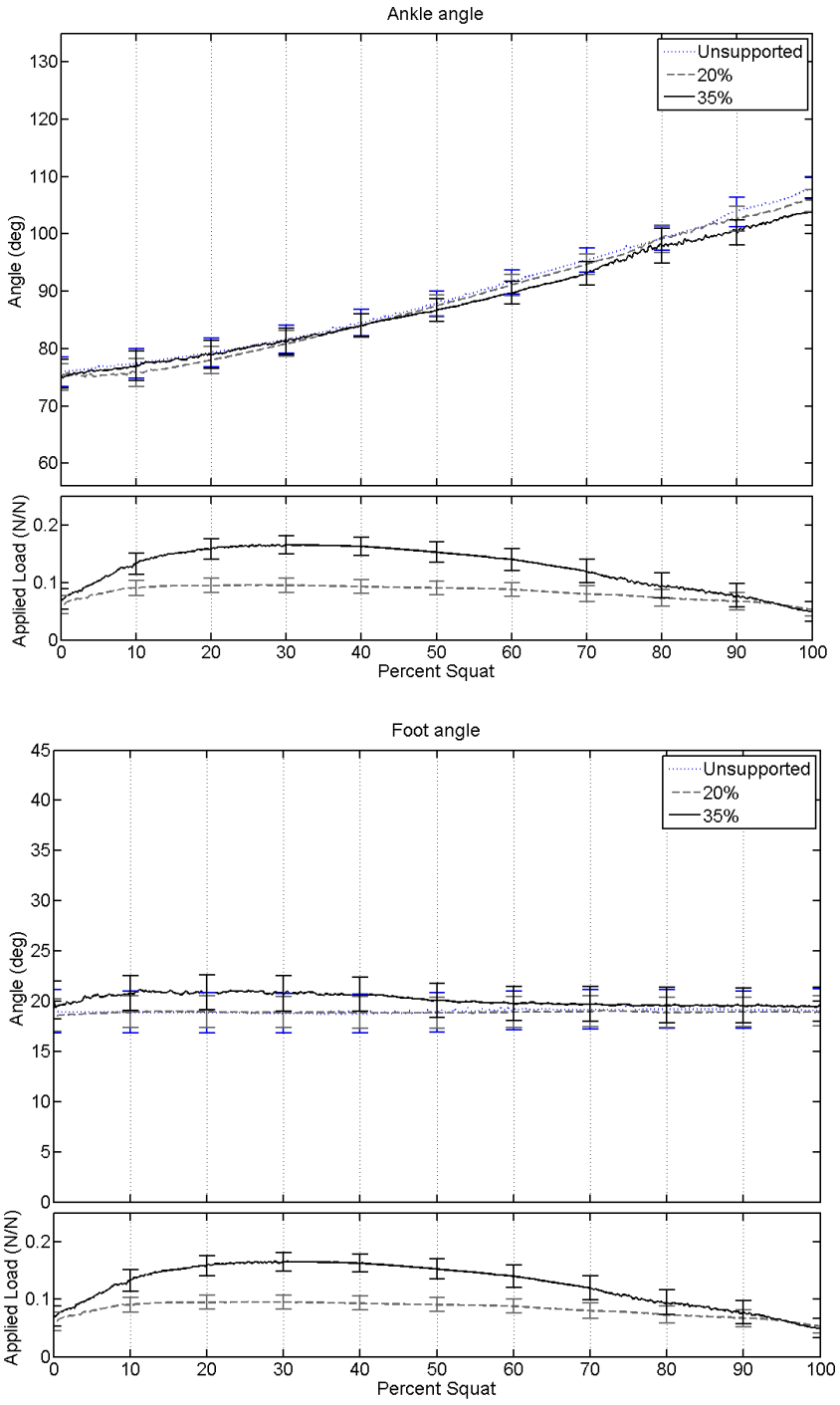

Figure 66. Angles of the foot and ankle over the course of the squat. Ankle angle is measured as the angle between foot and shank. Foot angle is measured as the angle between the horizontal and the line from ankle to base of the middle toe.

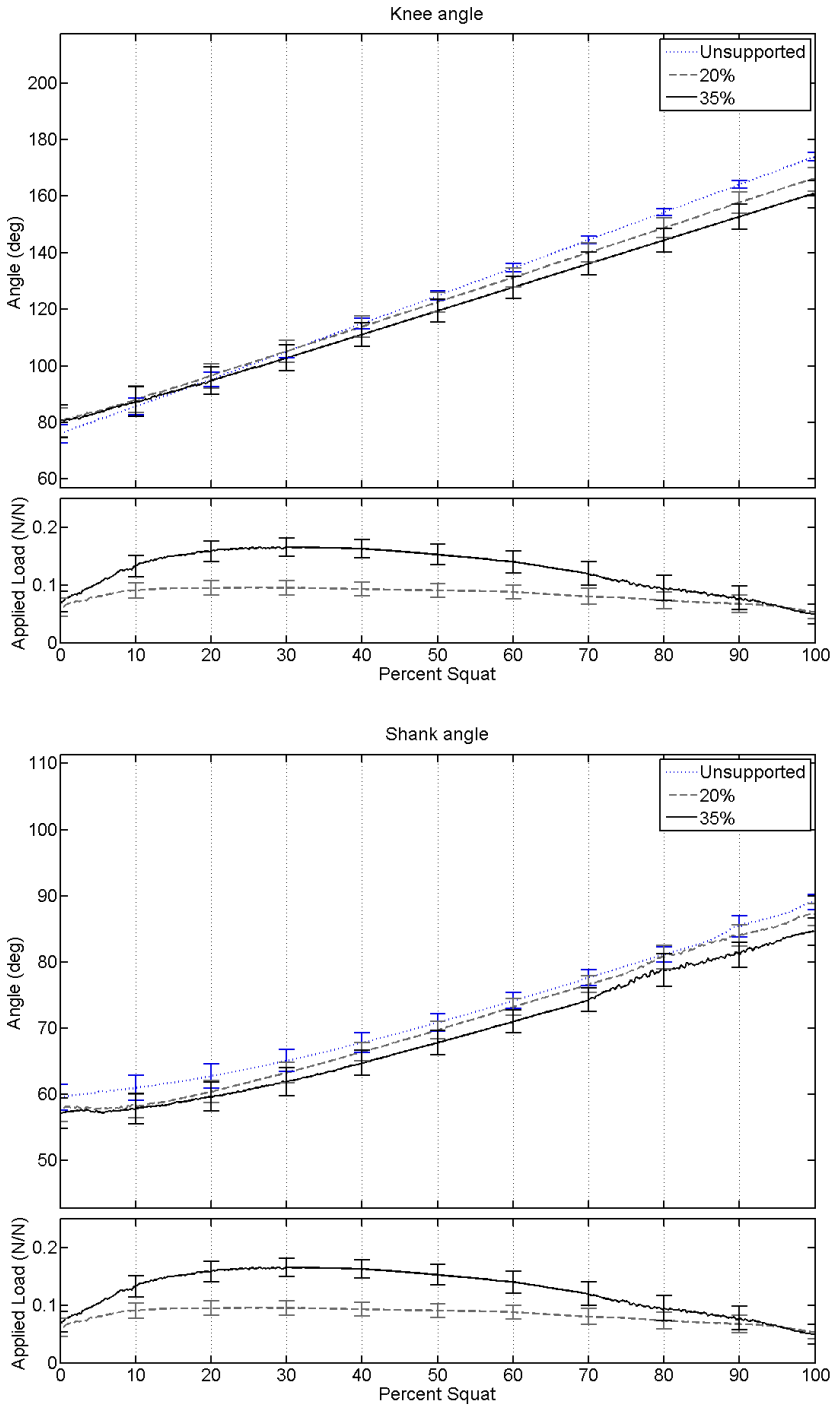

Figure 67. Angles of the knee and shank over the course of the squat. Knee angle is measured as the angle between the shank and the thigh. Shank angle is measured as the angle of the shank with the horizontal.

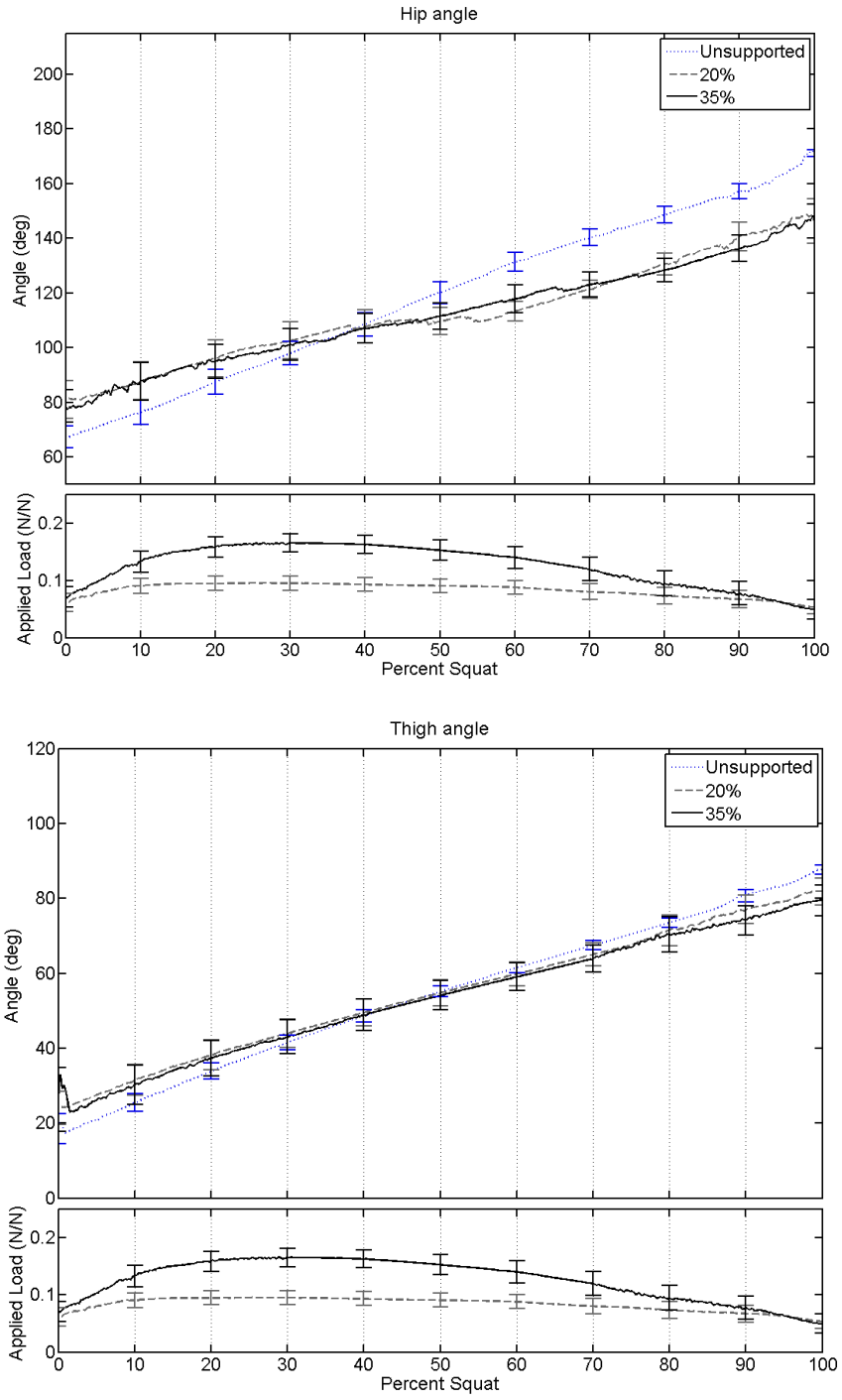

Figure 68. Angles of the hip and thigh over the course of the squat. Hip angle is measured as the angle between the thigh and the trunk. Thigh angle is measured as the angle of the thigh with the horizontal.

APPENDIX J. SUBJECT QUESTIONNAIRE

Subject Questionnaire
Ginina Vitucci
12/15/2014

Did the harness hinder your ability to squat in any way (ex. weight, fit, size, elasticity, rigidity, etc.)?

YES NO

If yes, how?

_____

_____

_____

Comfort – FIT

Circle the position in which you felt most comfortable in the harness.

Box the position in which you felt the least comfortable in the harness.

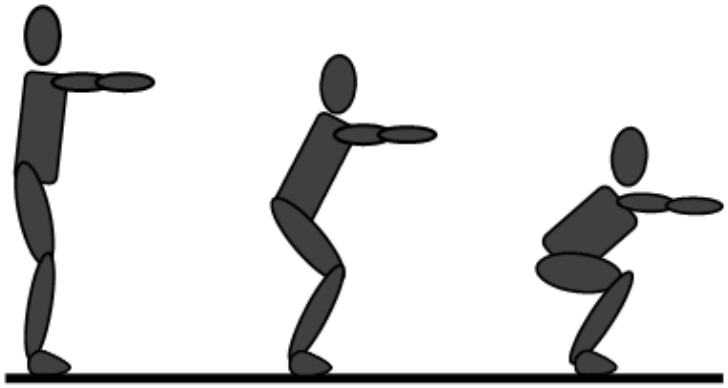

Referring to the figure on the right, how did the fit of the harness in each of these locations change over the duration of the experiment?

1 – Waist	Tighter	Looser	Remained the same
2 – Right hip	Tighter	Looser	Remained the same
3 – Left hip	Tighter	Looser	Remained the same
4 – Right outer thigh	Tighter	Looser	Remained the same
5 – Left outer thigh	Tighter	Looser	Remained the same
6 – Right inner thigh	Tighter	Looser	Remained the same
7 – Left inner thigh	Tighter	Looser	Remained the same

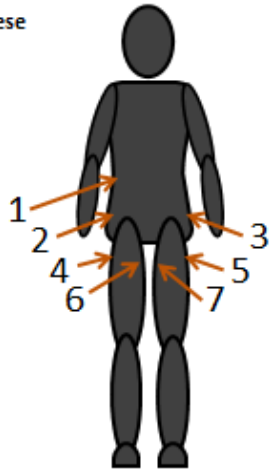

Subject Questionnaire
Ginina Vitucci
12/15/2014

If we hadn't told you, would you have noticed each time the applied load increased?

YES NO

Did the harness slide up your legs, hips, or waist to an uncomfortable point?

YES NO

If yes, when?

20% BW 35% BW

Comfort – FEEL

Would you choose to wear this harness if it enabled you to be more independent?

YES NO

Where would you wear this harness?

At home To school/work Recreationally Only with close family and friends

What is one specific improvement you would like to see in this harness scheme?

_____

_____

_____

How complicated was putting on the harness?

Easy Somewhat easy Acceptable Somewhat difficult Difficult

What was the hardest part of putting on the harness?

_____

_____

_____

Don/Doff

How long did it take you to put the harness on?

1-3 minutes 4-5 minutes 6-7 minutes 8-10 minutes

How long did it take you to take the harness off?

1-3 minutes 4-5 minutes 6-7 minutes 8-10 minutes